M. Tech (Environmental Engineering)

SOHOM CHATTERJEE

2023

MULTIPARAMETER RELATION WITH SOIL ORGANIC CARBON STOCK AT INDIAN WETLANDS

A DISSERTATION

SUBMITTED IN PARTIAL FULFILMENT OF THE REQUIREMENTS FOR THE AWARD OF THE DEGREE

OF

MASTER OF TECHNOLOGY

IN

ENVIRONMENTAL ENGINEERING

Submitted by,

SOHOM CHATTERJEE

(Roll No.: 2K21/ENE/11)

Under the supervision of

PROF. ANIL KUMAR HARITASH

DEPARTMENT OF ENVIRONMENTAL ENGINEERING

DELHI TECHNOLOGICAL UNIVERSITY

(Formerly Delhi College of Engineering)

Bawana Road, Delhi- 110042

MAY, 2023

MULTIPARAMETER RELATION WITH SOIL ORGANIC CARBON STOCK AT INDIAN WETLANDS

A DISSERTATION

SUBMITTED IN PARTIAL FULFILMENT OF THE REQUIREMENTS FOR THE AWARD OF THE DEGREE

OF

MASTER OF TECHNOLOGY

IN

ENVIRONMENTAL ENGINEERING

Submitted by,

SOHOM CHATTERJEE

(Roll No.: 2K21/ENE/11)

Under the supervision of

PROF. ANIL KUMAR HARITASH

DEPARTMENT OF ENVIRONMENTAL ENGINEERING
DELHI TECHNOLOGICAL UNIVERSITY
(Formerly Delhi College of Engineering)
Bawana Road, Delhi- 110042
MAY, 2023

DEPARTMENT OF ENVIRONMENTAL ENGINEERING
DELHI TECHNOLOGICAL UNIVERSITY
(Formerly Delhi College of Engineering)
Bawana Road, Delhi- 110042

CANDIDATE'S DECLARATION

I, Sohom Chatterjee, 2K21/ENE/11 of M. Tech Environmental Engineering, hereby declare that the report entitled "**Multiparameter Relation with Soil Organic Carbon Stock at Indian Wetlands**" submitted by me, for the partial fulfilment of the degree of Master of Technology to Department of Environmental Engineering, Delhi Technological University is a record of the M. Tech thesis project work carried out by me under the supervision of Prof. Anil Kumar Haritash, Delhi Technological University.

I further declare that this written submission represents my ideas in my own words and where other's ideas or words have been included, I have adequately cited and referenced the original sources. I affirm that I have adhered to all principles of academic honesty and integrity and have not misrepresented or falsified any idea/data/fact/source to the best of my knowledge. I understand that any violation of the above will cause for disciplinary action by the Institute and can also evoke penal action from the sources which have not been cited properly.

Place: Delhi

Date: SOHOM CHATTERJEE

DEPARTMENT OF ENVIRONMENTAL ENGINEERING
DELHI TECHNOLOGICAL UNIVERSITY
(Formerly Delhi College of Engineering)
Bawana Road, Delhi- 110042

CERTIFICATE

I hereby certify that the Project Dissertation titled "**Multiparameter Relation with Soil Organic Carbon Stock at Indian Wetlands**" which is submitted by **Sohom Chatterjee, Roll No. 2K21/ENE/11**, Department of Environmental Engineering, Delhi Technological University, Delhi in partial fulfilment of the requirement for the award of the degree of Master of Technology, is a record of the project work carried out by the student under my supervision. To the best of my knowledge this work has not been submitted in part or full for any Degree or Diploma to this University or elsewhere.

Place: Delhi

Date:

PROF. ANIL KUMAR HARITASH

SUPERVISOR

ABSTRACT

Carbon Storage can be of two types i.e., 1) Organic Carbon storage and 2) Inorganic Carbon Storage. Research studies depicts that in arid, semiarid area and coastal area with high alkalinity and salinity in soil is of great importance to store Carbon in inorganic form. However, Soil Organic Carbon (SOC) is a widely accepted indicator to predict the soil health and carbon storage in soil. Soil Organic Carbon stock (tonnes/hector) data (0 – 30 m) from the latest release of SoilGrids (May 2020) has been used in this study to correlate the SOC stock with multiple indices derived from Landsat 8 band dataset. The study areas selected here are East Calcutta Wetland (Ramsar site no. 1208) & Sundarban Wetland (site no. 2370) which are inscribed in a single Landsat 8 tile (WRS Path/Row: 138/45) and are of international importance for rich biodiversity and climate change. Several studies by numerous scholars have been proved that SOC stock has a deep correlation with NDVI and crop phenology. Numerous physical, chemical, and biological parameters regulate the carbon cycle and this complex interaction is hard to predict with a few laboratories analysis and can be cost-extensive or site accessibility for sampling is often denied for numerous bio-geophysical constraints. However, spatiotemporal changes of parameters derived from satellite data can be a good option to specify the sampling area with more certainty and cross validation for lab analysis. Built-up area, cloud cover and presence of surface water plays important role to regulate the prediction of subsurface SOC stock. Hence Multiparameter (NDVI, NDBI, NDWI, LST & SMI) analysis, variation, and best possible correlation (r, Pearson correlation coefficient) is established here which can be used for further research progress in these study areas. Sampling in the study areas is done by Google Earth Engine to generate 1000 and 19000 random sampling points at the site no. 1208 and 2370, consequently. ArcGIS 10.8.2 software is used in this analysis to estimate the band statistics and interpolation of SOC data input, data extraction, resampling, and raster calculation for derived indices (NDVI, NDBI, NDWI, SMI) and LST. Predictability of SOC stock using Ordinary Kriging method with spherical variogram has been established in this study through the variation trend of covariates like Root Mean Square (RMSE) and R^2 are shown here where extracted point dataset is used as measured and interpolated point dataset are used as predicted value in SOC stock analysis. Linear Regression method is also to compare statistical outcome between the two study areas. Monthly variation of the derived multiparameter with SOC stock data is

the key concern throughout this work. Excel and Tableau software are used to analysis the data in this study. The results showing the variation of statistical metrices and linear regression has done to fit the line with a minimum R^2 values for both extracted and interpolated SOC data points at both study sites. In this analysis, the monthly variation of multiparameter in case of EKW is higher than Sundarban Wetlands which is mainly due to anthropogenic activity at Ramsar site 1208. Though both the wetlands are of different types, but they have a good on an average amount of SOC stock as per the data collection. The importance of wetland in environmental balance is the key moto which has tried to be established in through this study.

Keywords: **East Calcutta Wetlands, Sundarban Wetland, SOC, NDVI, NDBI. NDWI, LST, SMI, R^2, RMSE**

ACKNOWLEDGEMENT

I would like to express my deepest gratitude to my Major Project-II guide Prof. Anil Kumar Haritash, the HOD of Department of Environmental Engineering at Delhi Technological University. The door to Prof. Anil Kumar Haritash office and laboratory was always open whenever I ran into a trouble spot or had a question about my research or writing. I also want to endeavour my heartiest thanks to all the PHD scholars of Department of Environmental Engineering to consistently help me in due needs. I also must acknowledge the unconditional freedom to think, plan, execute and express, that I was given in every step of my project work, while keeping faith and confidence on my capabilities.

SOHOM CHATTERJEE

2K21/ENE/11

CONTENTS

LIST OF TABLES

LIST OF FIGURES

LIST OF SYMBOLS, ABBREVIATIONS & NOMENCLATURE

BT	Brightness Temperature
EKW	East Kolkata (Calcutta) Wetlands
LSE	Land Surface Emissivity
LST	Land Surface Temperature
Multiparameter	NDVI. NDBI, NDWI, LST, SMI
NDBI	Normalized Difference Built-up Index
NDVI	Normalized Difference Vegetation Index
NDWI	Normalized Difference Water Index
P_v	Proportion of Vegetation
r	Pearson's correlation coefficient
Ramsar	Ramsar Convention on Wetlands of International Importance Especially as Waterfowl Habitat
RMSE	Root Mean Square Error
SMI	Soil Moisture Index
SOC	Soil Organic Carbon
SoilGrids	Global Grided Soil Information
Spatiotemporal	Variation of a parameter at a space with time
Temporal	Time Wise Variation
TOA	Top of Atmosphere

CHAPTER 1

INTRODUCTION

1.1 Overview

The biogeochemical cycle through which Carbon (C) is interchanged between various layers of earth such as biosphere, geosphere, pedosphere, hydrosphere, and atmosphere, is referred to as Carbon Cycle. The primary concern behind Carbon storage and Carbon management is to reduce climate risk and enhance climate resiliency. In today's world, atmospheric Carbon pool is getting higher day by day with respect to the underground and fixed carbon stock. Carbon can be stored in various forms in earth such as Soil Organic Carbon (SOC) including Particulate Organic Carbon (POC); Dissolved Organic Carbon (DOC), other type of carbon fixation mechanism is in the form of Soil Inorganic Carbon (SIC). There are several nature-based solutions for Carbon sequestration like afforestation, conservation of biosphere and mangroves, conservation of wetlands, grasslands, peatlands etc. Research study shows that in dryland Carbon gets stored in the form of Soil Inorganic Carbon whereas, in peatland and wetland Carbon storage in the form of Soil Organic Carbon dominates. It has been also studied that two-third of carbon storage in the world is in Soil Organic Carbon form whereas, rest of the portion stores Carbon in inorganic form. Here, in this study SOC storage in two different types of wetlands is of primary concern. Based on the types of wetlands, vegetation type in wetland, several physical, chemical, and biological factors present in wetland soil; carbon sink for long term assurance differs. All wetlands are enabled of sequestering and storing carbon through photosynthesis and accumulation of organic matter in sediments, soils, and vegetation biomass. During the study of complex processes that occur in wetlands, it is observed that in general, wetland plants grow at a faster rate than they decompose, contributing to a net annual carbon sink. As a result of waterlogging in wetland, anaerobic condition generated in soils, limits oxygen diffusion into sediment profiles. Consequently, the decomposition rates slow down, leading to significant accumulation of organic carbon in wetland sediments. However, the presence of

anaerobic conditions creates an ideal environment to produce greenhouse gases, including methane (CH_4) and nitrous oxide (N_2O). In periodically flooded systems like floodplains, methane emissions can vary significantly. During periods of inundation and anaerobic conditions, methane production may occur. Conversely, when these wetlands are dry, they can serve as methane sinks. Additionally, salinity acts as an inhibiting factor for methane production, resulting in lower methane emission rates in coastal wetlands compared to freshwater wetlands.

1.2 Carbon Cycle & Carbon Storage in Wetland

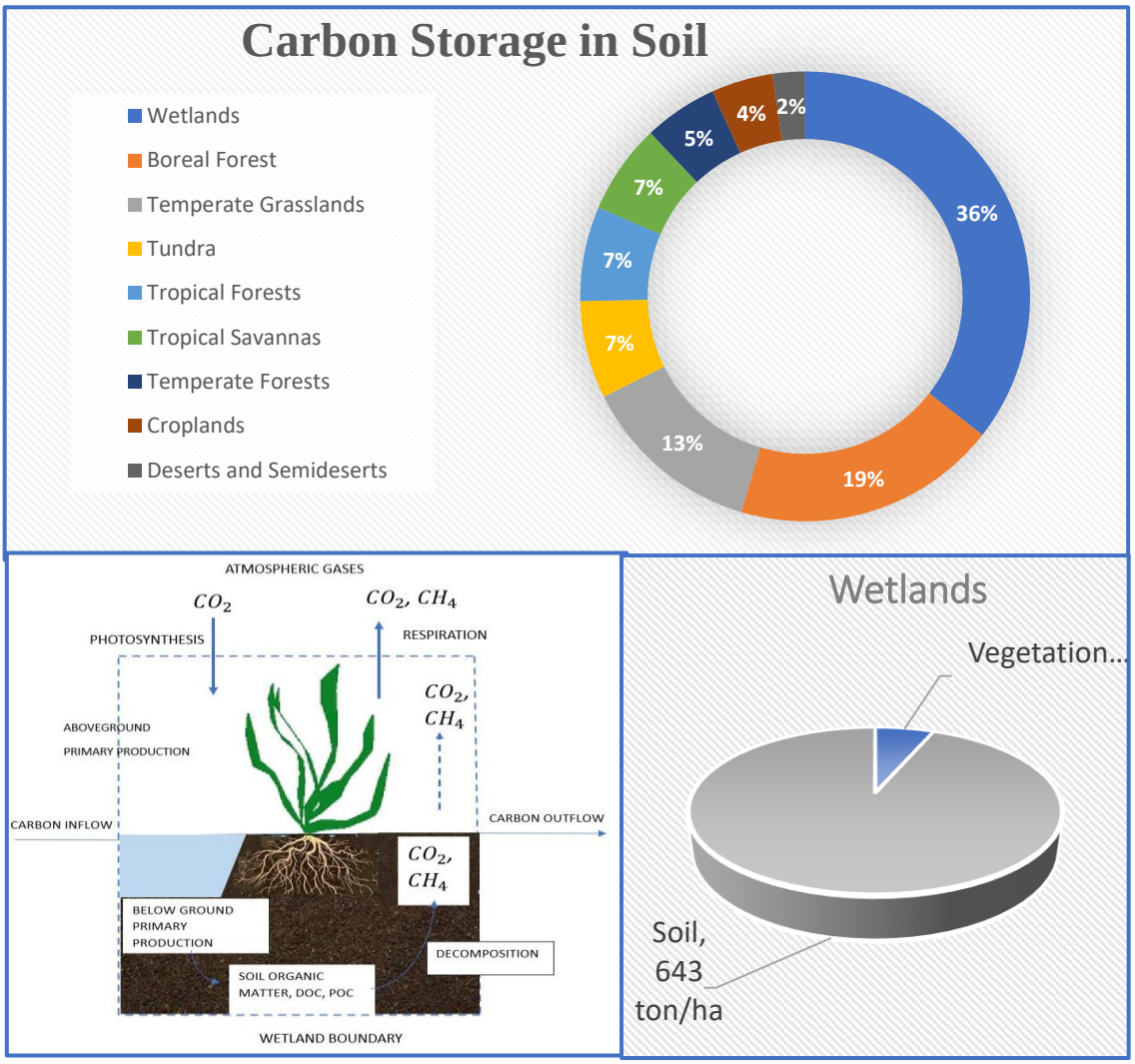

Figure 1.1: Carbon Cycle and Carbon Storage in Wetland

1.3 Soil in-situ Factors Affecting Carbon Storage

There are several physical, chemical & biological factors inside soil which actively regulate the Carbon cycle and carbon storage in soil.

1.3.1 Physical

Bulk Density, Clay Content, Coarse Fragment, Sand, Silt these are some important physical properties of soil.

1.3.2 Chemical

Cation Exchange capacity, Nitrogen, Soil Organic Carbon, pH of water are some important chemical properties of soil.

Based upon these physical and chemical properties, soil organic carbon stock (tons/hector) and organic carbon density (gm/dm^3) are derived by ISRIC team with the help of machine learning algorithm.

1.4 About SoilGrids

SoilGrids TM is a digital soil mapping system designed for global-scale mapping of soil properties, utilizing advanced machine learning techniques. The models used in this system are trained using a vast dataset of over 230,000 soil profile observations sourced from the WoSIS database, along with a wide range of environmental covariates. More than 400 environmental layers derived from Earth observation data, including climate, land cover, and terrain morphology, were incorporated to extract relevant covariates.

The outcome of SoilGrids is a collection of global maps depicting various soil properties at six standard depth intervals (as per the specifications of the Global Soil Map IUSS working group). These maps have a spatial resolution of 250 meters, an improvement from the previous resolution of 1 km. To assess prediction uncertainty, a 90% prediction interval is calculated using the lower and upper limits. Additionally, an uncertainty layer is provided on the SoilGrids website, which represents the ratio between the inter-quantile range and the median. The SoilGrids data is publicly accessible under the CC-BY 4.0 License.

For generating SOC stock maps at depths ranging from 0 to 30 cm, a two-step process was followed. Firstly, carbon stocks were computed at the sampling locations by modelling carbon density based on SOC concentration, bulk density, and the proportion of coarse fragments for each observation. Then, a weighted sum of carbon densities was

calculated for observations within the 0-30 cm depth range. Finally, a Quantile Random Forest model was calibrated and applied to generate the global SOC stock map.

It is important to note that the calculations and models excluded organic layers present on top of mineral soils. The total global carbon stocks estimated using version 2 of SoilGrids amounted to 599 Pg of carbon for the 0-30 cm depth range, which aligns more closely with other global estimates. SoilGrids has homolosine projection. Hence, it can be used by any GIS software.

1.5 About Landsat-8

Landsat 8, also known as the Landsat Data Continuity Mission (LDCM), is a satellite operated by NASA and the United States Geological Survey (USGS) that plays a crucial role in Earth observation and monitoring. Launched on February 11, 2013, Landsat 8 is the eighth satellite in the Landsat program, which has been providing valuable data about our planet's land surface since 1972.

Landsat 8 carries two main instruments: the Operational Land Imager (OLI) and the Thermal Infrared Sensor (TIRS). The OLI captures images with improved resolution and accuracy compared to its predecessors, offering nine spectral bands ranging from visible to shortwave infrared. This multispectral capability allows scientists and researchers to study a wide range of phenomena, such as vegetation dynamics, land cover changes, urban development, and the health of coastal and inland water bodies.

The TIRS instrument on Landsat 8 measures thermal energy emitted from the Earth's surface. It provides valuable data for monitoring surface temperatures, identifying thermal anomalies, and studying processes like volcanic activity, wildfire detection, and urban heat island effects. The combination of OLI and TIRS data allows for a more comprehensive understanding of Earth's land surface dynamics and helps in managing and protecting our planet's resources.

Landsat 8 orbits the Earth in a sun-synchronous polar orbit, which means it passes over the same area at approximately the same local solar time on each orbit. This consistent viewing geometry is crucial for comparing images over time and monitoring changes in land use and land cover. The satellite covers the entire globe every 16 days, capturing high-quality images with a spatial resolution of 30 meters for most of its spectral bands.

One significant advancement introduced by Landsat 8 is its onboard data storage capacity. It can store up to 4 terabytes of data, enabling the satellite to collect and store a considerable amount of imagery even in areas with limited ground receiving stations. The stored data can be downlinked to ground stations during subsequent passes over those stations, ensuring that valuable observations are not lost.

The data captured by Landsat 8 is freely available to the public, making it a valuable resource for a wide range of applications. Scientists, policymakers, land managers, and researchers around the world rely on Landsat imagery to monitor environmental changes, assess the impacts of natural disasters, plan urban development, manage water resources, study climate change, and support various other applications aimed at understanding and protecting our planet.

Landsat 8 continues the legacy of the Landsat program, providing a long-term and consistent record of Earth's land surface observations. Its high-quality data, improved capabilities, and open data policy make it an indispensable tool for studying our changing planet and making informed decisions for a sustainable future.

Table 1.1: Landsat 8 OLI Bands Identity

Band Type	OPERATIONAL LAND IMAGER (OLI) BANDS								
Band No.	Band 1	Band 2	Band 3	Band 4	Band 5	Band 6	Band 7	Band 8	Band 9
Band Name	Ultra-Blue	Blue	Green	Red	NIR	SWIR 1	SWIR 2	Panchromatic	Cirrus
Wavelength (µm)	0.435-0.451	0.452-0.512	0.533-0.590	0.636-0.673	0.851-0.879	1.566-1.651	2.107-2.294	0.503-0.676	1.363-1.384
Resolution (Meter)	30	30	30	30	30	30	30	15	30

Table 1.2: Landsat 8 TIRS Bands Identity

Band Type	Thermal Infrared Sensor (TIR) Bands	
Band No	Band 10	Band 11
Band Name	TIRS 1	TIRS 2
Wavelength (μm)	10.60-11.19	11.50-12.51
Resolution (Meter)	100 (30)	100 (30)

1.6 Multiparameter of This Study

1.6.1 Normalized Difference Vegetation Index (NDVI)

NDVI estimates vegetation with the measurement of the difference between Near-infrared (which is strongly reflected by greeneries) and red light (which is absorbed by greeneries). It is considered as the foundation of remote sensing. It has several uses like:

1. To identify vegetation separately, from other types of Land-use & Land-cover
2. To estimate vegetation density and health of the vegetation
3. To some extent NDVI can measure the phase of crops as it has a strong correlation with crop phenological parameters.
4. NDVI can be used in vine vigor assessment, though the accuracy depends on proper soil management
5. Additionally, NDVI has other uses like optimizing fungicide application, Eradicating Weed Infestation, deforestation monitoring, forage abundance measurement and many more.

The outcomes of the NDVI estimation range are -1 to 1. The negative values indicate to areas with water bodies & surfaces with water, human made structures, clouds, rocks & snow. Bare soil typically exhibits NDVI values in the range of 0.1 to 0.2, while plants generally display positive values between 0.2 and 1. A healthy and dense vegetation canopy is expected to have an NDVI above 0.5, whereas sparse vegetation typically falls within the 0.2 to 0.5 range. It is important to note that these are rough guidelines, and the interpretation of NDVI values should always take into account factors such as season, plant types, and regional variations to gain a precise understanding of their meaning.

1.6.2 Normalized Difference Built-up Index (NDBI)

NDBI is estimated by the difference of NIR and SWIR bands to focus on manufactured built-up areas. NDBI is ratio based on mitigating the effects of terrain illumination differences and atmospheric effects.

Indexes representing built-up area can be of several types as follow:

1. Normalized Difference Built-up Index (NDBI)
2. Built-up Index (BU)
3. Urban Index (UI)
4. Index-based Built-up Index (IBI)
5. Enhanced Built-up and Bareness Index (EBBI)

These are the most usual indexes to estimate the built-up areas. These different indexes having their own empirical equation for estimation which is used as raster formula in various geoprocessing software by using the input band data of several geoinformatics sources like Sentinel, MODIS or Landsat. It has seen that, soil at built-up areas and barren land reflects more SWIR and less NIR. Infrared spectrum cannot be reflected by water bodies. In case of surface with green vegetation, NIR spectrum reflection is more than SWIR spectrum. For a better result, we can use Built-up Index (BU). Built-up Index is a satellite data processed indicator to estimate the urban pattern by using the difference of NDBI and NDVI. Built-up index is the binary image with only higher positive value indicates built-up and barren thus. Thus, it allows BU to generate a processed map the built-up area in an efficient way.

NDBI value lies in between the range of -1 to +1. The negative values represent wasteland areas where no structures have been built up since now and positive values indicates highly built-up areas.

1.6.3 Normalized Difference Water Index (NDWI)

NDWI is used widely to estimate the water bodies. The index can be estimated by using Green and NIR bands of remote sensing images. The NDWI is used to get accurate water information in an efficient way. It has a high sensitivity for build-up land and result in over-estimated water bodies. The NDWI products can be used in conjunction with NDVI change products to assess context of apparent change areas.

NDWI value lies in between -1 to +1. The range breaks are as following:

0.2 to 1 – This indicates the water surface,

0.0 to 0.2 – This indicates the flood situation and humidity,

-0.3 to 0.0 – This indicates the moderate drought and surfaces with no or less water

-1 to -0.3 – This indicates the drought situation and completely non-aqueous surfaces

1.6.4 Land Surface Temperature (LST)

LST refers to the perceived heat of the Earth's "surface" in a specific location. When observed from a satellite, the "surface" encompasses whatever is visible through the atmosphere, such as snow, ice, grass, rooftops, or forest canopies. It is important to note that LST differs from the air temperature reported in daily weather forecasts.

LST represents the radiative temperature of the land surface as detected by remote sensors. It is derived from Top-of-Atmosphere brightness temperatures obtained from the infrared spectral channels of geostationary satellites like Meteosat Second Generation, GOES, and MTSAT/Himawari. The estimation of LST also considers factors such as albedo (surface reflectivity), vegetation cover, and soil moisture.

LST reflects a combination of temperatures from both vegetation and bare soil. Since both components respond rapidly to changes in solar radiation caused by cloud cover, aerosol concentration, and diurnal variations in illumination, LST exhibits rapid fluctuations as well. In turn, LST influences the energy exchange between the ground and vegetation, ultimately impacting the surface air temperature.

Calculation of LST is still challenging. Some of the proposed Algorithm for LST calculation is as follow:

1. The retrieval of LST involves the utilization of the Radiative Transfer Equation along with atmospheric parameters. These parameters are used to estimate the temperature of the Earth's surface from remote sensing data.
2. A Single-Channel Algorithm developed by Jiménez-Muñoz et al. (2014) can be employed for LST retrieval. This algorithm utilizes specific coefficients and equations to calculate the temperature based on data from a single spectral channel.
3. Another option is the Split-Window Algorithm, also developed by Jiménez-Muñoz et al. (2014), which utilizes coefficients and equations designed for split-

window spectral channels. This algorithm allows for the estimation of LST using the data from multiple spectral channels.

4. Alternatively, the Split-Window Algorithm developed by Du et al. (2015) can be utilized. This algorithm incorporates specific coefficients and equations suitable for split-window spectral channels, enabling the retrieval of LST from remote sensing data.

1.6.5 Soil Moisture Index (SMI)

The measurement known as the soil moisture index (SMI) quantifies the relationship between the current soil moisture and the permanent wilting point relative to the field capacity and residual soil moisture. The SMI is expressed as a numerical value ranging from 0 to 1, where 0 represents extremely dry conditions, and 1 represents extremely wet conditions. This index serves as an indicator of soil moisture levels and provides valuable insights into the moisture status of an area. It has an important use in drought monitoring.

1.7 Objectives

This study is based on remote sensing data entirely. Here, in this study, Soil Organic Carbon stock (in tons/hector) has been collected from SoilGrids 250 m and time series variation of indices (NDVI, NDBI, NDWI, SMI) & LST are calculated from Landsat 8 OLI & TIR bands to fulfill the following objectives:

1) Inter-comparison of SOC stock between the two types of wetlands (Inland-human made wetland & coastal-intertidal wetland)
2) To check the correlation of monthly variation of Multiparameter with SOC stock for following cases:
   (a) Soil Organic Carbon Stock & Normalized Difference Vegetation Index (NDVI) [Jan – Dec]
   (b) Soil Organic Carbon Stock & Normalized Difference Built-Up Index (NDBI) [Jan – Dec]
   (c) Soil Organic Carbon Stock & Normalized Difference Water Index (NDWI) [Jan – Dec]
3) To analyze the Lansat 8 data with SOC data collected from SoilGrids and establish the decision on the Carbon storage in both type of wetland from the statistical outcomes along with interpolation accuracy in random sampling

CHAPTER 2

REVIEW OF LITERATURE

Research study carried out by **(H. Xu)** introduces a “Modified” NDWI (MNDWI) as a novel approach, based on Mcfeeters' NDWI from 1966. The MNDWI utilizes MIR (Band 5) instead of NIR (Band 4) to construct the index. Experimental testing of the MNDWI was conducted in various environments, including ocean, lake, and river areas with built-up lands, as well as vegetated lands with both clean and polluted water bodies, using Landsat TM ATM imagery.

The results of this study demonstrate that the MNDWI significantly improves the accuracy of water detection, particularly in areas predominantly consisting of built-up land. By effectively suppressing information related to built-up land, the MNDWI successfully highlights water features and enables accurate extraction of water body information within the study areas.[1] On the other hand, using the NDWI alone for enhancing and extracting water information in built-up land-dominated areas leads to mixed results, as it tends to incorporate noise from the built-up land, resulting in overestimation of the water body extent.

Moreover, the MNDWI exhibits enhanced capability in capturing subtle water features compared to the NDWI and other visible spectral bands. Additionally, the MNDWI image proves effective in identifying non-point pollution surrounding Xian en Island, resulting from agricultural activities. Notably, the ratio computation employed in the MNDWI facilitates the removal of shadow noise from water information, eliminating the need for complex procedures that would otherwise be required

Research work carried out by **(L. Yang et al)** Mapping the spatial distribution of soil organic carbon (SOC) content or stock is crucial for climate change studies and land management decision-making. In croplands, crop species/crop rotations and agricultural management practices significantly influence the spatial variability of SOC. In regions where climatic conditions and farming practices are relatively consistent within a crop species' cultivation territory, crop phenology serves as a reliable indicator of the crop's response to soil conditions. Therefore, integrating phenological parameters

with crop rotation information can be an effective approach for mapping soil organic carbon in these areas.

In this study conducted in Anhui province, China, phenological parameters were derived from time series data of the NDVI. These parameters, along with crop rotation information, were utilized to predict topsoil organic carbon content in cropland areas. The results revealed that the base levels (average of the left and right minimum values of a time series profile) for both seasons emerged as the most significant predictors in the study area.[2] Incorporating both crop rotation and the two phenological parameters into the analysis, in addition to the natural environmental variables, resulted in a substantial improvement in prediction accuracy. Specifically, the inclusion of these variables enhanced the R2 value by 50% and reduced the root mean square error (RMSE) by 13.4%.

In the context of digital soil mapping, study conducted at a regional scale by **(L. Yang, Y. Cai, L. Zhang, M. Guo, A. Li, and C. Zhou)** have encountered challenges when attempting to map SOC due to the complex relationships between SOC and environmental factors. One potential approach to address this challenge is to incorporate vegetation phenology as an environmental covariate, as it directly reflects the long-term characteristics of vegetation growth.

This paper investigates the effectiveness of ten-year MODIS MCD12Q2 phenology variables for SOC prediction using a convolutional neural network (CNN) model in Anhui province, China. To compare the performance, a random forest (RF) model was also employed, and three sets of environmental variables were utilized. The results demonstrate that the inclusion of land surface phenology variables in conjunction with natural environmental variables significantly improved the prediction accuracy of the CNN model. Specifically, the addition of land surface phenology variables led to a reduction of 5.57% in root mean square error (RMSE) and an increase of 31.29% in R2 compared to the CNN model without these variables.[3]

The evaluation of SOC accumulation in tropical forests was conducted at Ranthambhore Tiger Reserve Forest area by **(P. Kumar et al),** utilizing both remote sensing images and field methods. Multiple soil samples were randomly collected from various locations within the region for laboratory analysis to estimate surface soil carbon concentrations. The study employed regression analysis to establish relationships

between bare soil index, NDVI, SOC, and the correlation between SOC and NDVI. By comparing reference SOC (SOC measured in the field) with predicted SOC (estimated from satellite imagery), the study derived results and findings.

Remote sensing images were utilized to accurately predict the carbon content associated with organic matter in the soil using NDVI and relevant equations. These predictions were then utilized to generate a digital map of soil organic carbon, providing a spatial representation of SOC in the study area.[4] The relationship between NDVI and both reference and predicted SOC was established using equations to derive digital SOC values from remote sensing data. The study also presented the statistical relationship between reference SOC, pH concentrations, and NDVI values, demonstrating the variations among these variables in relation to predicted SOC

The findings of this study conducted by **(S. Pal, S. Manna, A. Aich, B. Chattopadhyay, and S. K. Mukhopadhyay)** revealed that East Calcutta Wetlands has significant potential for storing organic matter in the soil, thereby contributing to carbon sequestration. The efficient carbon storage capacity of EKW highlights its importance from both economic and ecological perspectives, emphasizing the need for conservation, sustainable development, and responsible management of this valuable wetland ecosystem. The study also observed that the application of composite wastewater increased the concentration of cations in soil samples. Elevated concentrations of these cations can lead to competition among them, thereby reducing their uptake by plants. This competition negatively impacts plant species development and overall system productivity. Given the economic importance of EKW for activities such as pisciculture and agriculture, it is crucial to implement control measures to prevent excessive waste discharge from this delicate ecosystem.[5]

Spatial distributions of chemical factors in surface soils exhibited notable variability within the East Kolkata Wetland, and distinct patterns of distribution were observed among the seven studied sites. This highlights the necessity of employing a spatially explicit sampling approach to accurately assess the underlying variability of soil properties. In this study, by combining geographical information with a spatially explicit sampling approach, a model was developed for estimating soil properties. This approach can also serve as a guide for formulating a comprehensive conservation plan for the fragile ecosystem of East Kolkata Wetlands.

In another study, correlation and single regression analyses were performed to examine the relationship between SOC and various geochemical properties done by **(K. Ashida et al).** Specifically, the correlations and quantitative relationships were assessed between SOC and oxalate extractable Al and Fe, pyrophosphate extractable Al and Fe, and the combined content of clay and silt.

In the subsurface soils, strong correlations were observed between SOC and oxalate extractable Al and Fe ($Al_o + Fe_o$) as well as pyrophosphate extractable Al and Fe ($Al_p + Fe_p$) (r = 0.79–0.85 and 0.58–0.85, respectively). The quantitative relationships between SOC and these properties were consistent across different weathering groups (4–5 and 5–8, respectively). However, no strong correlation or similar quantitative relationships were found between SOC and the combined content of clay and silt.

This study remained a key note on required caution when using Al_p and Fe_p for SOC estimation, as their measurements can be significantly influenced by experimental procedures such as centrifugation speed and filter pore size. In the present study, (clay + silt), ($Ca_e + Mg_e$) (calcium and magnesium exchangeable cations), and free Fe oxides showed weaker correlations with SOC, except in surface soils with a pH of 6.[6] In surface soils with higher pH, ($Ca_e + Mg_e$) and (clay+ silt) exhibited higher correlation coefficients compared to ($Al_p + Fe_p$) and ($Al_o + Fe_o$). The study also revealed that in the acidic subsoils, SOC content was primarily influenced by active and/or organically bound Al and Fe, with a similar molar ratio of SOC to ($Al_o + Fe_o$) (4–5) and ($Al_p + Fe_p$) (5–8).

Significant variation in soil organic carbon (SOC) stocks among several land-cover types within the park, with wetland soils exhibiting the highest SOC content (13.99 ± 1.05 kg/m^2), followed by forest, lawn, and bare soils as per investigated by **(J. Bae and Y. Ryu).** This study discovered a deep-seated "cultural layer" preserving the historical land use significantly contributed to the higher SOC stocks observed in the wetland. In terms of SOC concentrations in the topsoil, there was an approximately three-fold increase from 2003 to 2013 (256 ± 130%). By analyzing the NDVI derived from MODIS and Landsat satellite images, it was observed that land-use history, expansion of plant areas, and plant growth played a role in the observed increase in SOC concentrations over the 10-year period.[7] These findings suggest that urban park soils have the potential to act as carbon sinks, and careful consideration of land-use

history and land-cover choices in park planning can significantly impact the carbon budget of urban parks.

An investigation of the temporal and spatial trends of NDVI in the northern region of China and its response to meteorological factors was the primary focus of the research work carried out by **(S. Pan, X. Zhao, and Y. Yue).** Over the past 30 years, the study area has exhibited a slow growth trend in NDVI with increased fluctuations. The minimum NDVI value was recorded in 2004 at 0.4048, while the maximum was observed at 0.4683. The growth rate of NDVI was calculated to be 1.5%.

The research findings indicate that the influence of precipitation and temperature varies across different terrains in the northern region. In higher alpine and subalpine regions, NDVI shows a higher correlation and partial correlation with temperature compared to precipitation. Conversely, in northern grasslands, the correlation coefficient between NDVI and precipitation is higher than that of temperature, as confirmed by partial correlation analysis. This suggests that typical grasslands and desert grasslands in arid and semi-arid areas are particularly sensitive to precipitation, while plateau grasslands and woodlands at higher altitudes exhibit greater sensitivity to temperature.[8]

Mineralogy plays a crucial role in soil's ability to store carbon. In this study, the composition of sediments rich in mud was analysed by **(L. Borromeo, S. Andò, C. France-Lanord, G. Coletti, A. Hahn, and E. Garzanti)** in terms of their mineralogy and geochemistry. To ensure accuracy and precision comparable to that achieved for sand samples, a range of techniques were employed. These techniques included laser granulometry, optical microscopy, Raman spectroscopy, X-ray diffraction (XRD), inductively coupled plasma optical emission spectrometry/mass spectrometry (ICP-OES/ICP-MS), and X-ray fluorescence (XRF). The analysis was conducted on both the bulk sample and the low-density LM (light minerals) and high-density HM (heavy minerals) fractions of six different grain-size classes, which spanned from particles smaller than 5 μm to larger than 63 μm. The separation of minerals was achieved using wet sieving.

For grains as small as 5 μm, a meticulous approach involving a combination of optical observations under a microscope and Raman spectroscopy was utilized to accurately identify transparent-heavy-mineral species on a grain-by-grain basis. Standard XRD and XRF methods were employed to analyse the <5-μm class of particles. By adopting this

comprehensive approach, the researchers were able to investigate both the compositional variability between different sediment samples and the variability within each individual sample.[9] The sieve analysis conducted during the study confirmed that the fine mode in all the samples predominantly consisted of very fine silt and clay. This finding validated the observation that laser granulometry tends to underestimate the clay content in the analysed sediment samples.

Artificial neural networks (ANNs) were utilized to develop models for predicting soil organic carbon density (SOCD) at various depths within the soil layers. The input variables in this study done by **(S. Falahatkar, S. M. Hosseini, S. Ayoubi, and A. Salmanmahiny)** considered for the models consisted of selected environmental factors such as vegetation indices, soil particle size distribution, land use type, and primary and secondary terrain attributes. The results revealed that the developed ANN models accounted for 77% and 72% of the variability in SOCD for the soil layers at depths of 0–20 cm and 20–40 cm, respectively, at the study site.

In this study, sensitivity analyses were conducted to determine the significant contributions of variables in predicting SOCD. The findings indicated that the most influential variables for predicting SOCD in the 0–20 cm soil layer were land use type, NDVI, NDWI, silt, clay, and elevation, in descending order.[10] Conversely, for the 20–40 cm soil layer, the order of importance in predicting SOCD was land use type, followed by NDVI, NDWI, clay, and silt.

Role of Wetlands in Carbon cycle was issued by a paper published by Department of Sustainability, Environment, Water, Population, and communities of Australian Government on July 2012. This paper gave an overview on Carbon sequestration in different types of wetlands globally along with degradation of wetlands and potentiality for carbon capture by the wetland. This paper reveals the data about Australian wetland, climate change and it's impact on wetland, international policies and Australian policies for wetland security and management.[11]

A research work done by **(Ayala Izurieta et al. 2021)** reveals Multi-predictor mapping of SOC in the alpine tundra region through the development of SOC multi-predictor model specifically for the complex Andean páramo area. The model was calibrated with high accuracy, achieving 82% for SOC in weight percentage and 77% for SOC in

Mg/ha. Estimating SOC distribution in such complex areas is challenging due to various factors such as climate, topographical variability, and geological diversity.[12]

To overcome these challenges, an optimization process was conducted using a Random Forest (RF) machine learning algorithm. This algorithm selected nine environmental variables that are closely related to SOC sequestration dynamics. These variables include geological unit, soil taxonomy, precipitation, height, orientation, LS factor, BI index, average annual temperature, and TOA Brightness Temperature. These variables were found to be highly relevant in quantifying SOC in the study area.

An article published by **(Hengl et al. n.d)** reveals the technical advancements and accuracy evaluation of the latest version of the SoilGrids system, which offers improved soil mapping at a resolution of 250 meters (June 2016 update). These improvements can be attributed to three main factors: (1) the adoption of machine learning techniques instead of linear regression, (2) the generation of covariate layers at a finer resolution, and (3) the inclusion of additional soil profiles to enhance the modeling process.

To further enhance the SoilGrids system, future developments could focus on refining methodologies to incorporate input uncertainties and deriving posterior probability distributions at the pixel level.[13] Moreover, there is potential for automating spatial modeling to facilitate the generation of soil maps for numerous soil variables. Additionally, a promising area for future research involves developing techniques for merging SoilGrids predictions with local or national gridded soil products at different scales, such as resolutions up to 50 meters. This integration would contribute to the production of increasingly accurate, comprehensive, and consistent global soil information.

A research work that shows a clear representation of NDVI temporal variation to predict SOC was done by **(Zhang et al. 2019)**. In this study several models like OK, SLR, PLSR, SVM and ANN were used and intercomparison was done. The results showed that ANN is the best tool for prediction. However, OK method is significantly good to predict just after ANN. In this research, a practical demonstration was presented on the effective mapping of regional soil organic carbon (SOC) in plains, addressing the challenges associated with selecting auxiliary variables. The utilization of NDVI time series data demonstrated significant potential in predicting SOC, and the application of artificial neural networks (ANN) effectively extracted valuable information for digital

soil mapping. Therefore, it is recommended to explore and implement approaches that leverage the time series characteristics of multiple key auxiliary variables using ANN in various geographical areas to predict other soil properties. Enhancing our understanding of the spatial distribution of soil properties through such methods supports improved soil management practices, enhances agricultural productivity, and facilitates ecological planning.[14]

To calculate Land Surface temperature, various algorithms are followed. Such a study in Bangladesh, to calculate LST, four algorithms and their intercomparison was carried out by (**Sajib et al. 2020)**. In this study, the results obtained from the Single-Channel algorithm for Land Surface Temperature (LST) exhibit a higher Root Mean Square Error (RMSE) with an average RMSE of 4.11°C, compared to the RTE-based method. In contrast, the Split-Window Algorithm developed by Jiménez-Muñoz et al. demonstrates superior performance with the lowest average RMSE of 1.19°C among the evaluated methods. These two algorithms, the Split-Window Algorithm and the Single-Channel algorithm, are recommended in situations where (a) accurate measurement of water vapor content is available and (b) other atmospheric parameters are not necessary. It is important to note that the Single-Channel algorithm may not be suitable for images that contain multiple thermal bands and, therefore, caution should be exercised when employing this method in such cases.[15]

Another comparison study for LST calculation was done by **(Yu et al. 2014)** to compare among Radiative Transfer Equation-Based Method, Split Window Algorithm and Single Channel Method. In this research, three different methods were applied to Landsat 8 Thermal Infrared Sensor (TIRS) data, namely the radiative transfer equation (RTE) based method, the split-window (SW) algorithm, and the single-channel (SC) method. For the RTE method, the National Centers for Environmental Prediction (NECP) data was utilized to simulate the required parameters using the MODTRAN model. In the SW algorithm, coefficients were adjusted based on the spectral response functions of TIRS bands 10 and 11. Atmospheric transmittance was derived from the MODTRAN model, employing a standard atmospheric profile. As for the SC method, parameters were obtained through regression analysis using a general spectral function corresponding to simulated atmospheric absorption profiles.[16] Land surface emissivity was estimated using the NDVI threshold method. To validate the results, forty-one imagery scenes were compared with measurements from four SURFRAD

sites that possess high-frequency irradiance data and the MODIS Land Surface Emissivity (LSE) product.

Research progress by (Sobirno et al. 2008) depicts Retrieval From Different VNIR and TIR Sensors show us This study to calculate LST was done by TES algorithm. This study highlights several key advantages TES algorithm. Firstly, it enables the simultaneous retrieval of surface temperature and emissivity. Secondly, it can be applied to various natural surfaces, making it suitable for mineral mapping even with high spatial resolution data. However, there are some notable disadvantages. Firstly, accurate atmospheric correction is essential for obtaining reliable results. Additionally, challenges arise in classifying pixels with low or high spectral contrast, leading to artificial discontinuities in the emissivity products.[17] Furthermore, the TES algorithm is not applicable to most operational sensors, as it necessitates a minimum of four Thermal Infrared (TIR) bands located in atmospheric windows.

The literature survey done here, ensure more versatile and accurate approach is to adapt for the calculation of LST. Most of the studies of SOC mapping focuses to correlate it with NDVI. However, other various indices such as NDBI, NDWI and NDBI are requires to acknowledge to enlighten the SOC mapping from all aspects. LU-LC classification for more particular and in-depth study in SOC mapping, interpolation and prediction can be adapted as a future research scope.

Spatial Resolution is a key element for remote sensing accuracy. However, study shows that SoilGrids 250m is a open data source of 250 m spatial resolution which was earlier at 1 km spatial resolution. This is a good sign for betterment and accuracy of the research work. However, more research should be done on it and comparison of remote sensing database with field data connection should be taken as a long term future research scope to enhance the security and accuracy of existing research work.

CHAPTER 3

MATERIALS & METHODOLOGY

3.1 Study Area

In this study, two Ramsar designated wetlands in India are considered as Study area. These are:

1. East Calcutta Wetland (Ramsar site 1208); also known as EKW (East Kolkata Wetland)
2. Sundarban Wetland (Ramsar site 2370)

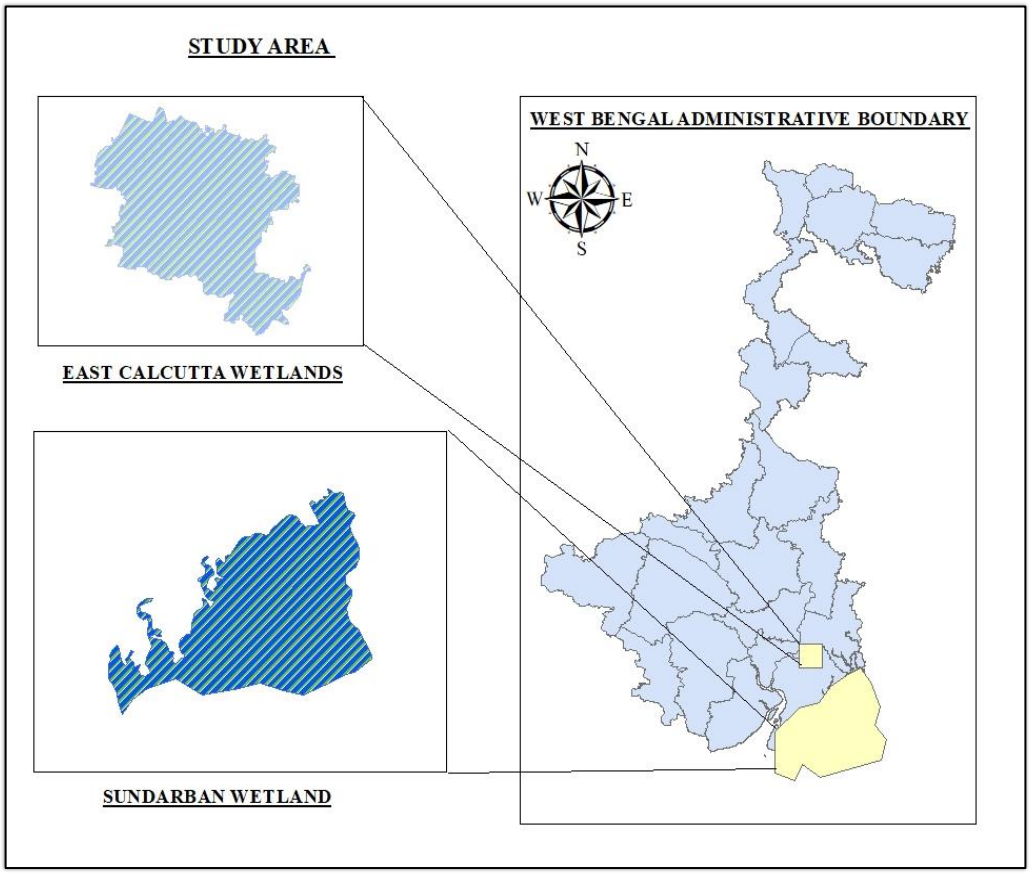

Figure 3.1: Study Area Identity

3.1.1 Ramsar Site 1208

3.1.1.1 Description

Located east of Kolkata in West Bengal, the East Calcutta Wetlands is a remarkable man-made inland wetland recognized worldwide as "an exceptional model of environmental protection and development management." Its primary purpose is to

serve as an urban facility for wastewater treatment, employing an efficient nutrient recovery system that allows the utilization of treated water for pisciculture and agriculture. Spanning around 4,000 hectares, the wetland comprises fish ponds where water flows, facilitating the treatment process.

The East Calcutta Wetlands received its designation as a Ramsar site on August 19, 2002, based on its compliance with criterion 1, which recognizes its unique wetland type. The wetland encompasses intertidal marshes, including salt marshes and salt meadows, alongside significant wastewater treatment areas such as sewage farms, settling ponds, and oxidation basins. Notably, it holds the distinction of being the largest congregation of sewage-fed fish ponds in the world, all concentrated in a single location. The wetland plays a crucial role in sustaining the local economy by providing approximately 150 tons of fresh vegetables daily and supporting the production of around 10,500 tons of table fish per year. These fisheries directly support the livelihoods of over 50,000 people and indirectly benefit many more.

Over the years, the East Calcutta Wetlands has evolved into a natural water-logged area, fostering a diverse range of fauna and flora. It serves as a habitat for various mammal species, including the marsh mongoose, small Indian mongoose, palm civet, and small Indian civet. The wetland is also home to an impressive avian population, with over 40 bird species recorded, including both resident and migratory species. Notable avian inhabitants include grebes, coots, darters, shags, cormorants, teals, egrets, jacanas, snipes, terns, eagles, sandpipers, gulls, rails, and kingfishers.

The East Calcutta Wetlands stands as a testament to the harmonious coexistence of human development and environmental preservation. Its unique combination of wastewater treatment, sustainable aquaculture, and agricultural practices has not only transformed it into a vital ecological hub but also contributed significantly to the local economy and livelihoods of thousands of people.

3.1.1.2 Salient Observations

Table 2.1: Salient Observations at East Calcutta Wetlands

Name	East Calcutta Wetlands
Location	22°28'00" to 22°35'18" N Latitude 88° 22'55" to 88° 30'16" E Longitude
Type Of Wetland	Waterlogged (man-made)
Area of Wetland	12512 ha
Perimeter	83 km
Elevation	2 m
Open-water Post-monsoon: Pre-monsoon:	 362 ha 65 ha

3.1.2 Ramsar Site 2370

3.1.2.1 Description

The Sundarbans, an extensive region comprising numerous islands and an intricate network of rivers, tributaries, and creeks, is situated at the delta region formed by the Ganga and Brahmaputra rivers, where they meet the Bay of Bengal. It stretches across India and Bangladesh and holds more than 60% of India's mangrove forest area. Notably, it has been officially recognized as the 27th Ramsar Site in India, highlighting its significance as a protected wetland. Covering a vast area of 4,23,000 hectares, it stands as the largest protected wetland in the country.

The Ramsar designation for the Indian Sundarbans was granted based on the fulfillment of multiple criteria. It satisfied four out of the nine criteria necessary for the status of a 'Wetland of International Importance.' These criteria include the presence of rare species and vulnerable ecological communities, remarkable biodiversity, substantial fish populations with important spawning and migration areas. Additionally, the Sundarbans holds the esteemed title of a UNESCO World Heritage site and serves as a vital habitat for the majestic Royal Bengal Tiger. It also provides a sanctuary for various rare and globally endangered species, such as the critically endangered northern river terrapin (Batagur baska), the endangered Irrawaddy dolphin (Orcaella brevirostris), and the vulnerable fishing cat (Prionailurus viverrinus). Moreover, the region boasts the existence of two out of the world's four horseshoe crab species and eight out of India's twelve kingfisher species. Remarkably, it supports a total of 2,626 faunal species and hosts 90% of the mangrove varieties found in the country.

However, the Sundarbans face multiple threats arising from human activities. The northern and northwestern periphery of the Indian Sundarbans is densely populated, exerting significant pressure on the ecosystem. The Ramsar Information Sheet identifies fishing and the exploitation of aquatic resources as high-impact threats to the wetland. Other detrimental factors include dredging, oil and gas extraction, logging, wood harvesting, hunting, and the collection of terrestrial animals. While salinity levels pose a moderate actual threat, tourism poses a relatively low actual threat to the region.

Preserving and safeguarding the Sundarbans is of utmost importance to protect this distinctive and ecologically vital habitat, ensuring the survival of its diverse species and upholding the integrity of this invaluable wetland ecosystem

3.1.2.2 Salient Observations

Table 3.2: Salient Observations at Sundarban Wetland

Name	Sundarban Wetland
Location	21° 32’00” to 22° 40’00” N Latitude 88° 05’00” to 89° 00’ E Longitude
Type of Wetland	Coastal Wetland
Wetland Area	423,000 ha
Elevation	0.9 to 2.1 m

3.2 Tools & Techniques

3.2.1 ArcGIS

ArcGIS is a comprehensive geographic information system (GIS) software suite developed by Esri. It provides a powerful platform for capturing, managing, analyzing, and visualizing spatial data. ArcGIS is widely used across various industries, including environmental management, urban planning, transportation, natural resource exploration, and many others.

At the core of ArcGIS lies its ability to integrate and manipulate different types of spatial data, such as maps, satellite imagery, aerial photographs, and geospatial databases. The software enables users to create, edit, and organize geographic information, allowing for efficient data management and exploration.

ArcGIS offers a diverse set of tools and functionalities that enable users to perform complex spatial analysis. These tools allow for the identification of patterns, relationships, and trends within the data, aiding in decision-making processes. With ArcGIS, users can perform spatial queries, conduct proximity analysis, generate heatmaps, perform network analysis, and create models to simulate real-world scenarios.

The software also provides advanced mapping capabilities, allowing users to create visually compelling and informative maps. ArcGIS offers a wide range of cartographic tools for symbolizing and labeling features, adjusting map layouts, and creating interactive map applications. Users can generate maps that effectively communicate spatial information and support data-driven insights.

ArcGIS extends its capabilities through various extensions and add-ons, catering to specific industry needs. These extensions provide specialized tools and workflows for fields such as spatial statistics, 3D visualization, image analysis, geostatistics, and more. This flexibility makes ArcGIS a versatile and adaptable GIS software suite.

Furthermore, ArcGIS provides a collaborative environment through its ArcGIS Online platform. This web-based platform allows users to share maps, data, and applications with others, facilitating data collaboration and decision-making. It also enables the creation of interactive web maps and web applications that can be accessed and utilized by a broad audience.

In conclusion, ArcGIS is a powerful GIS software suite that enables users to effectively manage, analyze, and visualize spatial data. Its comprehensive set of tools and functionalities make it an asset across various industries, supporting data-driven decision-making, spatial analysis, and the creation of informative maps and applications. ArcGIS continues to evolve and innovate, remaining at the forefront of geospatial technology. In this Study, Spatial Analyst tool, Resampling, Clipping and Raster Calculation has been done through ArcGIS 10.8.2

3.2.2 Google Earth Engine

Google Earth Engine is a unique platform that combines an extensive collection of satellite imagery and geospatial datasets with advanced analysis capabilities on a global scale. It serves as a valuable resource for scientists, researchers, and developers who

seek to identify changes, track trends, and quantify differences across the Earth's surface. While commercial use of Earth Engine is now available, it continues to be freely accessible for academic and research purposes. The platform operates on a cloud-based infrastructure, enabling efficient processing of remote sensing data on a large scale. By consolidating trillions of scientific measurements obtained from satellite imagery spanning nearly four decades, Earth Engine provides a comprehensive online repository for scientists, independent researchers, and nations to leverage this vast pool of data in order to detect changes, analyze trends, and assess variations in Earth's features. Numerous applications of Earth Engine exist, including deforestation detection, land cover classification, estimation of forest biomass and carbon, and mapping of areas without roads across the globe. Among the tools available within Earth Engine, the Earth Engine Code Editor stands out as a web-based integrated development environment (IDE) that simplifies the creation of complex geospatial workflows.

3.2.2.1 Sampling at Ramsar Site 1208

```
//IMPORTS
var geometry = /* color: #00ffff */ee.Geometry.Polygon(
        [[[88.42629076327229, 22.581559604094647],
          [88.41393114413167, 22.56539157809551],
          [88.40878130282307, 22.558099494948554],
          [88.40225817049885, 22.55080702625915],
          [88.39710832919026, 22.53970905177128],
          [88.39470506991292, 22.529244430042137],
          [88.39710832919026, 22.52353612034532],
          [88.40157152499104, 22.513704589692118],
          [88.39985491122151, 22.503237998305867],
          [88.39333177889729, 22.486109140182116],
          [88.39024187411214, 22.481033515790187],
          [88.42011095370198, 22.462632817773475],
          [88.4540999063387, 22.445816250109164],
          [88.49770189608479, 22.433440492212625],
          [88.52104784335042, 22.42645880850978],
          [88.54164720858479, 22.43693120236426],
          [88.55812670077229, 22.499748958459957],
          [88.53993059481526, 22.508947146373398],
          [88.5368406900301, 22.534952503840316],
          [88.51521135653401, 22.558416550059558],
          [88.48808885897542, 22.57204923026097],
          [88.47229601229573, 22.583144602582937],
          [88.4654295572176, 22.581559604094647],
          [88.45101000155354, 22.581876605251168],
          [88.43830705965901, 22.58124260220875],
          [88.43178392733479, 22.583144602582937]]]);
```

```
//Random samples
//Create 1000 random sample points in the region.
var randomPoints = ee.FeatureCollection.randomPoints(geometry, 1000);
//Display the points.
Map.addLayer(randomPoints, {}, 'random points');
Map.centerObject(geometry);
//Exporting Tabular Data
//Export the FeatureCollection to a KML File
Export.table.toDrive({
  collection: randomPoints,
  description: 'ExportKML',
  fileFormat: 'KML'
});
//Export the FeatureCollection to a CSV File
Export.table.toDrive({
  collection: randomPoints,
  description: 'ExportCSV',
  fileFormat: 'CSV'
});
//Display the points.
Map.addLayer(randomPoints, {}, 'random points');
Map.centerObject(geometry);
```

3.2.2.2 Sampling at Ramsar Site 2370

```
//IMPORTS:
var table = ee.FeatureCollection("projects/ee-wetland-sohom/assets/Sundarban");
Map.addLayer(table, {},'projects/ee-wetland-sohom/assets/Sundarban');

//Random samples
//Create 19000 random sample points in the region.
var randomPoints = ee.FeatureCollection.randomPoints(table, 19000);

//Display the points.
Map.addLayer(randomPoints, {}, 'random points');
Map.centerObject(table);
```

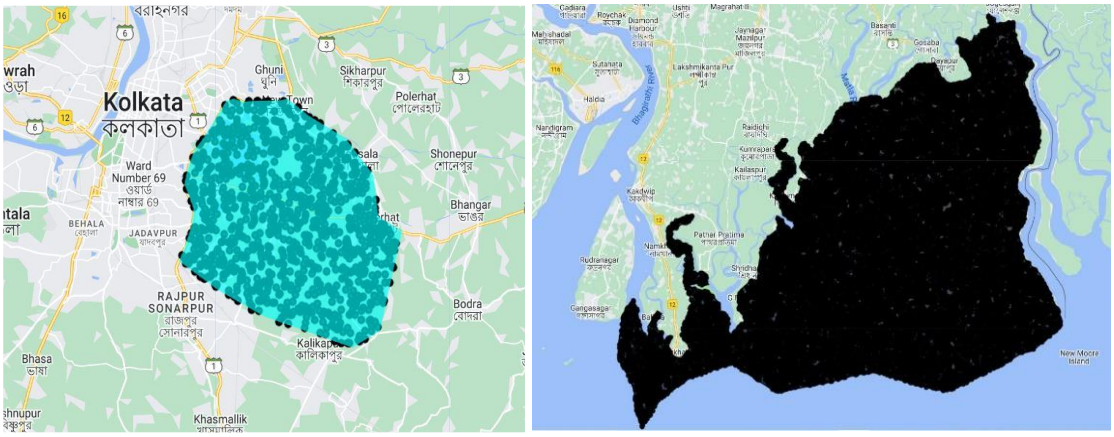

Figure 2.2: Random Sampling Points Generated at Site No. 1208 & 2370

3.3 Methodology for Multiparameter Measurement:

3.3.1 Measurement of Normalized Difference Vegetation Index (NDVI):

$$\boldsymbol{NDVI = \frac{(NIR - Red)}{(NIR + Red)} = \frac{(Band\ 5 - Band\ 4)}{(Band\ 5 + Band\ 4)}} \quad \textbf{...(3.1)}$$

The equation mentioned is a widely used formula for calculating the NDVI. It calculates NDVI based on the spectral reflectance measurements acquired in the red (visible) and near-infrared regions. The spectral reflectances represent the ratio of reflected radiation to incoming radiation for each spectral band, ranging between 0 and 1. As a result, the NDVI itself varies between -1 and +1, following its design and definition.

3.3.2 Measurement of Normalized Difference Built-up Index (NDBI)

NDBI is calculated according to the following raster formula:

$$\boldsymbol{NDBI = \frac{(SWIR - NIR)}{(SWIR + NIR)} = \frac{(Band\ 6 - Band\ 5)}{(Band\ 6 + Band\ 5)}} \quad \textbf{...(3.2)}$$

NDBI range from -1 to +1 where the negative values represent areas with no built-up structures and positive values represent highly built-up areas.

3.3.3 Measurement of Normalized Difference Water Index (NDWI)

Popularly, NDWI can be calculated according to the following raster formula suggested by Gao (1996):

$$\boldsymbol{NDWI = \frac{(NIR - SWIR)}{(NIR + SWIR)} = \frac{(Band\ 5 - Band\ 6)}{(Band\ 5 + Band\ 6)}} \quad \textbf{...(3.3)}$$

There is a modified formula suggested by Xu, H. (2005) as a research outcome.

$$\boldsymbol{MNDWI = \frac{(Green - SWIR)}{(Green + SWIR)} = \frac{(Band\ 3 - Band\ 6)}{(Band\ 3 + Band\ 6)}} \quad \textbf{...(3.4)}$$

The NDWI product is dimensionless and varies between -1 to +1, depending on the leaf water content but also on the vegetation type and cover (Figure 2). High values of NDWI (in blue) correspond to high vegetation water content and to high vegetation fraction cover.

3.3.4 Measurement of Land Surface Temperature (LST)

The End Formula to calculate LST is as follows as used here. However, the full calculation pathway is provided under Framework of LST calculation in the next section:

$$LST = \frac{B\_10\_11}{\left(1+\left(\frac{\lambda * B\_10\_11}{p}\right) * ln(LSE_{Mean})\right)} = \frac{B\_10\_11}{\left(1+\left(\frac{10.895 * B\_10\_11}{1438}\right) * ln(LSE_{Mean})\right)} \quad \ldots(3.5)$$

3.3.5 Measurement of Soil Moisture Index (SMI)

SMI is calculated according to the following raster formula:

$$SMI = \frac{(LST_{Max} - LST)}{(LST_{Max} - LST_{Min})} \quad \ldots(3.6)$$

3.4 Framework Methodology

3.4.1 Land Surface Emissivity Calculation

In quantitative terms, emissivity is defined as the ratio between the thermal radiation emitted by a surface and the radiation from an ideal black surface at the same temperature, as stated by the Stefan-Boltzmann law. LST from Top of Atmosphere (TOA) brightness temperature, it is crucial to consider the emissivity of land surfaces. The term Land Surface Emissivity (LSE) specifically refers to the emissivity of land surfaces, which can vary depending on the composition of materials present, including soils, vegetation, and water. One approach to obtain LSE is by utilizing the NDVI, which indicates the level of greenness in land surfaces and provides insights into the types of materials presents. Consequently, different NDVI values correspond to different land surface materials. For instance, an NDVI value below 0.2 signifies bare soil, and in this scenario, emissivity can be calculated using reflectivity values in the red region of the image. On the other hand, an NDVI value above 0.5 indicates a land surface consisting entirely of vegetation. In such cases, a constant emissivity value, typically 0.99, can be applied. However, when the NDVI falls between 0.2 and 0.5, the LSE for a given band can be related to the NDVI and the proportion of vegetation (Pv) can be calculated using the [Equation 3.7]:

$$P_v = \begin{cases} a_i \rho_{red} + b_i & NDVI < 0.2 \\ \epsilon_{v,i} + \epsilon_{s,i}(1 - P_v) + C_i & 0.2 \leq NDVI \leq 0.5 \\ \epsilon_{v,i} + C_i & NDVI > 0.5 \end{cases} \quad \text{...(3.7)}$$

In the provided equation, where $\epsilon_{v,i}$ represents the emissivity of fully vegetated surfaces and $\epsilon_{s,i}$ denotes the emissivity of barren soil in the band i. The proportion of vegetation, P_v, is calculated using the equation mentioned earlier. The coefficients a_i and b_i can be estimated from laboratory spectra of soils through statistical fits, assuming a linear relationship between emissivity and reflectivity in the red band. The symbol Ci in the equation represents the roughness of land surfaces. In the case of plain and homogeneous land surfaces, the roughness factor C_{i} can be disregarded by setting C_{i}= 0. However, for rough and heterogeneous surfaces like soil-vegetation mixed pixels, C_{i} accounts for the increment in emissivity resulting from the cavity effect and multiple scattering in these mixed pixels.

By incorporating the emissivity values for soil and vegetation and considering the range of NDVI values typically found in earth surfaces (around 0.2 to 0.5), the calculation of land surface emissivity (LSE) can be performed using the NDVI-threshold method, as indicated in the [Equation 3.8]:

$$LSE = \epsilon_v P_v + \epsilon_s (1 - P_v) + C \quad \text{...(3.8)}$$

The variable "C" mentioned in the equation above is equivalent to "d_ϵ" as described in the literature.

In accordance with the equation, the computation of Land Surface Emissivity (LSE) for Landsat 8 thermal bands requires the estimation of ϵ_s and ϵ_v values for both Thermal Infrared (TIR) bands. Yu et al. derived these values by utilizing the MODIS UCSB (University of California, Santa Barbara, CA, USA) emissivity library, accessible at the following link: https://icess.eri.ucsb.edu/modis/EMIS/html/em.html. The estimated ϵ_s and ϵ_v values are provided in the [Table 3.3].

Table 3.3: Emissivity values of soil and vegetation for TIR band 10 and band 11

TIR Band	Emissivity values	
	Vegetation (ϵ_v)	Soil (ϵ_s)
Band 10	0.9863	0.9668
Band 11	0.9896	0.9747

In Equation, an approximate estimation of C is given by:

$$\boldsymbol{C = (1 - \epsilon_s)(1 - P_v)F\epsilon_v} \quad \textbf{...(3.9)}$$

In this equation, the variable "F" represents a shape factor. In their study, Sobrino et al. examined this shape factor (F) across various geometrical distributions, with an average value of 0.55.

Considering Equations (3.8) and (3.9), the Land Surface Emissivity (LSE) can be computed using the following formula:[17]

$$\boldsymbol{LSE = mP_v + n} \quad \textbf{...(3.10)}$$

$$\boldsymbol{m = \epsilon_v - \epsilon_s - (1 - \epsilon_s)F\epsilon_v} \quad \textbf{...(3.11)}$$

$$\boldsymbol{n = \epsilon_s + (1 - \epsilon_s)F\epsilon_v} \quad \textbf{...(3.12)}$$

Using the provided emissivity values and the mathematical expression in Equation, we can compute the Land Surface Emissivity (LSE) for both thermal infrared (TIR) bands of Landsat 8 data. To begin, we need to determine the m and n values for the respective bands. For TIR band 10, the calculation is as follows:

$$m_{TIR\,10} = 0.9863 - 0.9668 - (1 - 0.9668) \times 0.55 \times 0.9863 \approx 0.0015$$

$$n_{TIR\,10} = 0.9668 - (1 - 0.9668) \times 0.55 \times 0.9863 \approx 0.9848$$

Thus, following the Equation (3.10), LSE for TIR band 10 can be estimated as below:

$$\boldsymbol{LSE_{TIR\,10} = 0.0015P_v + 0.9848} \quad \textbf{...(3.13)}$$

In the same way, for TIR band 11,

$$m_{TIR\,11} = 0.9896 - 0.9747 - (1 - 0.9747) \times 0.55 \times 0.9896 \approx 0.0011$$

$$n_{TIR\,11} = 0.9747 - (1 - 0.9747) \times 0.55 \times 0.9896 \approx 0.9885$$

$$LSE_{TIR\,10} = 0.0011P_v + 0.9885 \quad \text{...(3.14)}$$

3.4.2 Framework of LST calculation for this Study

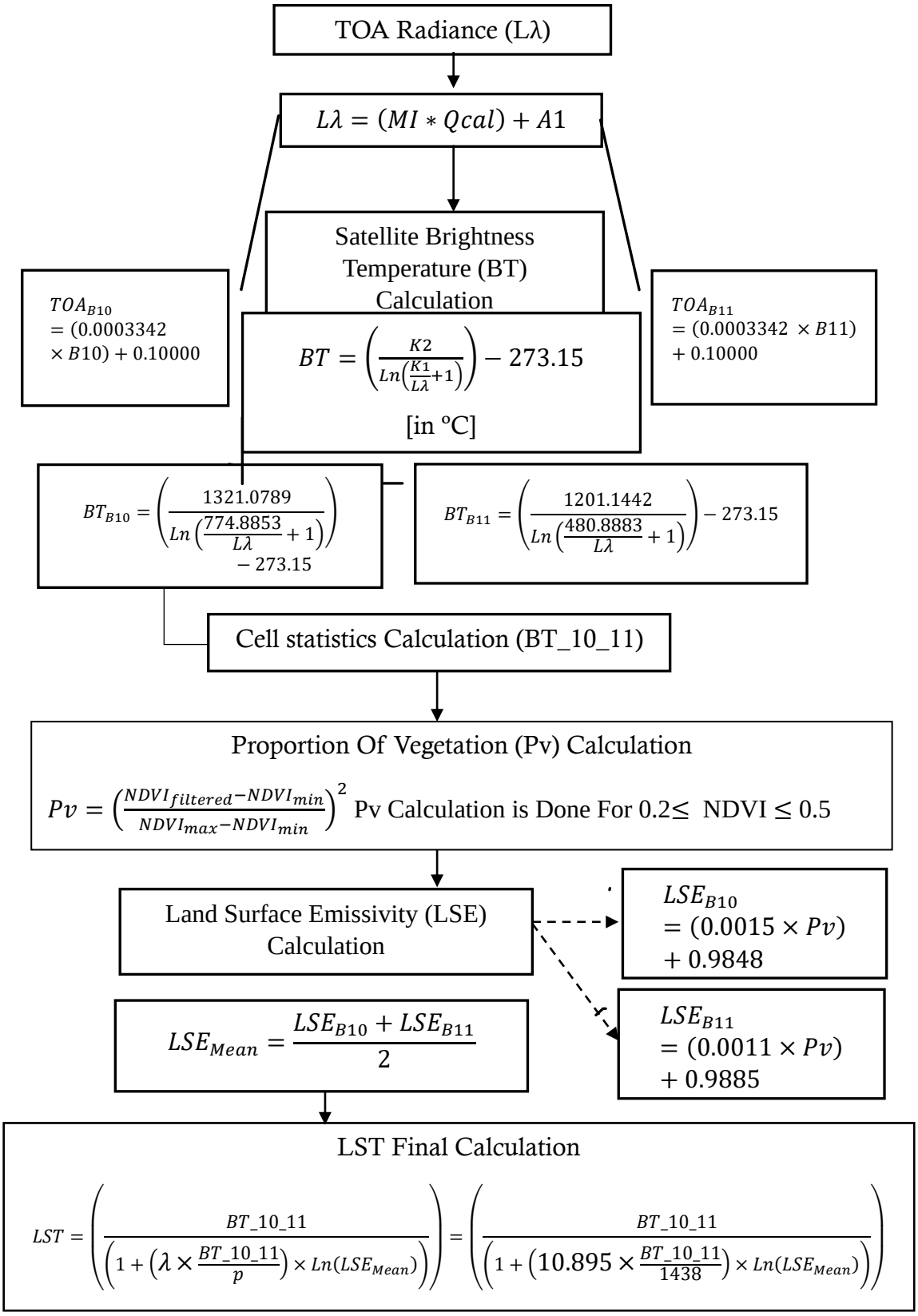

Figure 3.3: Framework of LST Calculation

3.4.3 Framework of Ordinary Kriging

The predicted model can be expressed as follows:

$$\boldsymbol{Z^*(x_0) = \sum_{i=0}^{n} \lambda_i * Z(x_i)} \quad \textbf{...(3.15)}$$

where Z (x_0) represents the estimated SOC value of variable Z at location x_0, $Z^*(x_i)$ is the measured SOC data, $\boldsymbol{\lambda_i}$ represents the weights combined with the measured values, and n is the number of measured values within a neighborhood of four or eight. In this study, the OK model was created using a spherical variogram model in ArcGIS 10.8.2. The equation for the spherical model is defined as follows:

$$= \begin{cases} 0 & h = 0 \\ C_0 + \left(\frac{3h}{2a} - \frac{h^3}{2a^3}\right) & 0 < h < a \\ C_0 + C & h > a \end{cases} \quad \textbf{...(3.16)}$$

where h is the spatial lag between two locations, a is the range, C_0 is the nugget value, and $C_0 + C$ is the partial sill.

3.5 Data Collection

3.5.1 Landsat-8 Data Collection

Table 3.4: Landsat-8 Data Collection Details

SL No.	Date of Image Capture	Details of Path/Row	Cloud Information (Percentage)	Scenario ID No.
1	06/01/2022	138/45	0.08	LC81380452022006LGN00
2	07/02/2022	138/45	0.00	LC81380452022038LGN00
3	19/03/2022	138/45	0.01	LC91380452022078LGN00
4	07/04/2023	138/45	1.15	LC91380452023097LGN00
5	06/05/2022	138/45	13.93	LC91380452022126LGN00
6	09/06/2020	138/45	45.48	LC81380452020161LGN00
7	27/07/2020	138/45	21.37	LC81380452020209LGN00
8	31/08/2021	138/45	32.84	LC81380452021243LGN00
9	27/09/2022	138/45	23.68	LC91380452022270LGN01
10	21/10/2022	138/45	0.01	LC81380452022294LGN00
11	114/11/2022	138/45	0.01	LC91380452022318LGN01
12	16/12/2022	138/45	0.04	LC91380452022350LGN02

3.5.2 Data Collection from SoilGrids-250

SOC Stock data has collected from SoilGrids 250 open data source. The collected SOC stock (Mean) raster is as below for the two study areas:

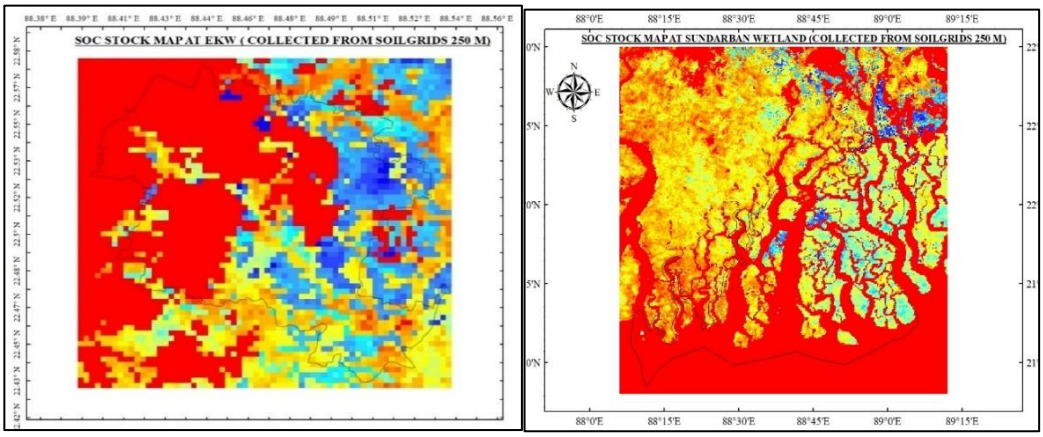

(a) **(b)**

Figure 3.4: (a & b): SOC Stock (t/ha) Mean Data Collected from SoilGrids 250 m

3.6 Calculation of Statistical Metrices

3.6.1 Formula for Pearson's correlation coefficient

$$r = \frac{\sum_{i=1}^{n}(x_i-\bar{x})(y_i-\bar{y})}{\sqrt{\sum_{i=1}^{n}(x_i-\bar{x})^2(y_i-\bar{y})^2}} \quad \text{...(3.17)}$$

r = correlation coefficient x_i= values of the x variable in a sample

$\bar{x}$ = mean of the values of the x variable y_i= values of the y variable in a sample

$\bar{y}$ = mean of the values of the y variable

3.6.2 Formula for Root Mean Square Error (RMSE) & R^2

$$RMSE = \sqrt{\frac{1}{n}\sum_{i=1}^{n}(M_i - P_i)^2} \quad \text{...(3.18)}$$

$$R^2 = \frac{\sum_{i=1}^{n}(P_i-\overline{M_i})^2}{\sum_{i=1}^{n}(M_i-\overline{M_i})^2} \quad \text{...(3.19)}$$

M_i = Measured (Here, Extracted) SOC value at site i, P_i = Predicted (Here, Interpolated) SOC value at site i, $\overline{M_i}$ = The average value of measured SOC, n = The total no. of modelling data.

CHAPTER 4

RESULTS & DISCUSSION

4.1 Interpolation Result for Soil Organic Carbon

4.1.1 At Ramsar Site 1208

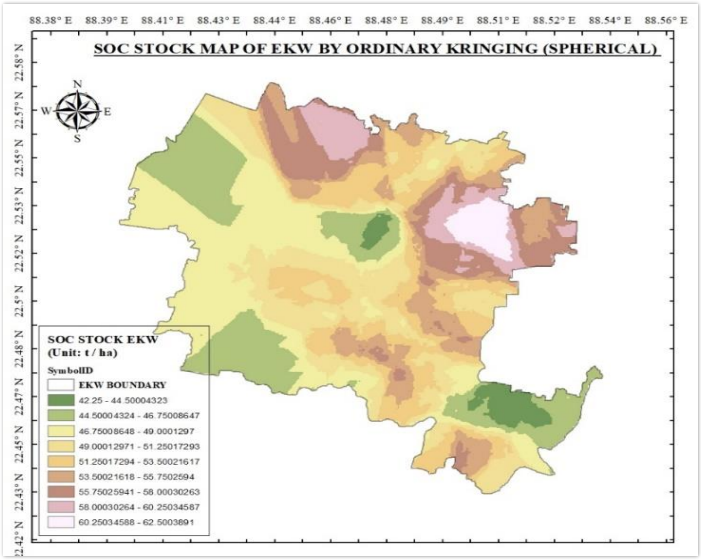

Figure 4.1: Interpolated (OK Method) SOC Stock Map at East Calcutta Wetlands

4.1.2 Resampling & Interpolation at Ramsar Site 2370

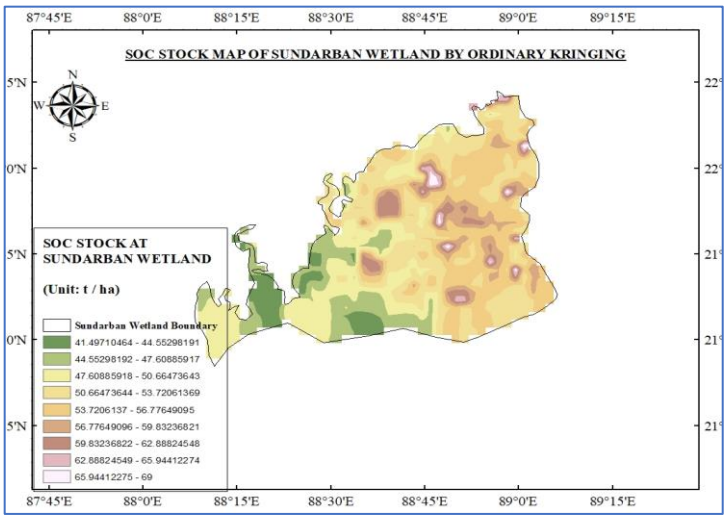

Figure 4.2: Interpolated (OK Method) SOC stock map of Sundarban Wetland

Table 4.1: Band Statistics of Interpolated SOC Stock Map at EKW

CELL SIZE (X, Y)	Band Statistics			
	Max	Min	Mean	Std Dev
0.00057, 0.00057	62.50038	42.25	50.92787	4.34799

Table 4.2: Resampling & Band Statistics of Interpolated SOC Stock Map at Sundarban Wetland

CELL SIZE (X, Y) (Before Resampling)	CELL SIZE (X, Y) (After Resampling)	Band Statistics			
		Max (t/ha)	Min (t/ha)	Mean (t/ha)	Std Dev
0.00057, 0.00057	0.02258, 0.02258	69	41.49710	52.18245	4.97682

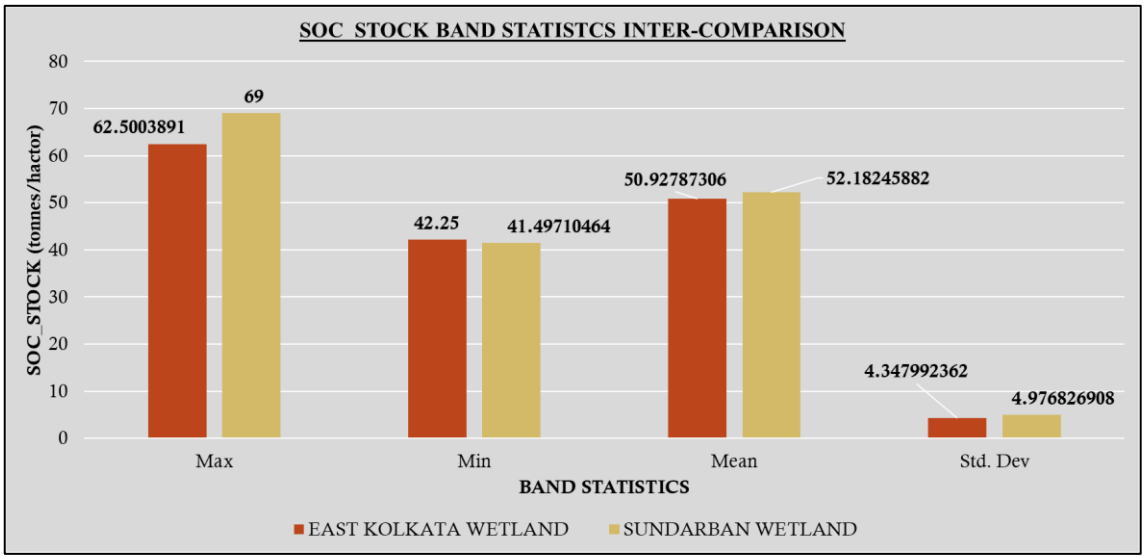

Figure 4.3: Inter-Comparison of SOC Stock Band Statistics

[See Table 4.1 & Table 4.2]

4.2 Result of Regression Analysis

4.2.1 At Ramsar Site 1208

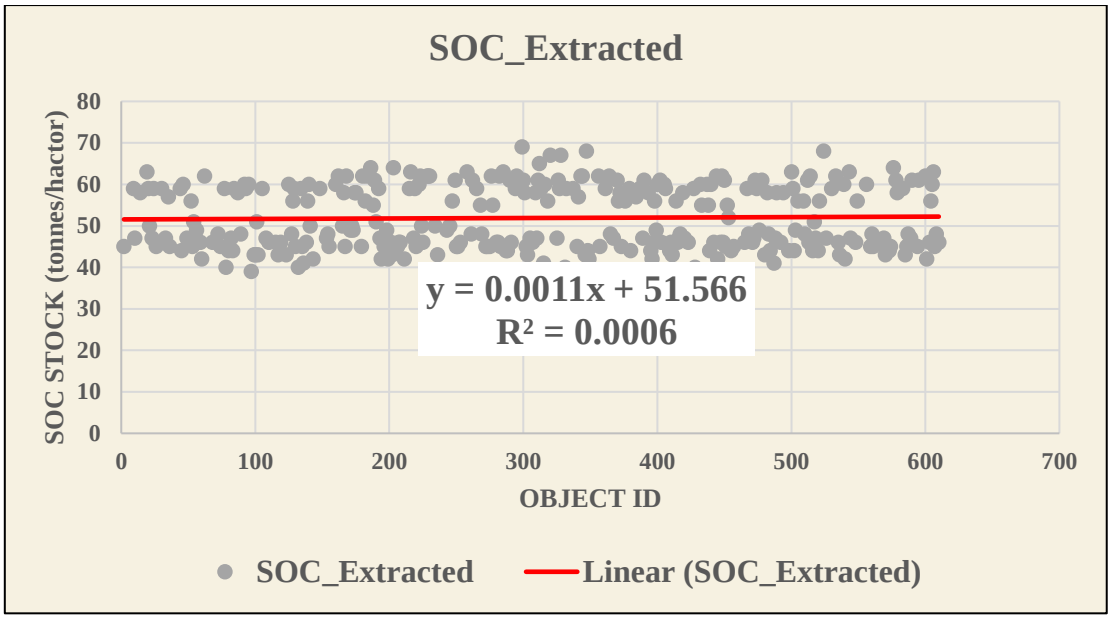

Figure 4.4: Linear Regression Curve Fitting for SOC Stock Data at EKW Extracted from SoilGrids-250

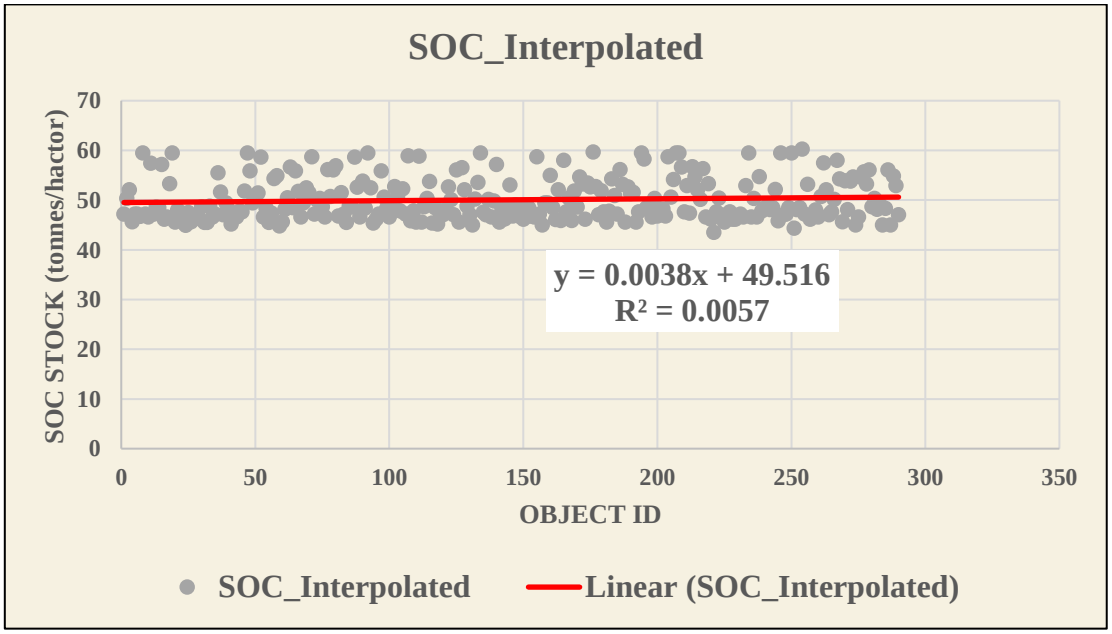

Figure 4.5: Linear Regression Curve Fitting for Interpolated SOC Stock Data at EKW

4.2.2 At Ramsar Site 2370

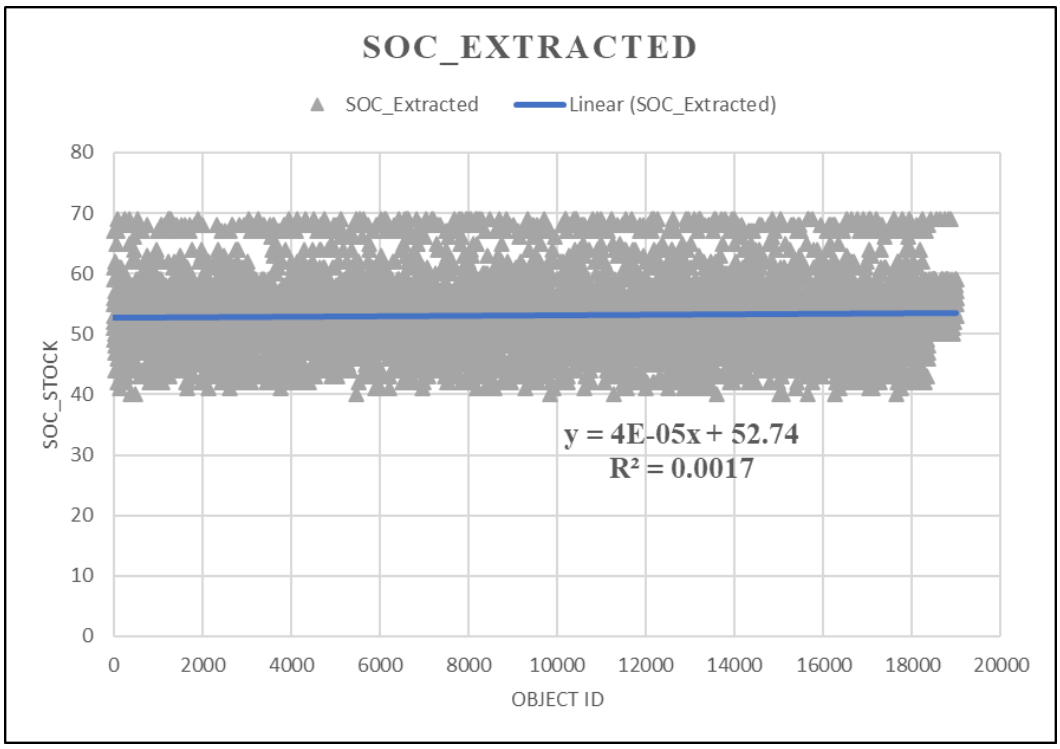

Figure 4.6: Linear Regression Curve Fitting for SOC Stock Data at Sundarban Wetland Extracted from SoilGrids-250

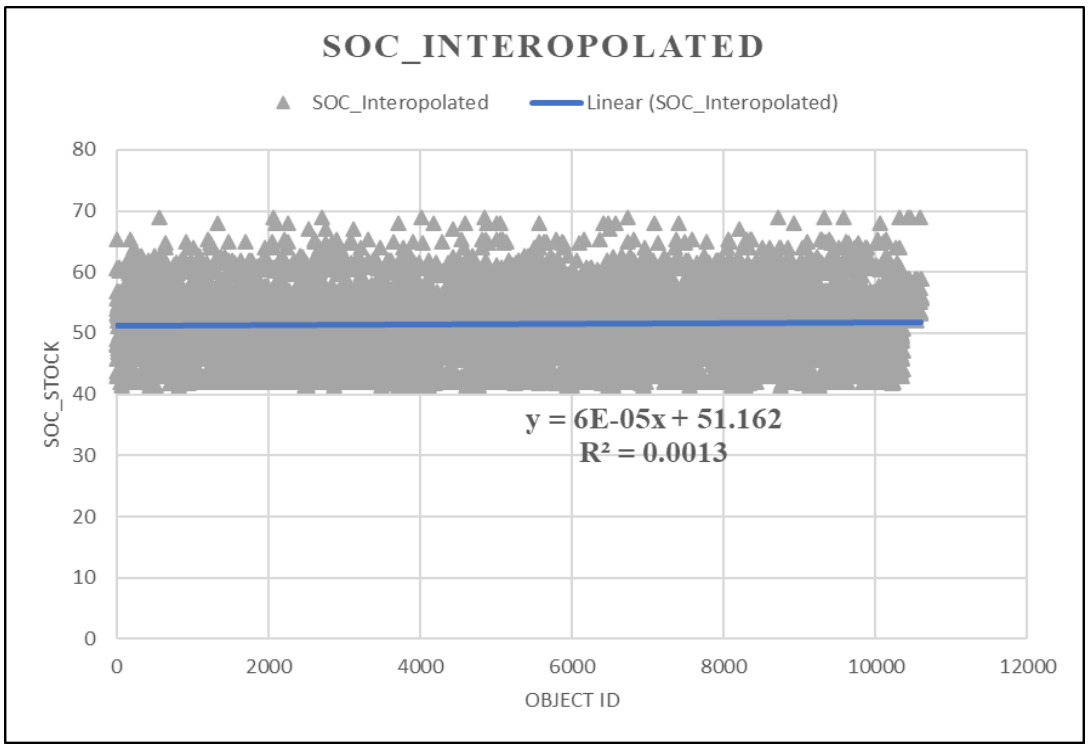

Figure 4.7: Linear Regression Curve Fitting for Interpolated SOC Stock Data at Sundarban Wetland

Table 4.3: Linear Regression Parameters Output

REGRESSION PARAMETERS	EKW_EXTRACTE	EKW_INTERPOLATED	SUNDARBAN_EXTRACTED	SUNDARBAN_INTERPOLATED
Slope	0.001095	0.003766	4E-05	5.753E-05
SE(Slope)	0.002471	0.002926	1.06E-05	1.557E-05
R^2	0.000617	0.00572	0.001686	0.0013351
F	0.19632	1.656855	14.18057	13.648509
ss reg	11.15639	28.82483	410.5852	315.56254
Intercept	51.56578	49.51582	52.73953	51.161754
SE(Intercept)	0.88258	0.49113	0.118421	0.0950459
SE(y)	7.538416	4.171009	5.380899	4.8083947
df	318	288	8397	10209
ss resid	18071.22	5010.427	243127.4	236038.82

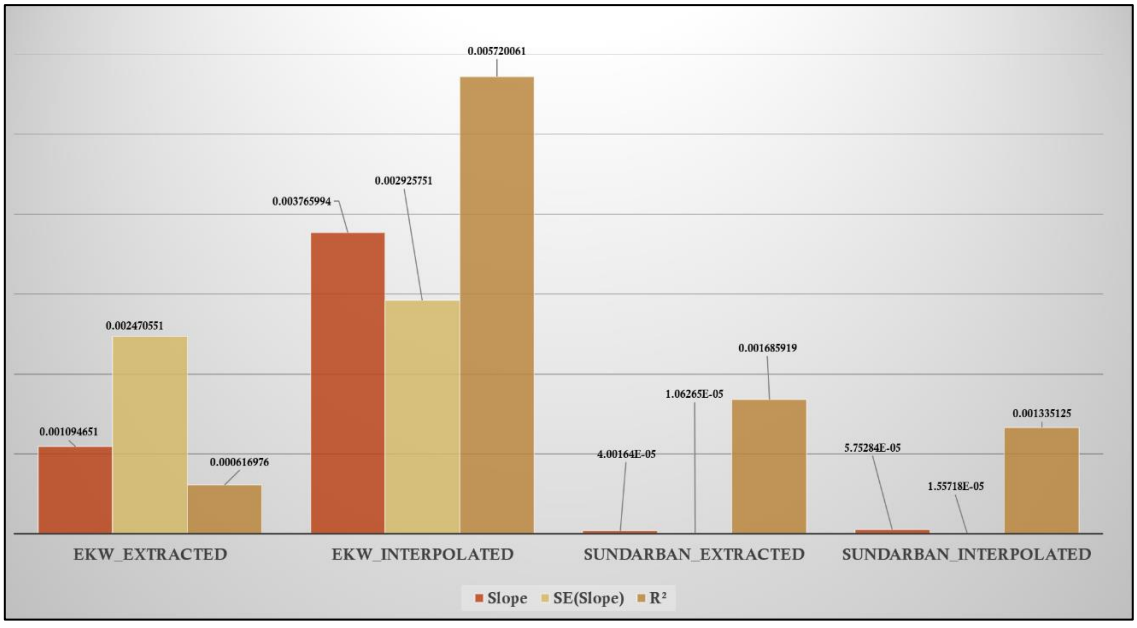

Figure 4.8: Linear Regression Outputs

4.3 Temporal Variation Results of NDVI

4.3.1 At Ramsar Site 1208

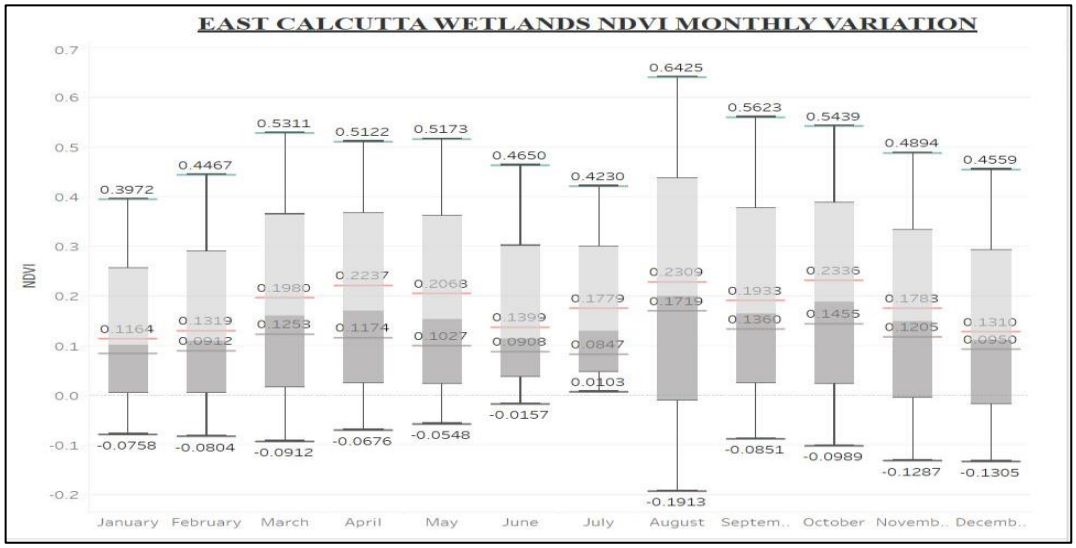

Figure 4.9: Temporal Variation of NDVI at Ramsar Site 1208

Table 4.4: Datasheet of NDVI Temporal Variation at Ramsar Site 1208

MONTHS	NDVI_Max	NDVI_Min	NDVI_Mean	NDVI_Std. Dev
January	0.397244781	-0.0758056	0.116440935	0.087325174
February	0.446687967	-0.08036109	0.131908248	0.091153838
March	0.531121433	-0.09117498	0.198024954	0.12534119
April	0.512178123	-0.06761719	0.22367931	0.117438534
May	0.517307103	-0.05478989	0.206843302	0.102650885
June	0.464955211	-0.0157484	0.139932686	0.090770185
July	0.423001945	0.01027084	0.177902393	0.084671393
August	0.642488956	-0.19129439	0.230869741	0.171901166
September	0.562286615	-0.08512764	0.193312146	0.136031542
October	0.543851197	-0.09886503	0.233585381	0.14547491
November	0.48940891	-0.1287002	0.178264461	0.120545324
December	0.455922157	-0.13046362	0.13104712	0.094993329

4.3.2 At Ramsar Site 2370

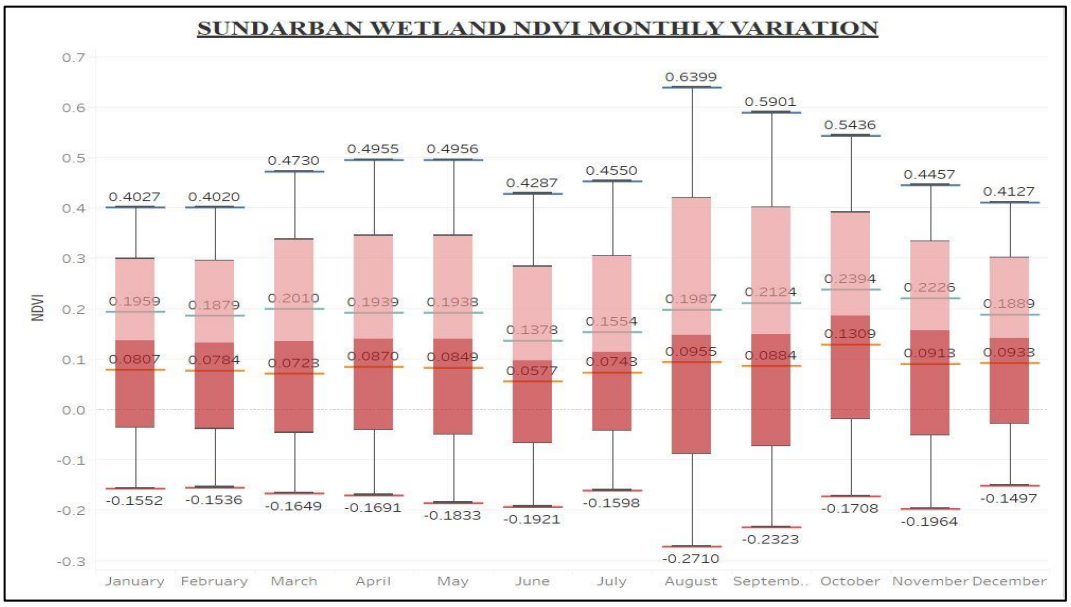

Figure 4.10: Temporal Variation of NDVI at Ramsar Site 2370

Table 4.5: Datasheet of NDVI Temporal Variation at Ramsar Site 2370

MONTHS	NDVI_Max	NDVI_Min	NDVI_Mean	NDVI_Std. Dev
January	0.402650535	-0.15518914	0.080741103	0.195919467
February	0.402016759	-0.15364763	0.078355574	0.187945599
March	0.473025262	-0.16489205	0.07232953	0.201001776
April	0.495476514	-0.16910741	0.086997665	0.193916895
May	0.495603323	-0.18332143	0.08486201	0.193803209
June	0.428662866	-0.1920556	0.057737242	0.137761653
July	0.455007941	-0.1597691	0.074286978	0.15542037
August	0.639933169	-0.27101067	0.095474982	0.198666546
September	0.590074718	-0.23227474	0.088388233	0.212394477
October	0.54363513	-0.17084812	0.130948787	0.239383579
November	0.445745498	-0.19635805	0.09129031	0.222643856
December	0.412745088	-0.14967172	0.093261763	0.188904692

4.4 Temporal Variation Results of NDBI

4.4.1 At Ramsar Site 1208

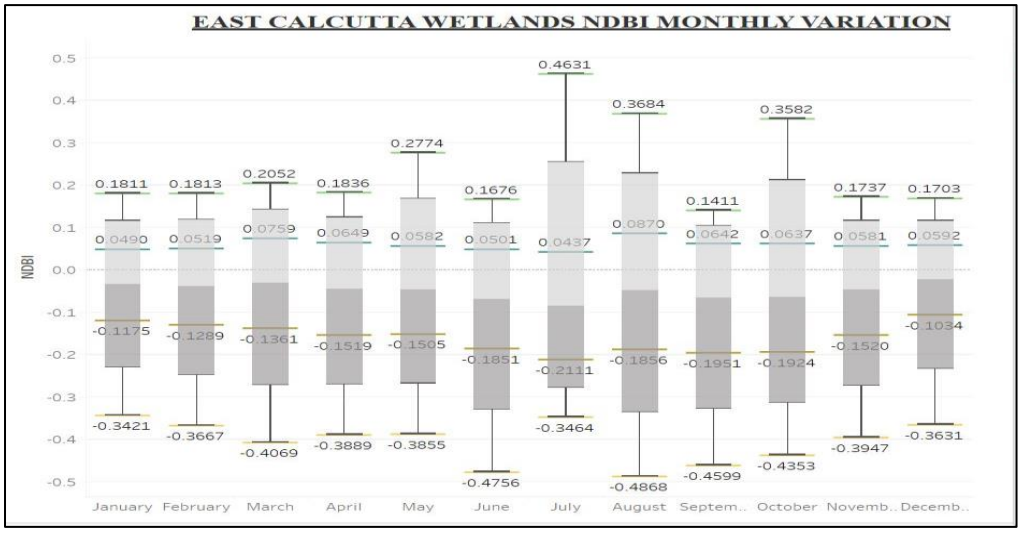

Figure 4.11: Temporal Variation of NDBI at Ramsar Site 1208

Table 4.6: Datasheet of NDBI Temporal Variation at Ramsar Site 1208

MONTHS	NDBI_Max	NDBI_Min	NDBI_Mean	NDBI_Std. Dev
January	0.181069702	-0.34214476	-0.117452741	0.048982574
February	0.181257859	-0.36665621	-0.128912413	0.051913248
March	0.205212787	-0.40690866	-0.136106994	0.075907805
April	0.183639959	-0.38886121	-0.15185873	0.06488309
May	0.277434886	-0.3854844	-0.150456427	0.058243549
June	0.167609483	-0.47561723	-0.185055817	0.050074372
July	0.463145077	-0.34638047	-0.211134219	0.043698741
August	0.368381619	-0.48675513	-0.185591434	0.087020838
September	0.141091615	-0.45992631	-0.195124333	0.064232748
October	0.358150959	-0.43528929	-0.192431299	0.063744753
November	0.173717886	-0.39474577	-0.151958893	0.058083738
December	0.170328617	-0.36313018	-0.103374522	0.059168268

4.4.2 At Ramsar Site 2370

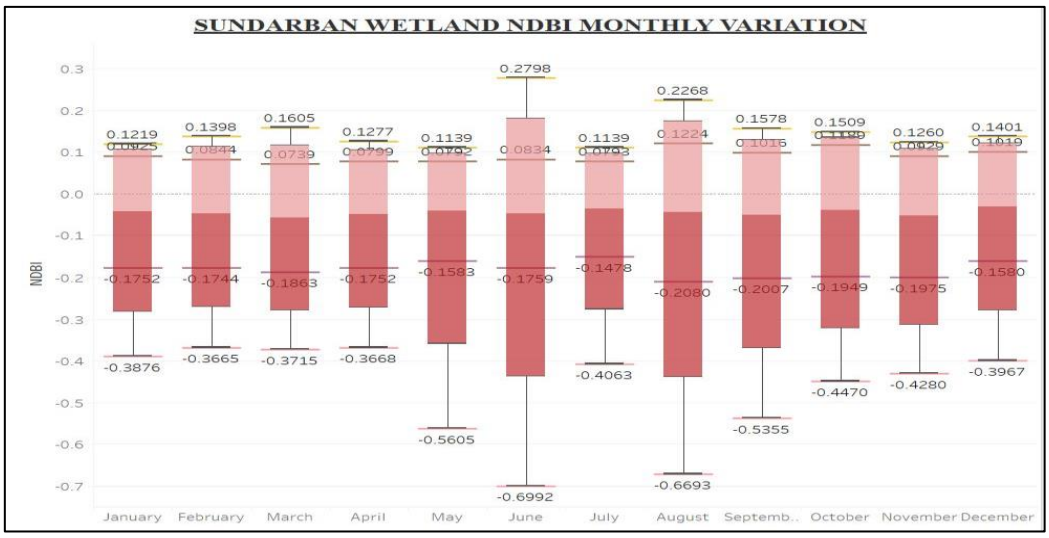

Figure 4.12: Temporal Variation of NDBI at Ramsar Site 2370

Table 4.7: Datasheet of NDBI Temporal Variation at Ramsar Site 2370

MONTHS	NDBI_Max	NDBI_Min	NDBI_Mean	NDBI_Std. Dev
January	0.121940911	-0.38757136	-0.175231281	0.092488983
February	0.139813349	-0.36646527	-0.174364747	0.084373584
March	0.160515532	-0.37148127	-0.186252323	0.073890795
April	0.127747089	-0.36683235	-0.17518502	0.079886819
May	0.113878623	-0.56052476	-0.158254364	0.079187114
June	0.279830962	-0.69921857	-0.175945932	0.083393028
July	0.113882549	-0.40630254	-0.147821974	0.079296278
August	0.22679393	-0.66932958	-0.208042172	0.122408101
September	0.157821044	-0.53549016	-0.200734604	0.101619403
October	0.150931761	-0.44701096	-0.194915625	0.118888684
November	0.125989795	-0.42802256	-0.197491958	0.092898714
December	0.140128449	-0.39674923	-0.15800744	0.101931654

4.5 Temporal Variation Results of NDWI

4.5.1 At Ramsar Site 1208

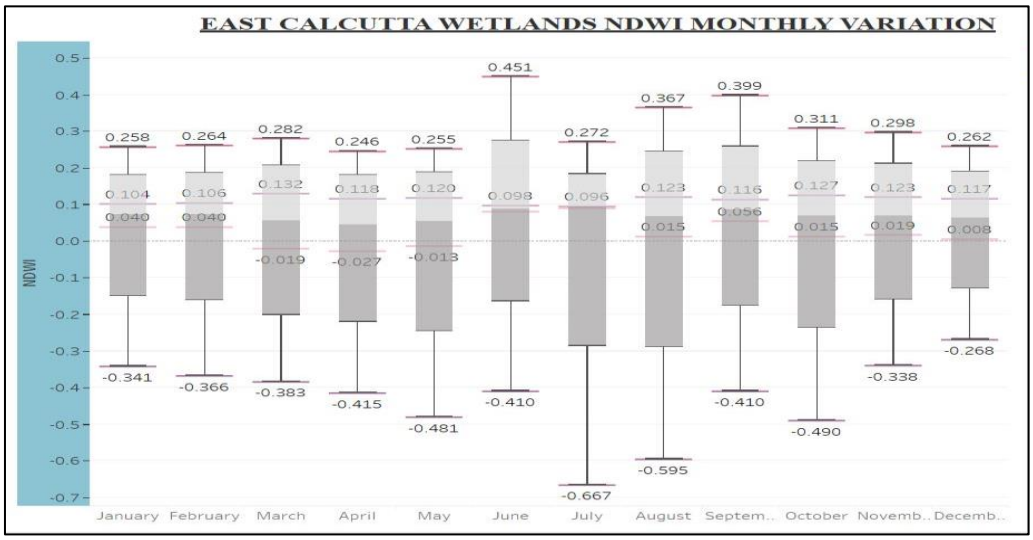

Figure 4.13: Temporal Variation of NDWI at Ramsar Site 1208

Table 4.8: Datasheet of NDWI Temporal Variation at Ramsar Site 1208

MONTHS	NDWI_Max	NDWI_Min	NDWI_Mean	NDWI_Std. Dev
January	0.258248776	-0.3409906	0.04009003	0.104082395
February	0.263539732	-0.36603287	0.039635176	0.106253075
March	0.281522602	-0.3833957	-0.019296234	0.13156409
April	0.246016681	-0.41457707	-0.026560515	0.117649493
May	0.254910111	-0.48056608	-0.012775029	0.120115591
June	0.451321542	-0.41008982	0.081402928	0.097802214
July	0.271540225	-0.66656071	0.090839007	0.096481479
August	0.367075354	-0.59457862	0.014909728	0.122609857
September	0.399166971	-0.4100315	0.055837848	0.115682128
October	0.310924381	-0.49005291	0.014568779	0.127343949
November	0.298408061	-0.33820102	0.019103439	0.122653758
December	0.261943072	-0.26820871	0.007605623	0.117263901

4.5.2 At Ramsar Site 2370

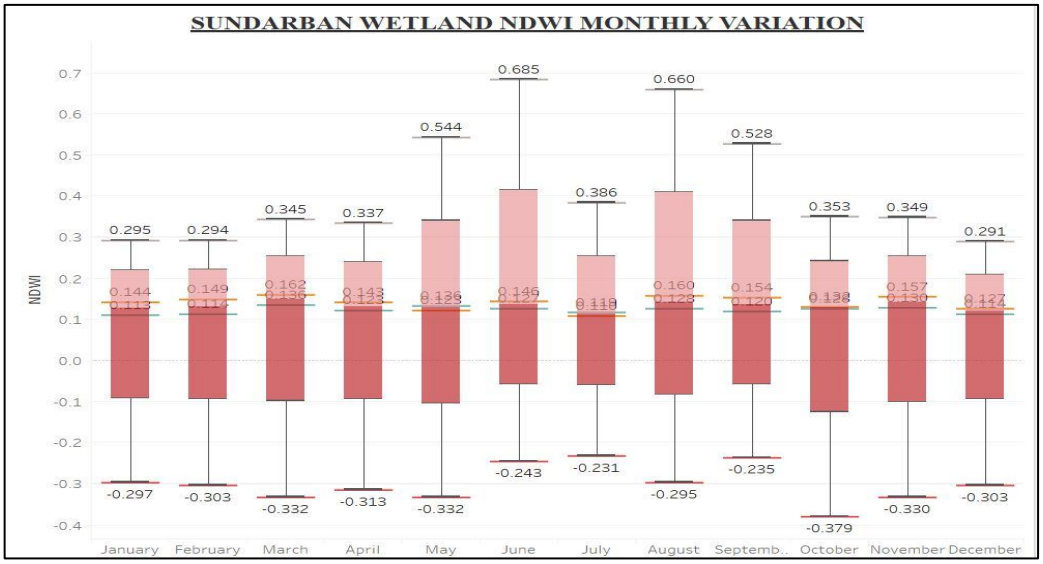

Figure 4.14: Temporal Variation of NDWI at Ramsar Site 2370

Table 4.9: Datasheet of NDWI Temporal Variation at Ramsar Site 2370

MONTHS	NDWI_Max	NDWI_Min	NDWI_Mean	NDWI_Std. Dev
January	0.294578552	-0.29656717	0.144137735	0.11287786
February	0.294124991	-0.30333233	0.149305653	0.114188318
March	0.345011979	-0.33200058	0.162221212	0.135999907
April	0.336712599	-0.3134726	0.142654067	0.12341841
May	0.544091225	-0.33153611	0.122539928	0.135597669
June	0.685478389	-0.24327727	0.145678892	0.127346458
July	0.386227936	-0.23143157	0.109767073	0.119345974
August	0.659827173	-0.29457363	0.160184481	0.127593592
September	0.528426766	-0.23463708	0.154197083	0.120367104
October	0.352544308	-0.37943476	0.131765305	0.128116413
November	0.349008441	-0.33042073	0.156658249	0.130465678
December	0.291388988	-0.3032344	0.126868741	0.113630098

4.6 Temporal Variation Results of LST

4.6.1 At Ramsar Site 1208

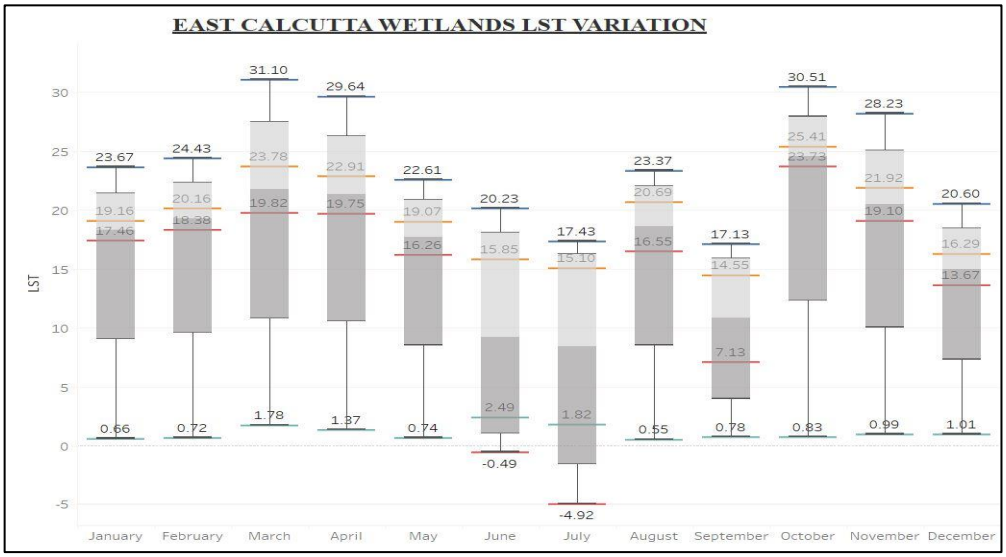

Figure 4.15: Temporal Variation of LST at Ramsar Site 1208

Table 4.10: Datasheet of LST Temporal Variation at Ramsar Site 1208

MONTHS	LST_Max	LST_Min	LST_Mean	LST_Std. Dev
January	23.66839218	17.4587498	19.16462053	0.663125599
February	24.43097305	18.3827076	20.16170856	0.716267041
March	31.10351372	19.8161354	23.77726492	1.782116246
April	29.63694382	19.7540207	22.91120611	1.367075348
May	22.6145916	16.2570515	19.07141573	0.744787591
June	20.22824097	-0.4941768	15.8458965	2.492941896
July	17.42556381	-4.9212250	15.09981016	1.82029203
August	23.36969566	16.5483589	20.68999697	0.551612008
September	17.12936783	7.13450956	14.5466955	0.784393144
October	30.5097084	23.7293854	25.40732741	0.832072701
November	28.22816467	19.1037655	21.92052498	0.986893333
December	20.60356522	13.6722498	16.29232374	1.009957533

4.6.2 At Ramsar Site 2370

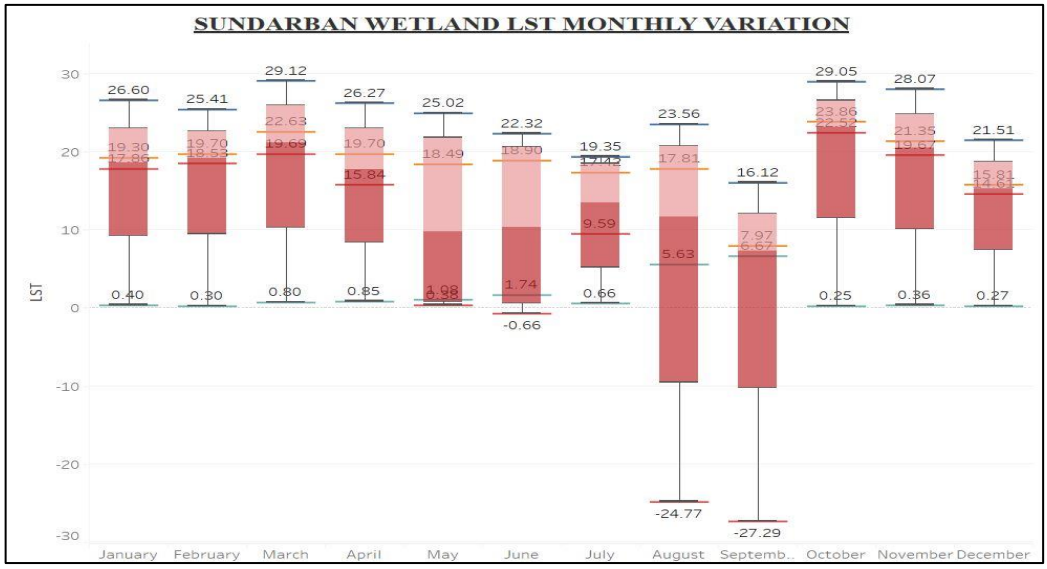

Figure 4.16: Temporal Variation of LST at Ramsar Site 2370

Table 4.11: Datasheet of LST Temporal Variation at Ramsar Site 2370

MONTHS	LST_Max	LST_Min	LST_Mean	LST_Std. Dev
January	26.60201645	17.8632278	19.29720054	0.4034337
February	25.40582466	18.5329018	19.70010982	0.299408935
March	29.11580276	19.6916866	22.63101264	0.799081076
April	26.27116394	15.8414907	19.69725869	0.852442963
May	25.01716614	0.37797475	18.48879879	1.075360901
June	22.31991005	-0.6599898	18.90397117	1.736642868
July	19.34545708	9.59361649	17.42291114	0.661245796
August	23.56080818	-24.771167	17.8097356	5.625965147
September	16.12379646	-27.288858	7.973501773	6.668869233
October	29.04547501	22.5156651	23.86341962	0.254975665
November	28.07186699	19.669529	21.35259561	0.363582407
December	21.50751686	14.6139755	15.81258383	0.273864291

4.7 Temporal Variation Results of SMI

4.7.1 At Ramsar Site 1208

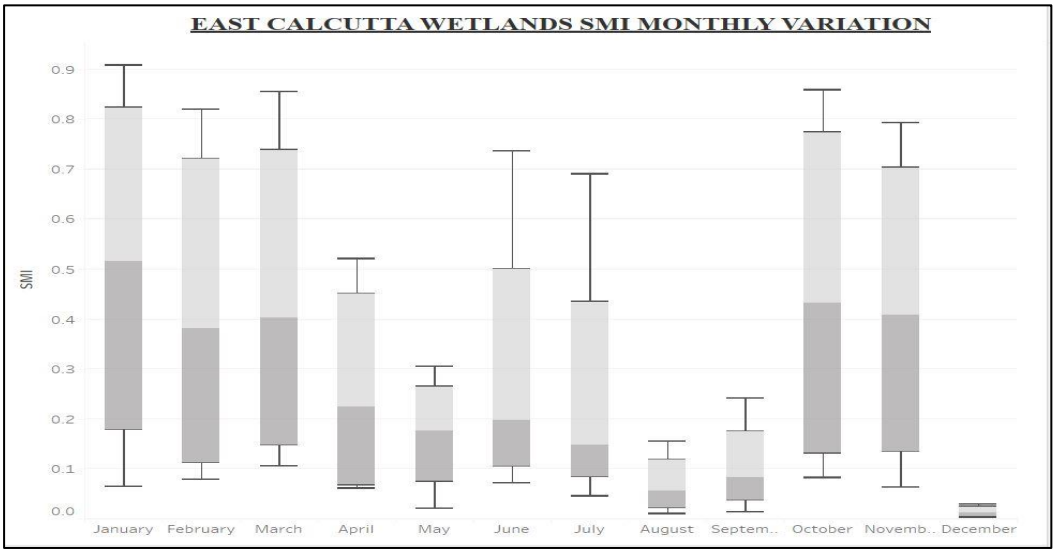

Figure 4.17: Temporal Variation of SMI at Ramsar Site 1208

Table 4.12: Datasheet of SMI Temporal Variation at Ramsar Site 1208

MONTHS	SMI_Max	SMI_Min	SMI_Mean	SMI_Std. Dev
January	0.908754289	0.29157335	0.739206518	0.065908539
February	0.820205569	0.14131927	0.620521964	0.080397243
March	0.855902612	0.18591724	0.620781705	0.105781151
April	0.522094727	0.07125363	0.37794651	0.062392996
May	0.304883927	0.12708731	0.22617669	0.020828925
June	0.73761797	0.13440001	0.261967602	0.072568139
July	0.690846801	0.11833668	0.17792097	0.046634693
August	0.156204492	0.03275345	0.08125004	0.009982952
September	0.242001578	0.0602346	0.107203204	0.014265013
October	0.858257234	0.17746778	0.689780729	0.083545627
November	0.793910325	0.20482892	0.612057172	0.063714934
December	0.030285235	0.0039748	0.02033975	0.003833677

4.7.2 At Ramsar Site 2370

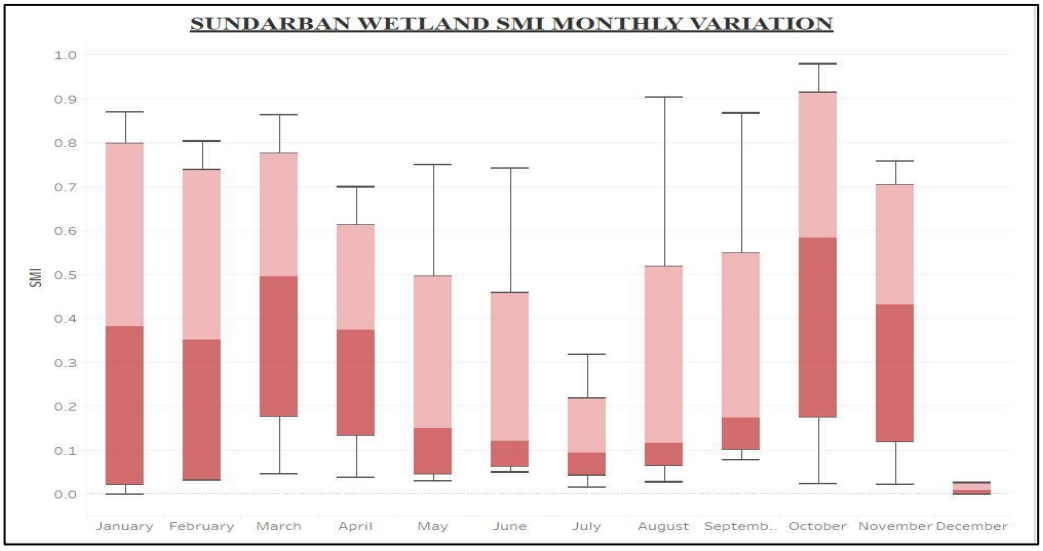

Figure 4.18: Temporal Variation of SMI at Ramsar Site 2370

Table 4.13: Datasheet of SMI Temporal Variation at Ramsar Site 2370

MONTHS	SMI_Max	SMI_Min	SMI_Mean	SMI_Std. Dev
January	0.868552864	-1.71E-06	0.726029295	0.040097571
February	0.803347051	0.03189726	0.672334017	0.033607093
March	0.863289535	0.30390188	0.688819851	0.04743109
April	0.700577259	0.22479442	0.524684081	0.038886906
May	0.748962343	0.05989627	0.242470308	0.030073825
June	0.742444694	0.0735127	0.172948765	0.050552699
July	0.318986058	0.06915027	0.118404639	0.016940686
August	0.90399611	0.02929474	0.133376372	0.101817469
September	0.868026674	0.07852197	0.226743634	0.121280389
October	0.980122864	0.32448655	0.844799328	0.025601251
November	0.757384002	0.21491967	0.648723325	0.023473286
December	0.026710559	0.0005435	0.022160785	0.001039556

4.8 Time Series Variation Results of Correlation Coefficient (r)

4.8.1 Case 1: SOC & NDVI

4.8.1.1 At Ramsar Site 1208

Table 4.14: SOC vs NDVI Correlation Coefficient chart at Ramsar Site 1208

	SOC	NDVI_Jan	NDVI_Feb	NDVI_March	NDVI_April	NDVI_May	NDVI_June	NDVI_July	NDVI_Aug	NDVI_Sept	NDVI_Oct	NDVI_Nov.	NDVI_Dec
SOC	1												
NDVI_Jan	0.00555	1											
NDVI_Feb	-0.13312	0.832663	1										
NDVI_March	0.040853	0.732691	0.679307	1									
NDVI_April	0.018556	0.7544	0.637129	0.76969	1								
NDVI_May	-0.09433	0.787475	0.761 78	0.7305	0.772393	1							
NDVI_June	-0.24963	0.516865	0.573918	0.407224	0.443235	0.529469	1						
NDVI_July	-0.17463	0.657615	0.700171	0.460333	0.564365	0.713658	0.665332	1					
NDVI_Aug	-0.08918	0.708901	0.702864	0.566525	0.643744	0.733716	0.539909	0.748296	1				
NDVI_Sept	-0.00902	0.611606	0.591957	0.587056	0.587525	0.575808	0.516201	0.543215	0.61794	1			
NDVI_Oct	-0.01014	0.85262	0.753213	0.766192	0.869792	0.826561	0.529293	0.691522	0.749311	0.678711	1		
NDVI_Nov.	-0.06387	0.833097	0.755029	0.737174	0.845694	0.825313	0.537142	0.689442	0.731311	0.656396	0.958118	1	
NDVI_Dec	-0.08003	0.812437	0.744	0.683538	0.802185	0.805281	0.528966	0.658589	0.707168	0.629085	0.895999	0.925492	1

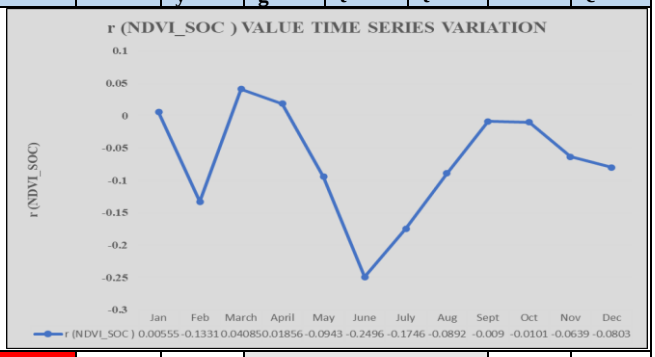

Fig. 4.19

Figure 4.19: r value variation at Ramsar site 1208 (SOC &NDVI)

Legend									
0.8-1	**0.6-0.8**	**0.4-0.6**	**0.2-0.4**	**0.0-0.2**	**-0.2-0.0**	**-0.4—0.2**	**-0.6—0.4**	**-0.8—0.6**	**-1—0.8**

4.8.1.2 At Ramsar Site 2370

Table 4.15: SOC vs NDVI Correlation Coefficient chart at Ramsar Site 2370

	SOC	NDVI_Jan	NDVI_Feb	NDVI_March	NDVI_April	NDVI_May	NDVI_June	NDVI_July	NDVI_Aug	NDVI_Sept	NDVI_Oct	NDVI_Nov.	NDVI_Dec
SOC	1												
NDVI_Jan	0.227337	1											
NDVI_Feb	0.218723	0.993821	1										
NDVI_March	0.217446	0.986921	0.984222	1									
NDVI_April	0.210234	0.980451	0.980183	0.991947	1								
NDVI_May	0.210324	0.955243	0.959909	0.958158	0.960313	1							
NDVI_June	0.230763	0.810169	0.811333	0.811754	0.805878	0.774733	1						
NDVI_July	0.245749	0.885834	0.890548	0.874789	0.873703	0.862004	0.734455	1					
NDVI_Aug	0.149	0.771673	0.784357	0.771948	0.781545	0.773688	0.657836	0.679834	1				
NDVI_Sept	0.221009	0.886829	0.887 37	0.892107	0.886 26	0.846216	0.776015	0.803581	0.682004	1			
NDVI_Oct	0.194851	0.987848	0.983596	0.989182	0.987617	0.955645	0.808653	0.869662	0.770475	0.888599	1		
NDVI_Nov.	0.218393	0.991087	0.989765	0.991943	0.989931	0.961631	0.813853	0.880793	0.779244	0.892678	0.994984	1	
NDVI_Dec	0.224082	0.993798	0.993998	0.984178	0.980736	0.957513	0.806545	0.885406	0.779136	0.884391	0.98743	0.991314	1

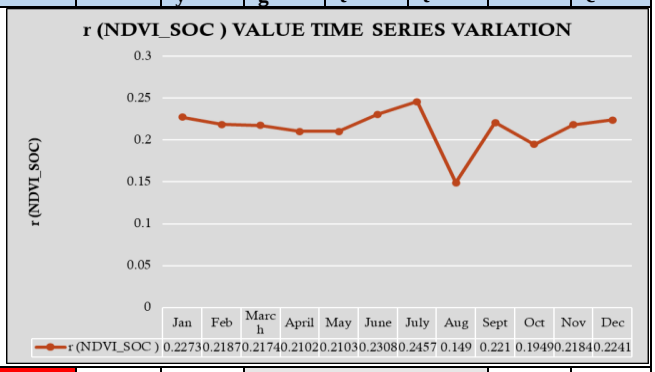

Fig. 4.20

Figure 4.20 r value variation at Ramsar site 2370 (SOC &NDVI)

Legend									
0.8-1	0.6-0.8	0.4-0.6	0.2-0.4	0.0-0.2	-0.2-0.0	-0.4—0.2	-0.6—0.4	-0.8—0.6	-1—0.8

4.8.2 Case 2: SOC & NDBI

4.8.2.1 At Ramsar Site 1208

Table 4.16: SOC vs NDBI Correlation Coefficient chart at Ramsar Site 1208

	SOC	NDBI_Jan	NDBI_Feb	NDBI_March	NDBI_April	NDBI_May	NDBI_June	NDBI_July	NDBI_Aug	NDBI_Sept	NDBI_Oct	NDBI_Nov.	NDBI_Dec
SOC	1												
NDBI_Jan	0.01585	1											
NDBI_Feb	-0.0274	0.695956	1										
NDBI_March	-0.06267	0.503488	0.714097	1									
NDBI_April	-0.14506	0.431191	0.543347	0.613236	1								
NDBI_May	0.077184	0.457146	0.451406	0.417027	0.445332	1							
NDBI_June	0.008226	0.284676	0.281188	0.263671	0.237961	0.312465	1						
NDBI_July	-0.12584	0.360907	0.363014	0.316074	0.390404	0.324825	0.416177	1					
NDBI_Aug	0.011161	0.167538	0.175167	0.13775	0.28482	0.182703	0.309649	0.328797	1				
NDBI_Sept	-0.12882	0.296003	0.298577	0.298722	0.394245	0.267871	0.319479	0.37351	0.497629	1			
NDBI_Oct	-0.12377	0.44789	0.415748	0.378268	0.563236	0.348136	0.406253	0.498333	0.506516	0.561238	1		
NDBI_Nov.	0.067408	0.587922	0.393982	0.338513	0.45826	0.509604	0.364944	0.403239	0.350884	0.418717	0.717519	1	
NDBI_Dec	0.126632	0.57767	0.370569	0.237936	0.308704	0.600769	0.246003	0.229887	0.116864	0.234892	0.381612	0.663298	1

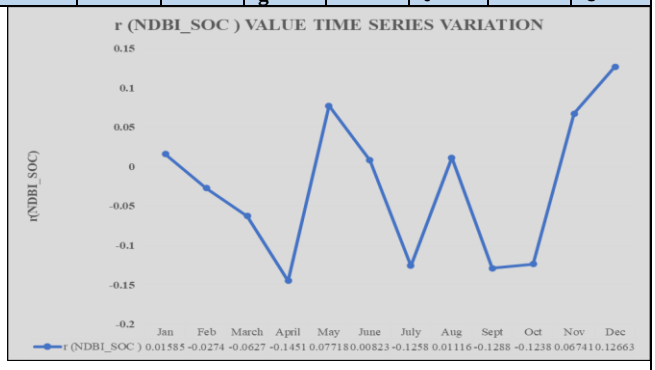

Fig. 4.21

Figure 4.21: r value variation at Ramsar site 1208 (SOC &NDBI)

Legend									
0.8-1	**0.6-0.8**	**0.4-0.6**	**0.2-0.4**	**0.0-0.2**	**-0.2-0.0**	**-0.4—0.2**	**-0.6—0.4**	**-0.8—0.6**	**-1—0.8**

4.8.2.2 At Ramsar Site 2370

Table 4.17: SOC vs NDBI Correlation Coefficient chart at Ramsar Site 1208

	SOC	NDBI_Jan	NDBI_Feb	NDBI_March	NDBI_April	NDBI_May	NDBI_June	NDBI_July	NDBI_Aug	NDBI_Sept	NDBI_Oct	NDBI_Nov.	NDBI_Dec
SOC	1												
NDBI_Jan	-0.24366	1											
NDBI_Feb	-0.25906	0.972239	1										
NDBI_March	-0.28027	0.932795	0.933936	1									
NDBI_April	-0.28529	0.919855	0.935165	0.944062	1								
NDBI_May	-0.21726	0.874217	0.860568	0.853886	0.843782	1							
NDBI_June	0.000135 8	0.362929	0.354829	0.351087	0.349111	0.343572	1						
NDBI_July	-0.17526	0.578822	0.603456	0.542391	0.584053	0.507356	0.218868	1					
NDBI_Aug	-0.29654	0.661165	0.704388	0.629746	0.686092	0.595106	0.209071	0.459015	1				
NDBI_Sept	-0.2425	0.737258	0.750384	0.721303	0.758143	0.647419	0.310437	0.501089	0.580845	1			
NDBI_Oct	-0.24017	0.926696	0.943478	0.874836	0.924689	0.817691	0.359885	0.627794	0.723844	0.779435	1		
NDBI_Nov.	-0.249	0.942979	0.959602	0.889383	0.922034	0.841888	0.359685	0.624036	0.727029	0.756162	0.974919	1	
NDBI_Dec	-0.23951	0.980586	0.969515	0.916625	0.915192	0.867529	0.362335	0.586612	0.666679	0.735307	0.934932	0.951085	1

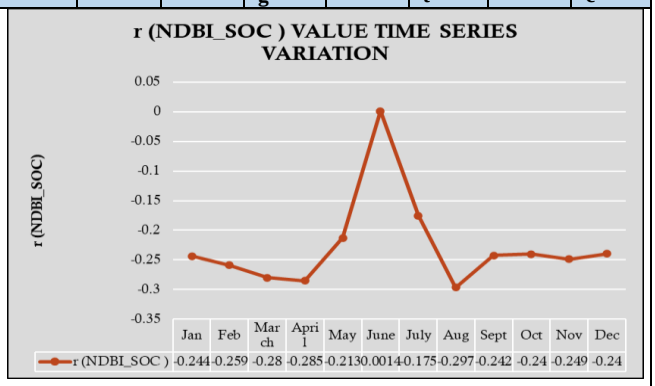

Fig. 4.22

Figure 4.22: r value variation at Ramsar site 2370 (SOC &NDBI)

Legend									
0.8-1	**0.6-0.8**	**0.4-0.6**	**0.2-0.4**	**0.0-0.2**	**-0.2-0.0**	**-0.4—0.2**	**-0.6—0.4**	**-0.8—0.6**	**-1—0.8**

4.8.3 Case 3: SOC & NDWI

4.8.3.1 At Ramsar Site 1208

Table 4.18: SOC vs NDWI Correlation Coefficient chart at Ramsar Site 1208

	SOC	NDWI_Jan	NDWI_Feb	NDWI_March	NDWI_April	NDWI_May	NDWI_June	NDWI_July	NDWI_Aug	NDWI_Sept	NDWI_Oct	NDWI_Nov.	NDWI_Dec
SOC	1												
NDWI_Jan	-0.01614	1											
NDWI_Feb	0.123346	0.818129	1										
NDWI_March	0.004322	0.844682	0.795186	1									
NDWI_April	0.080036	0.823008	0.763687	0.829484	1								
NDWI_May	0.030885	0.840003	0.761633	0.872698	0.861598	1							
NDWI_June	0.18743	0.528885	0.572778	0.505846	0.568236	0.49793	1						
NDWI_July	0.222379	0.643361	0.740847	0.626139	0.701699	0.63236	0.627016	1					
NDWI_Aug	0.127418	0.679034	0.719078	0.656392	0.699249	0.670312	0.542342	0.761837	1				
NDWI_Sept	0.09813	0.656987	0.633521	0.67424	0.692347	0.64574	0.576879	0.660909	0.628795	1			
NDWI_Oct	0.081233	0.880957	0.800251	0.859464	0.898233	0.879516	0.608427	0.753691	0.75948	0.76039	1		
NDWI_Nov.	0.023288	0.889011	0.75784	0.859026	0.890476	0.882097	0.559643	0.684097	0.700228	0.723443	0.963919	1	
NDWI_Dec	-0.01772	0.854561	0.679388	0.825123	0.852739	0.857992	0.471725	0.557645	0.607092	0.659582	0.893217	0.943551	1

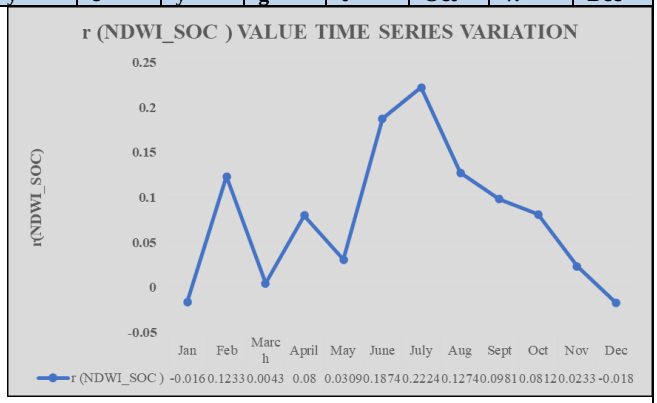

Fig. 4.23

Figure 4.23: r value variation at Ramsar site 1208 (SOC &NDWI)

Legend									
0.8-1	**0.6-0.8**	**0.4-0.6**	**0.2-0.4**	**0.0-0.2**	**-0.2-0.0**	**-0.4—0.2**	**-0.6—0.4**	**-0.8—0.6**	**-1—0.8**

4.8.3.2 At Ramsar Site 2370

Table 4.19: SOC vs NDWI Correlation Coefficient chart at Ramsar Site 2370

	SOC	NDWI_Jan	NDWI_Feb	NDWI_March	NDWI_April	NDWI_May	NDWI_June	NDWI_July	NDWI_Aug	NDWI_Sept	NDWI_Oct	NDWI_Nov	NDWI_Dec
SOC	1												
NDWI_Jan	-0.18662	1											
NDWI_Feb	-0.167	0.966913	1										
NDWI_March	-0.15546	0.970096	0.935208	1									
NDWI_April	-0.15284	0.964616	0.933845	0.985947	1								
NDWI_May	-0.18651	0.941029	0.914393	0.937484	0.938911	1							
NDWI_June	-0.22677	0.598862	0.576434	0.600202	0.595933	0.575255	1						
NDWI_July	-0.18524	0.642367	0.667945	0.611804	0.624384	0.61539903	0.393601	1					
NDWI_Aug	0.000506	0.551697	0.577447	0.531849	0.557658	0.542828	0.332805	0.430002	1				
NDWI_Sept	-0.18625	0.828505	0.811955	0.822591	0.815812	0.773625	0.527097	0.578884	0.458954	1			
NDWI_Oct	-0.15828	0.971914	0.9486	0.959837	0.961082	0.926712	0.598999	0.649804	0.579863	0.825175	1		
NDWI_Nov.	-0.19113	0.985947	0.969097	0.960527	0.962516	0.940766	0.602824	0.666789	0.581618	0.83491	0.98543	1	
NDWI_Dec	-0.16449	0.972961	0.971219	0.947578	0.945118	0.929319	0.579005	0.626072	0.546876	0.803568	0.945614	0.968542	1

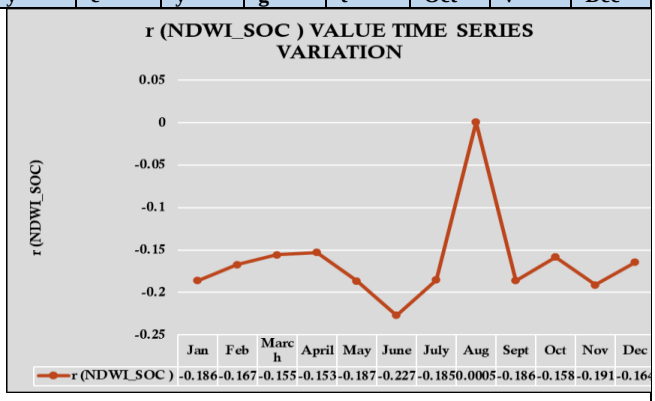

Fig. 4.24

Figure 4.24: r value variation at Ramsar site 2370 (SOC &NDWI)

Legend								
0.8-1	0.6-0.8	0.4-0.6	0.2-0.4	0.0-0.2	-0.2-0.0	-0.4—0.2	-0.6—0.4	-0.8—0.6	-1—0.8

4.9 Variation of Statistical Metrices:

4.9.1 Root Mean Square (RMSE) & R^2 Variation

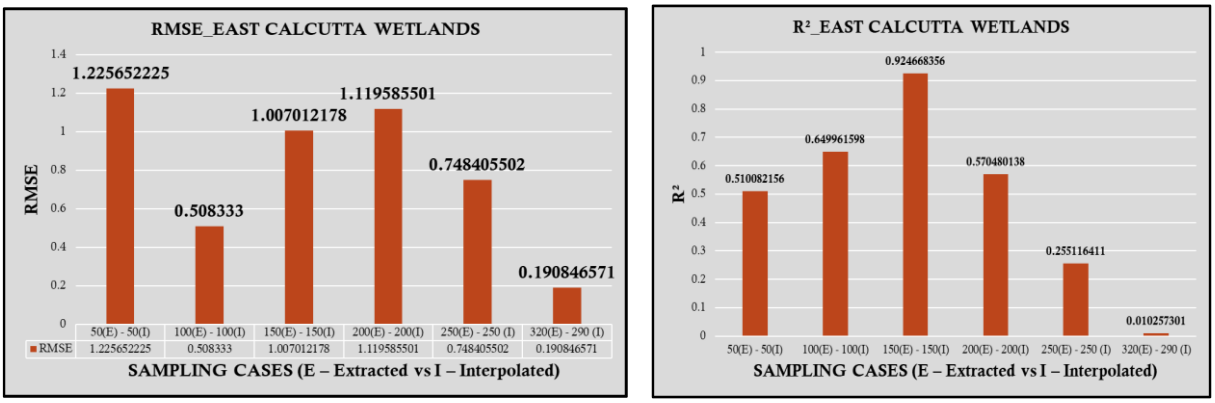

Figure 4.25: RMSE & R^2 Variation at East Calcutta Wetlands

Table 4.20: Datasheet for Root Mean Square (RMSE) & R^2 Variation at East Calcutta Wetlands [SOC stock Interpolation]

SAMPLING FOR RMSE CALCULATION	50(E) - 50(I)	100(E) - 100(I)	150(E) - 150(I)	200(E) - 200(I)	250(E) - 250 (I)	320(E) - 290 (I)
RMSE	1.225652	0.508333	1.007012	1.119586	0.748406	0.190846571
R^2	0.510082	0.649962	0.924668	0.57048	0.255116	0.010257301
E: Extracted			**I: Interpolated**			

4.9.3 Root Mean Square (RMSE) & R^2 Variation

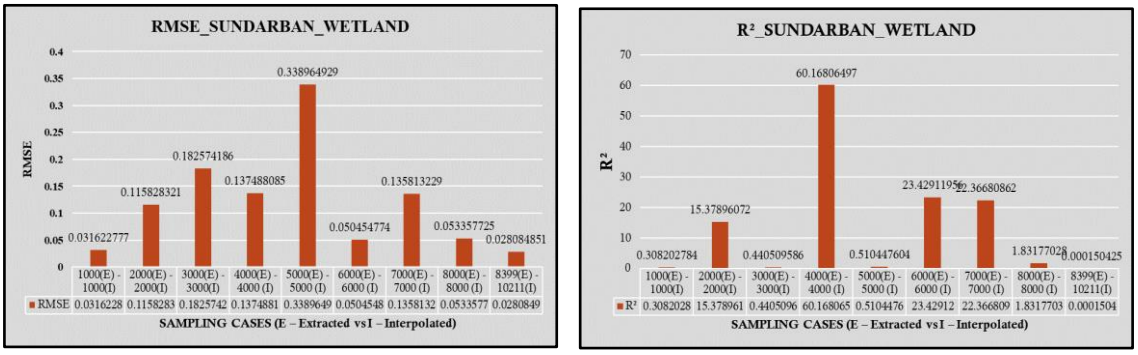

Figure 4.26: RMSE & R^2 Variation at Sundarban Wetland

Table 4.21: Datasheet for Root Mean Square (RMSE) & R^2 Variation at Sundarban Wetland [SOC stock Interpolation]

SAMPLING FOR RMSE CALCULATION	1000 (E) - 1000 (I)	2000 (E) - 2000 (I)	3000 (E) - 3000 (I)	4000 (E) - 4000 (I)	5000 (E) - 5000 (I)	6000 (E) - 6000 (I)	7000 (E) - 7000 (I)	8000 (E) - 8000 (I)	8399 (E) - 10211 (I)
RMSE	0.031623	0.115828	0.182574	0.137488	0.338965	0.050455	0.135813	0.053358	0.028085
R^2	0.308203	15.37896	0.44051	60.16806	0.510448	23.42912	22.36681	1.83177	0.00015
E: Extracted					**I: Interpolated**				

4.10 Discussion on Number of Sampling points vs. Statistical metrices output

It has been shown in Fig. 4.25 & 4.26 that RMSE and R^2 is varying with number of sampling points at both sites. The variation for RMSE was observed from a maximum value of 1.225 to minimum of a 0.19 at East Calcutta Wetlands and for Sundarban Wetland, the variation was in a range of 0.338 to 0.028. The variation for R^2 was observed from a maximum value of 0.92 to minimum of a 0.01 at East Calcutta Wetlands and for Sundarban Wetland, the variation was in a range of 60 to 0.0001. Here to say that, R^2 value cannot be greater than 1 and hence the cases of $R^2>1$ should not consider. As this RMSE and R^2 values at these site areas indicates towards the efficiency interpolation of Soil Organic Carbon stock through Ordinary Kriging method, therefore we can say that in case of East Calcutta Wetlands, as area is less than Sundarban Wetland, therefore uncertainty layer is also smaller and thus interpolation accuracy is higher than Sundarban Wetland and range variation is less. Whereas, in case of Sundarban Wetland, statistical metrices variation (for R^2) is quite wider.

4.11 Discussion on cloud cover for correlation output

Cloud Cover, surface emissivity, atmospheric reflection, and atmospheric absorption, these are quite important features behind the accuracy of remote sensing study. In highly cloud cover condition, it is not necessary to get an absurd value upon raster. It is because of the study area of our concern, may be out of the cloud interference whereas for a comparatively low cloud cover satellite image, the reverse phenomenon may be observed based upon the location of study area. Thus, as a result, correlation coefficient

varies accordingly as multiparameter measurement (NDVI, NDBI, NDWI, LST, SMI) changes in case to case.

5.3 Discussion on Correlation Output in this Study

From the [Table 4.14 to 4.19] and [Fig. 4.19 to 4.24], we get the total representation of correlation coefficients associated with this study. Except NDVI vs SOC correlation output at Sundarban Wetland and NDWI vs SOC correlation output at East Calcutta Wetlands, rest of the monthly correlation coefficient variations with multiparameter shows a net negative trend. Though the Landsat 8 data accumulation is in a range of year 2020 to 2023, the month-to-month correlation of multiparameter has a positive trend. It also indicates that no significant changes have occurred in the study areas. As, East Calcutta Wetlands is an inland wetland surrounded by Kolkata City and new extensions, hence a threat from anthropogenic activity always remains over it but from the functionality viewpoint and wetland health in terms of SOC stock, we can say that it is secured till now and requires a continuous management. At East Calcutta Wetlands, SOC vs NDVI monthly correlation variation has a net negative trend which indicates wetland plants are getting destroyed and a replantation and rejuvenation program is need to be taken to ensure wetland plant security because these plants not only store SOC in their biomass and rootzone, but also play a key role in the bioremediation and sewage treatment and also are of medicinal importance. Whereas, net positive trend of NDVI vs SOC correlation variation at Sundarban Wetland, reveals that new mangrove forest may be densified during the study period. As pisciculture dominates at East Calcutta wetland, therefore due to the seasonal change of water-logged area, bottom of the ponds may be exposed out which results into SOC vs NDWI net positive trends at East Calcutta Wetlands.

5.4 Discussion on Field Sampling vs Random Sampling

The conventional method for Soil Organic Carbon Testing is Walkley-black Method. However, this method needs to laboratory efficiency to execute and number of sample points and sample location accessibility by physically, may be restricted in some cases. In this case, remote sensing can be effectively used as a preliminary work out before laboratory execution.

CHAPTER 5

CONCLUSION

In this study, we have seen that the SoilGrids 250 m is a widely acceptable open source for Soil Organic carbon stock data collection. Through this work, we observed two different types of wetlands in a single Landsat -8 tile. The multiparameter with SOC correlation variation is less in Sundarban Wetland than East Calcutta Wetland. It indicates, how anthropogenic activities play a key role in the loss of underground Carbon stock.

Another feature which is important to predict the indices (NDVI, NDBI, NDWI, SMI etc.) in study, that is also depends upon the type of vegetation at Study area. Presence of Soil Organic Carbon indicates the healthy mineralogical profile of soil along with the presence of organic biomass. This indicates the source of nutrition to the plant. Presence of Mangrove in coastal line area are itself is a key indicator of Soil Organic Carbon stored in that area. Whereas, in case of inland wetland like East Calcutta Wetland, several wetland plant species along with pisciculture plays a conjugate role in Carbon capture and sequestration.

The most important parameters among the multiparameter considered in this study is NDVI. Temperature and Rainfall have key correlation with NDVI. However, water stored in soil voids and LST has more priority to the growth of plants. Hence, SMI and LST is considered in this study. Besides that, anthropogenic activity plays the key role to land cover and land use. Hence NDBI is considered in this study to check the correlation with SOC stock. Another parameter, NDWI as per Xu et al. recommendation, considered here so to identify the water-logged/ stream flow areas which is needed to done to separate terrestrial ecosystem from aquatic ecosystem in Soil parameters study.

More accurate interpolation could be done by using same sources of data with different interpolation technique, including Artificial Neural Network. Field Samples may be collected for cross validation of this study. Lastly, I want to convey the message to the fellow readers that we must act and make management plan with wide implementation opportunity to reduce emission and protect the wetlands.

APPENDICES

APPENDIX 1

SPATIOTEMPORAL VARIATION OF MULTIPARAMETER AT RAMSAR SITE (1208)

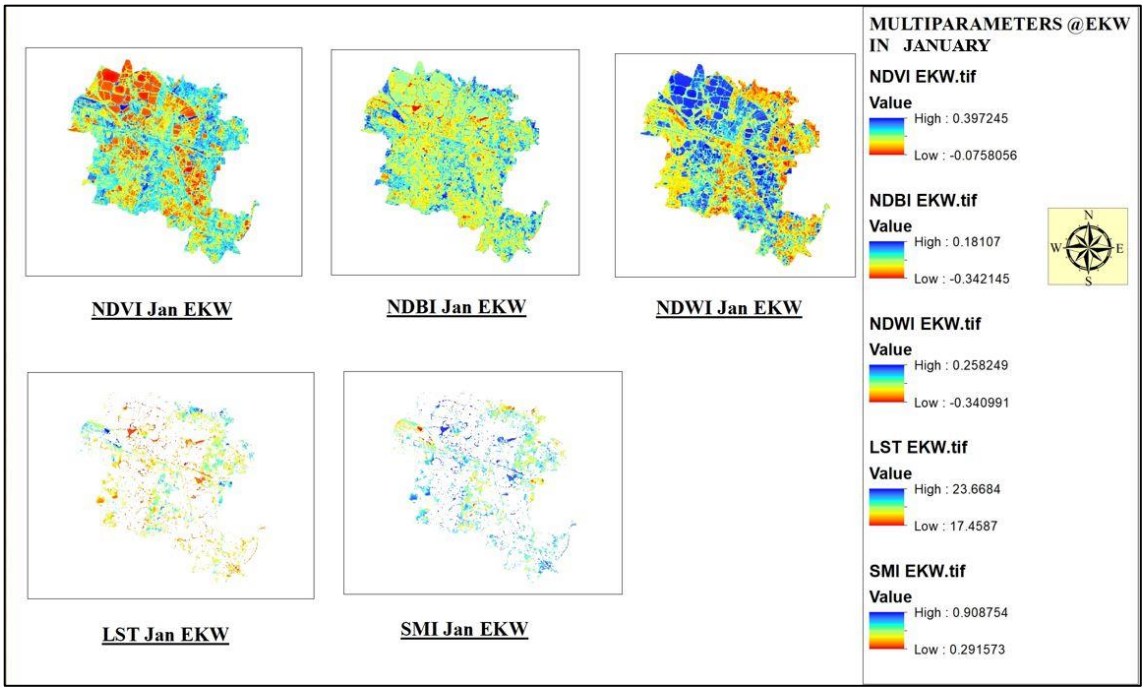

Figure A 1.1: Multiparameter at East Calcutta Wetlands in January

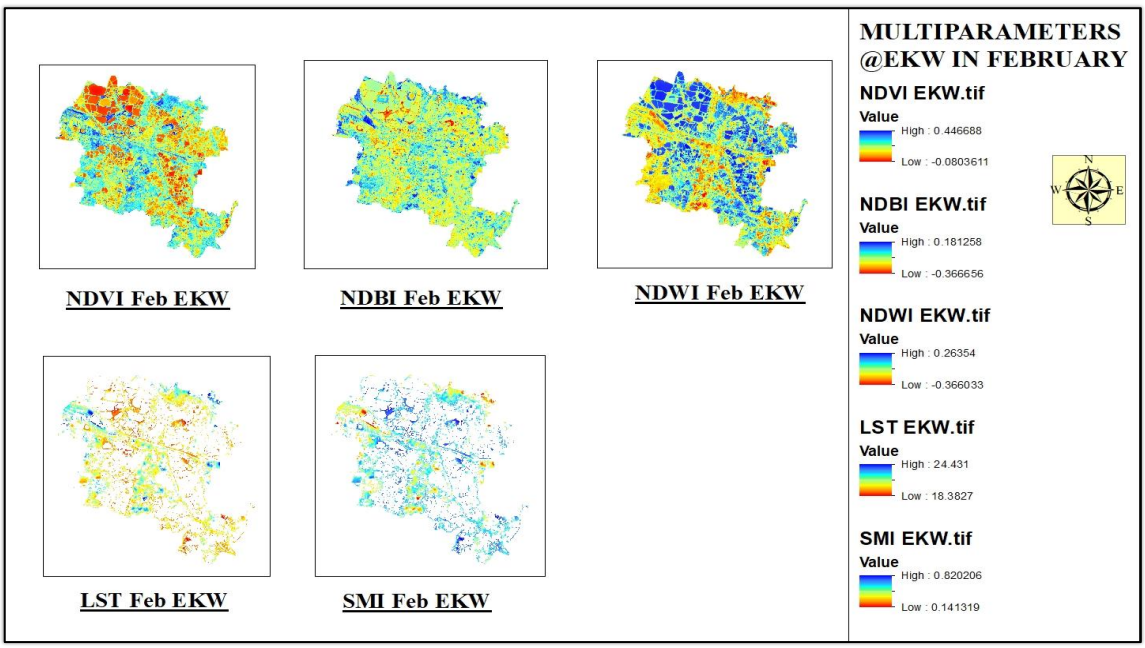

Figure A 1.2: Multiparameter at East Calcutta Wetlands in February

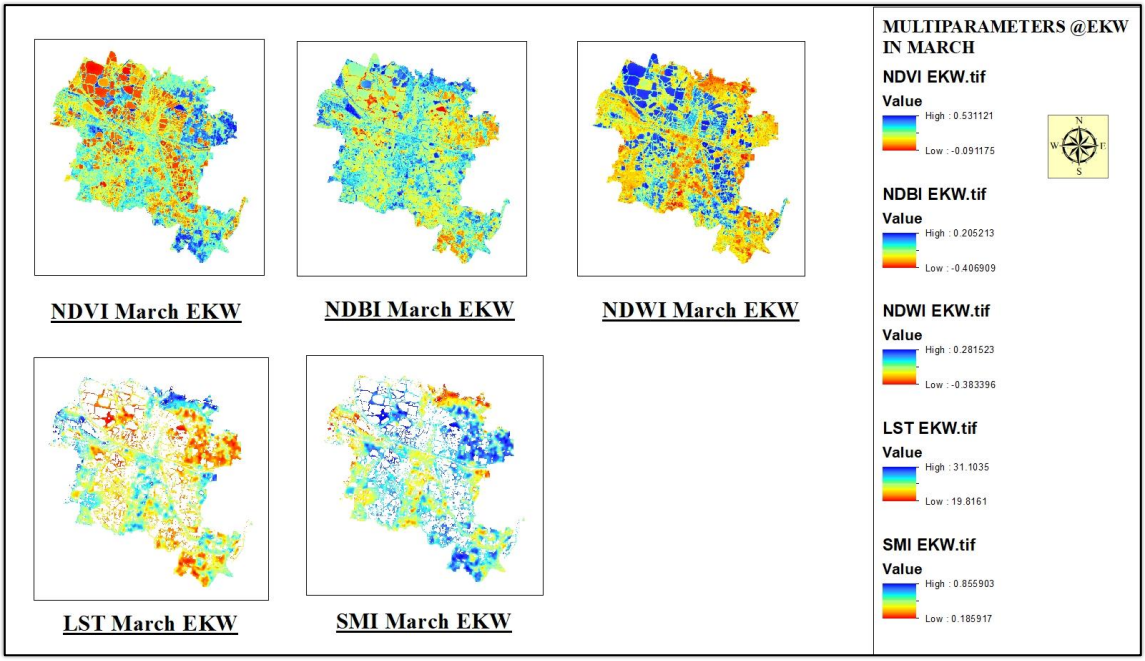

Figure A 1.3: Multiparameter at East Calcutta Wetlands in March

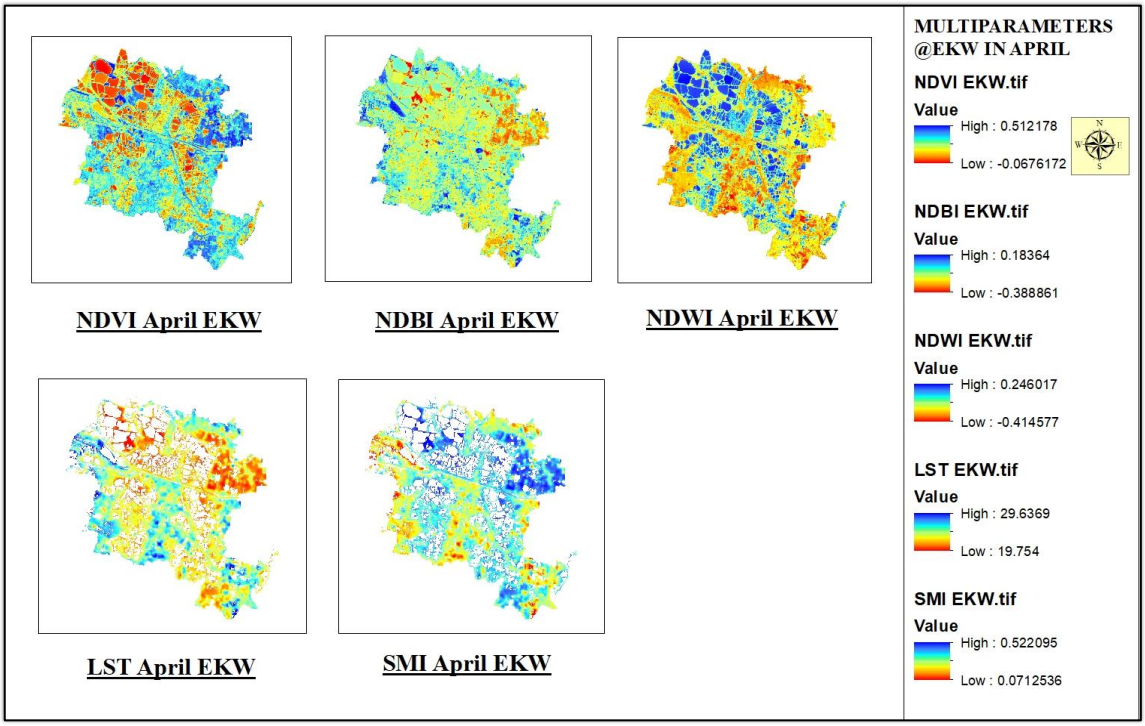

Figure A 1.4: Multiparameter at East Calcutta Wetlands in April

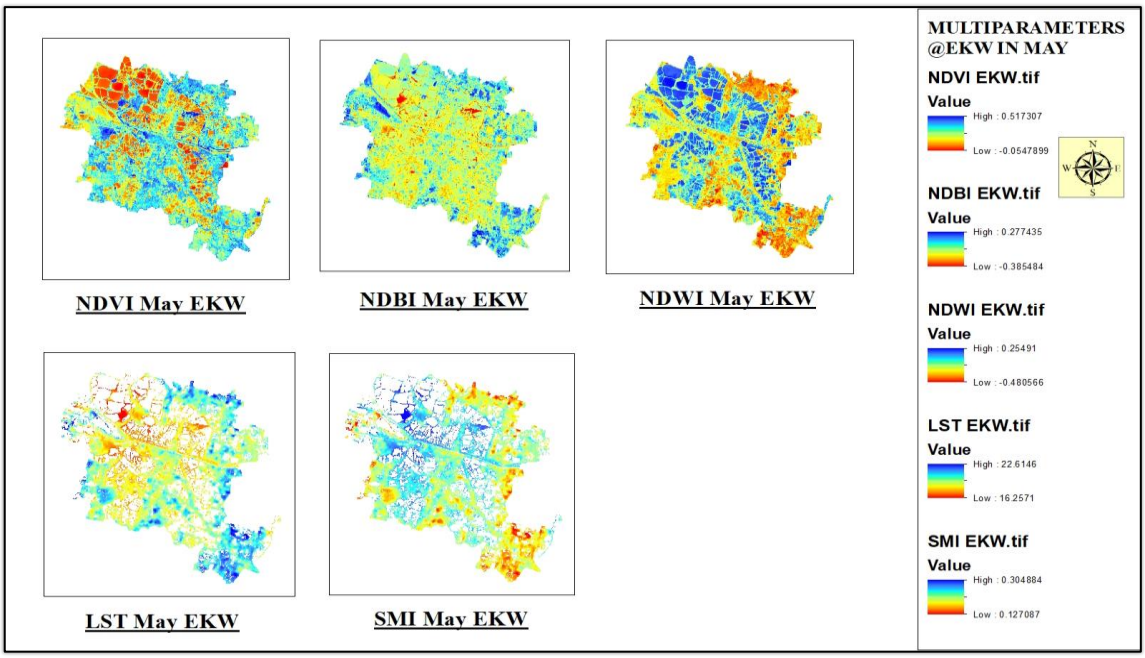

Figure A 1.5: Multiparameter at East Calcutta Wetlands in May

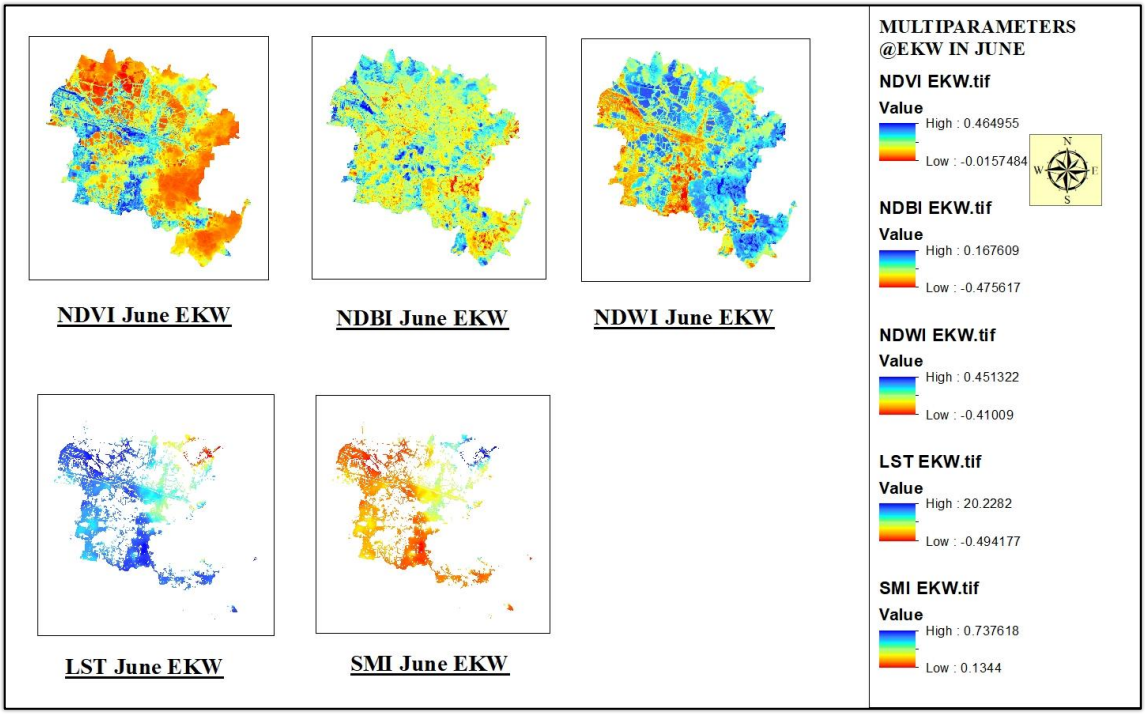

Figure A 1.6: Multiparameter at East Calcutta Wetlands in June

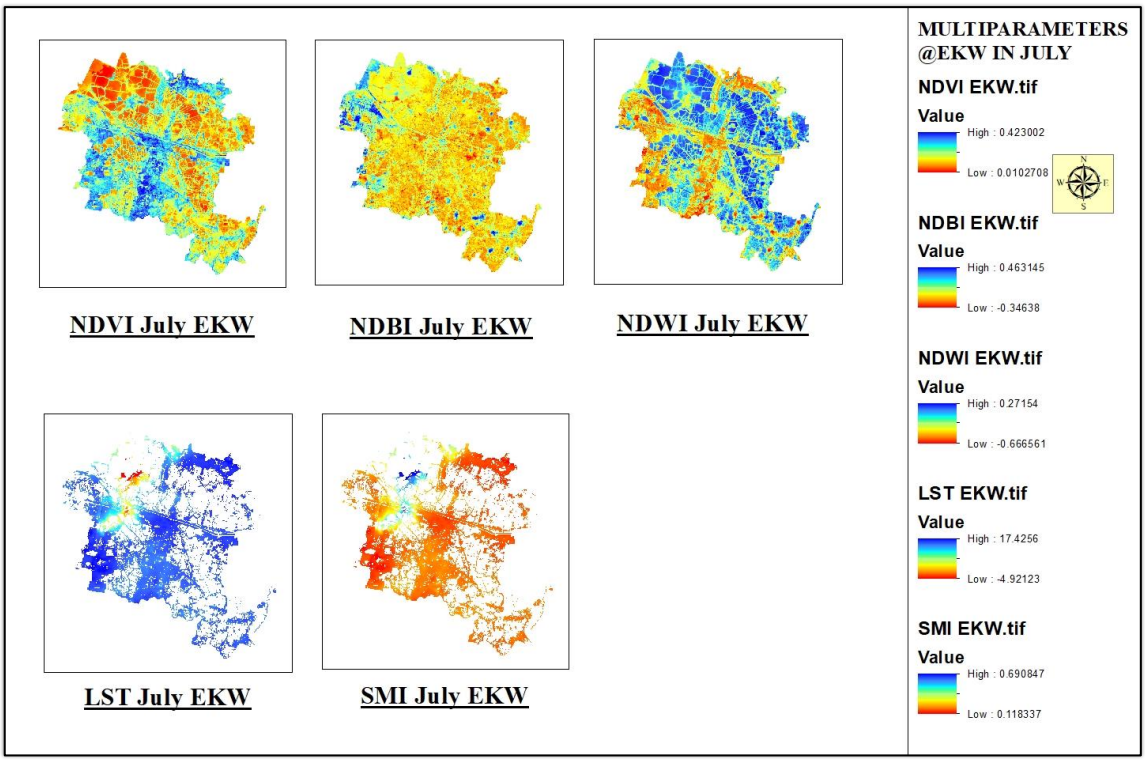

Figure A 1.7: Multiparameter at East Calcutta Wetlands in July

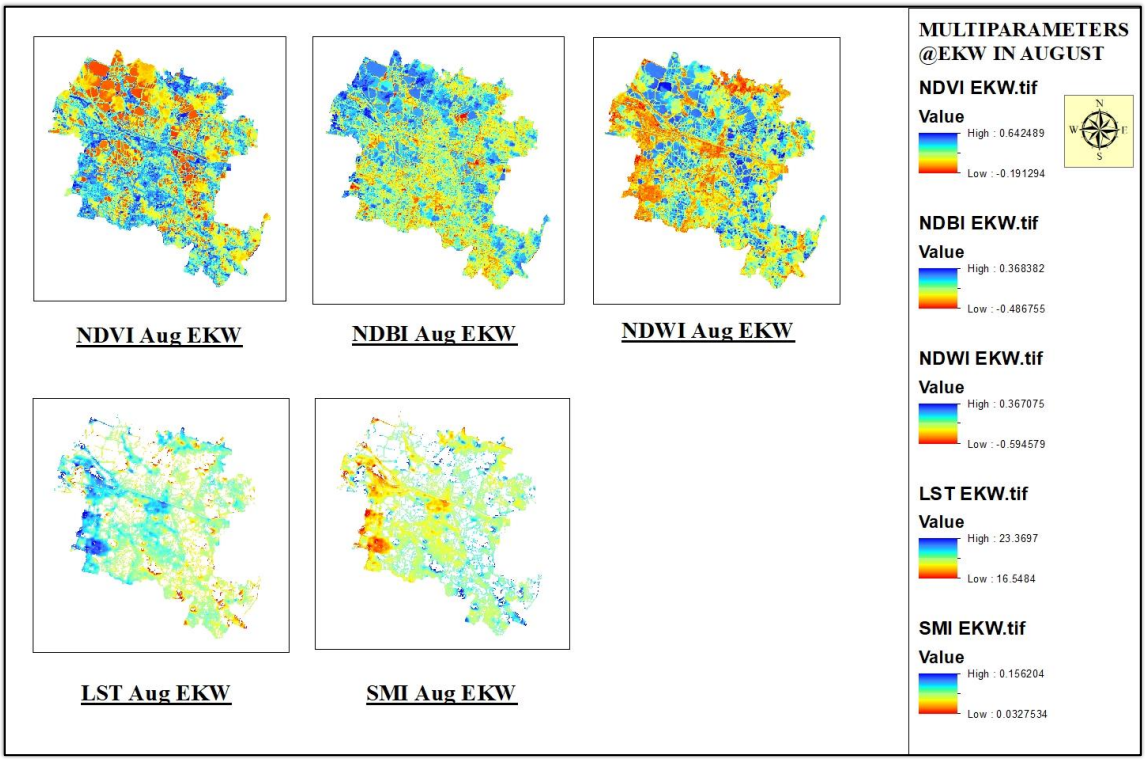

Figure A 1.8: Multiparameter at East Calcutta Wetlands in August

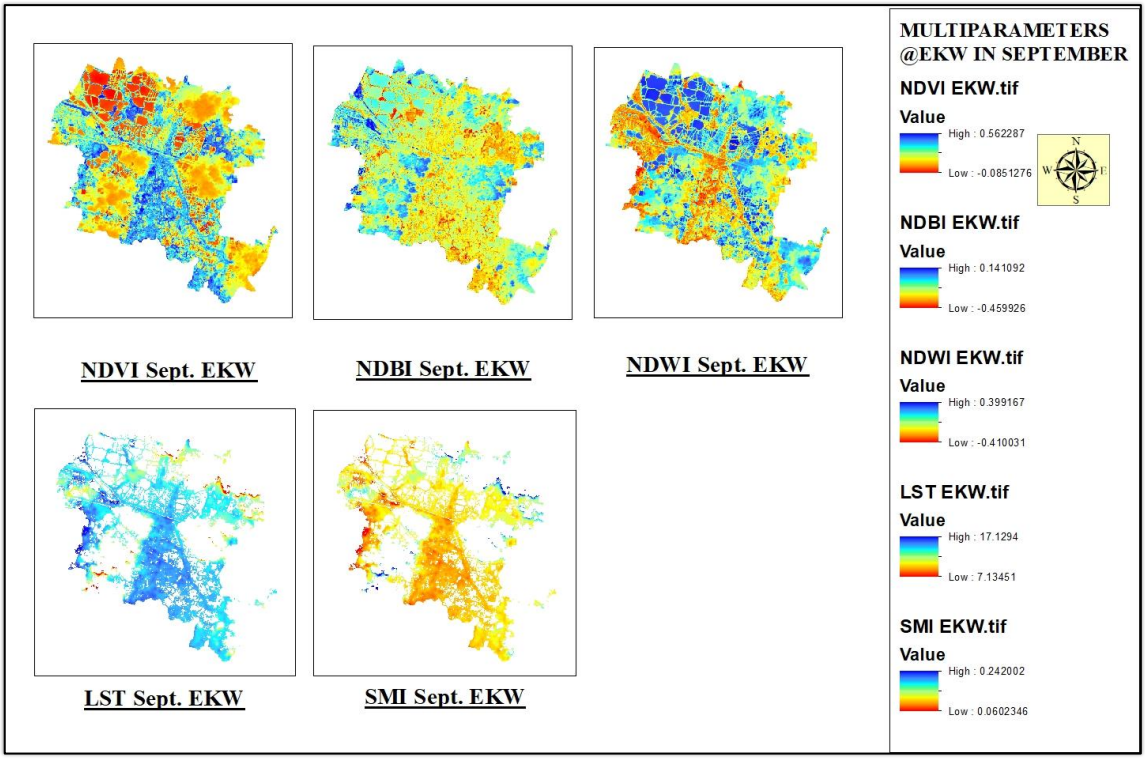

Figure A 1.9: Multiparameter at East Calcutta Wetlands in September

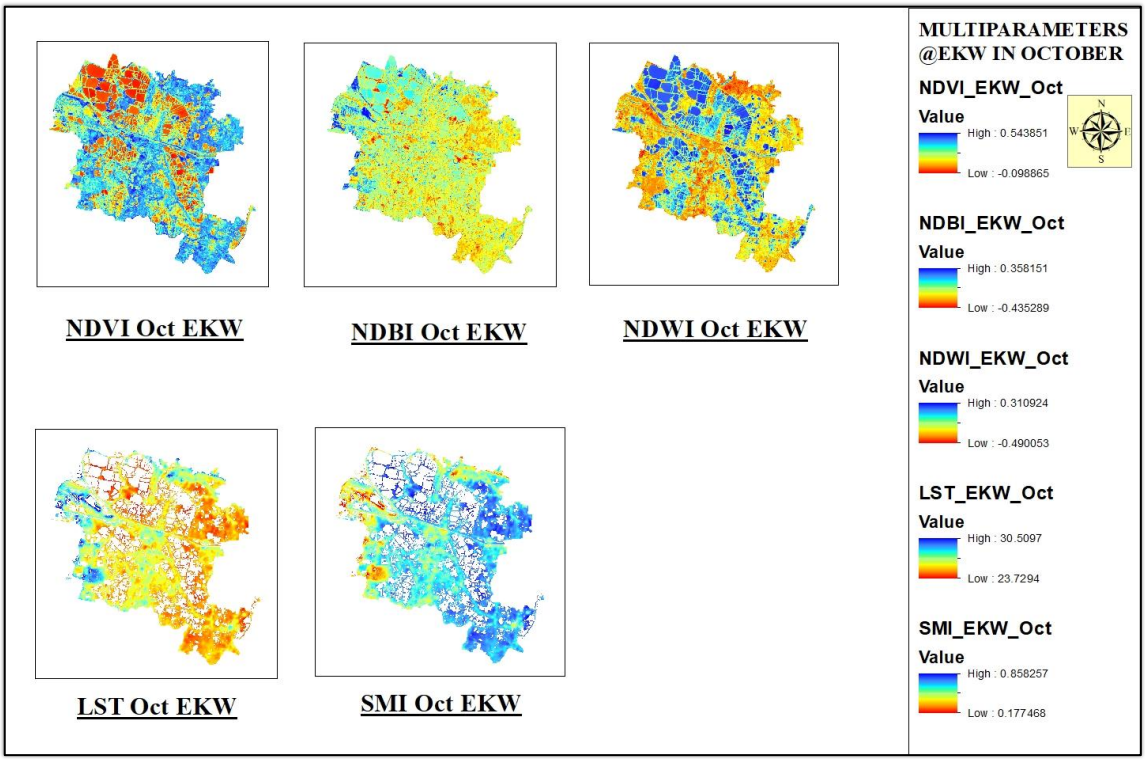

Figure A 1.10: Multiparameter at East Calcutta Wetlands in October

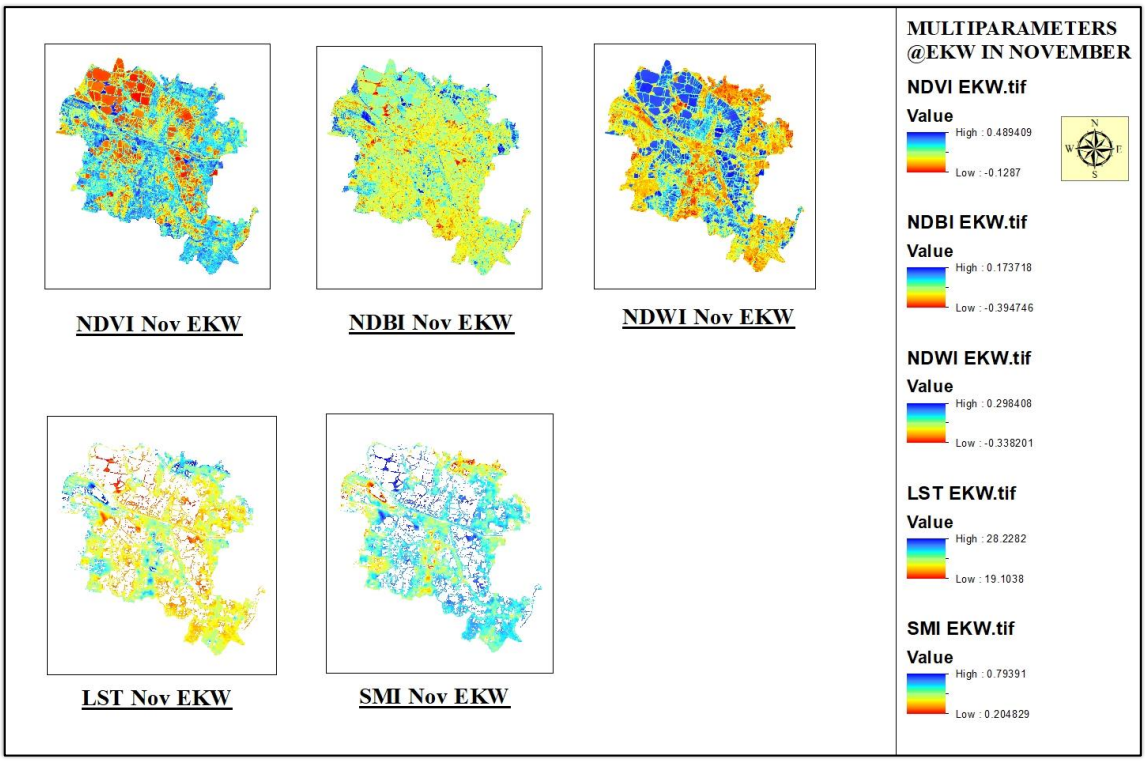

Figure A 1.11: Multiparameter at East Calcutta Wetlands in November

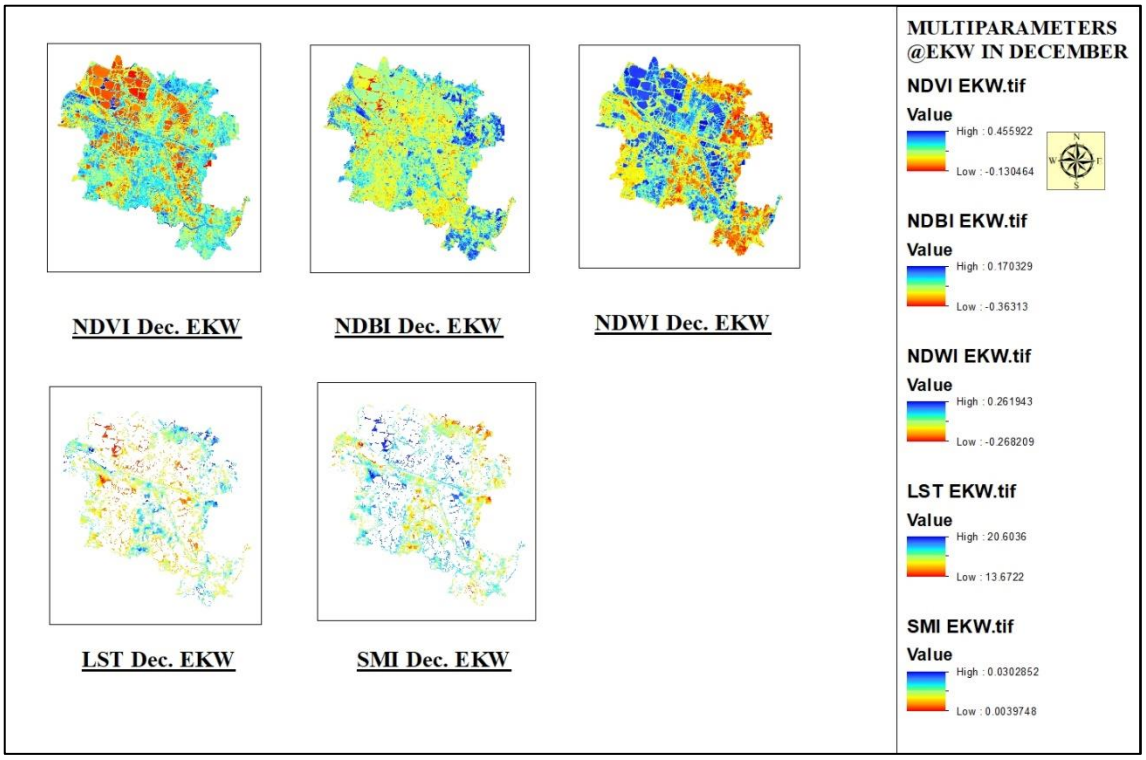

Figure A 1.12: Multiparameter at East Calcutta Wetlands in December

APPENDIX- 2

SPATIOTEMPORAL VARIATION OF MULTIPARAMETER AT RAMSAR SITE (2370)

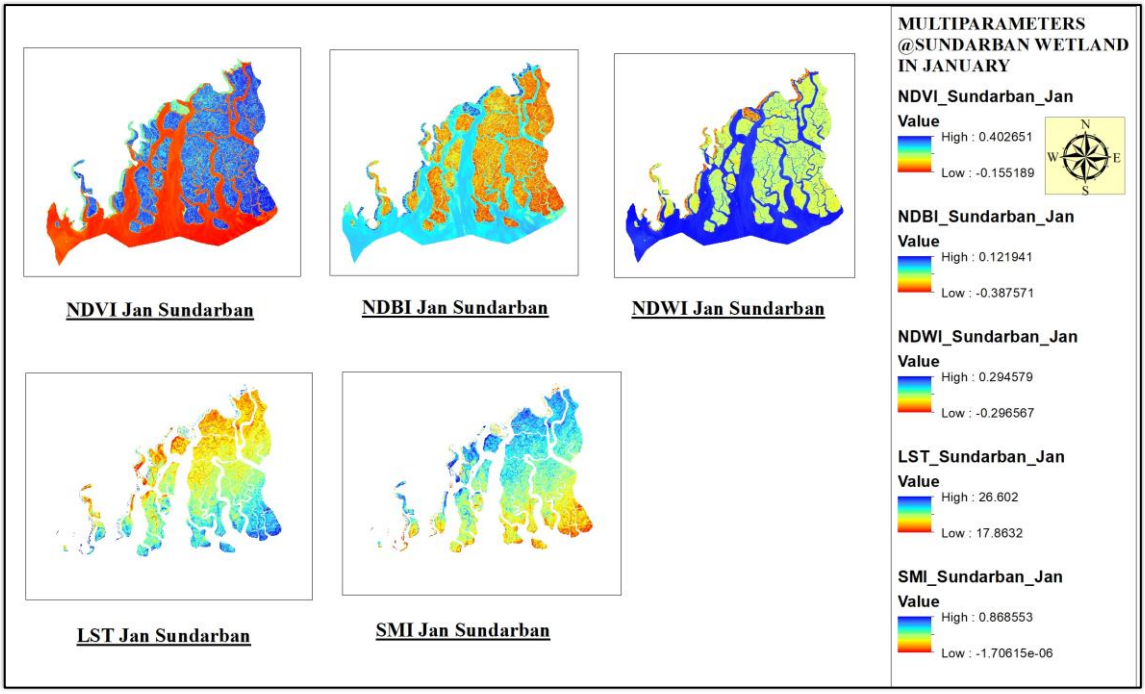

Figure A 2.1: Multiparameter at Sundarban Wetland in January

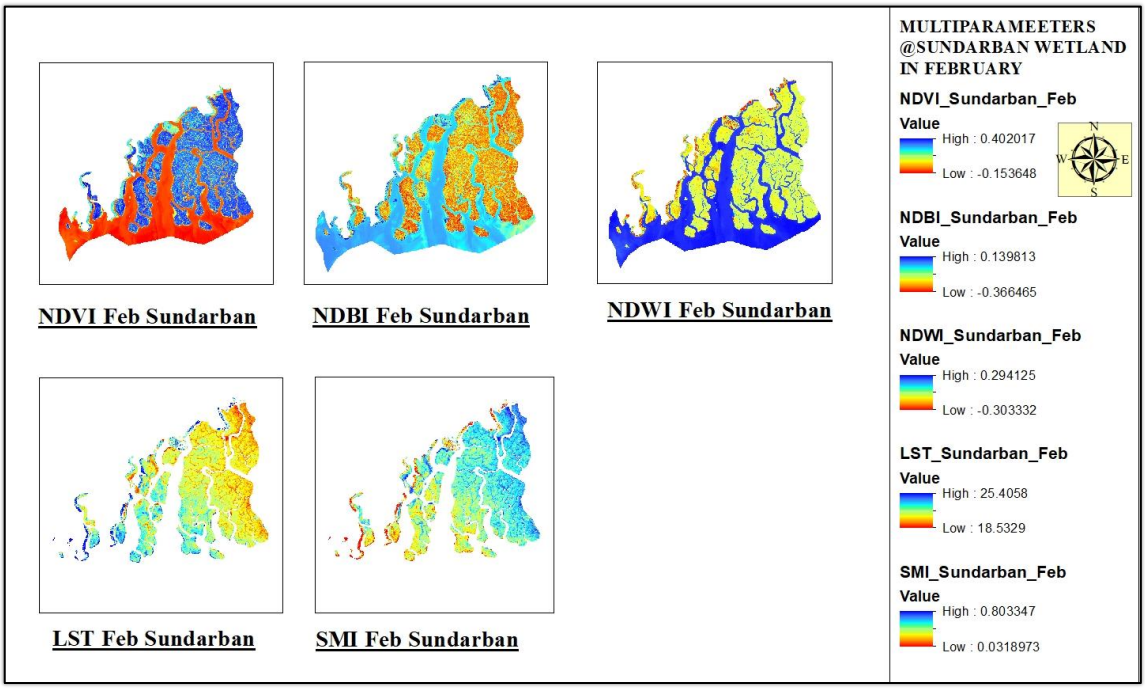

Figure A 2.2: Multiparameter at Sundarban Wetland in February

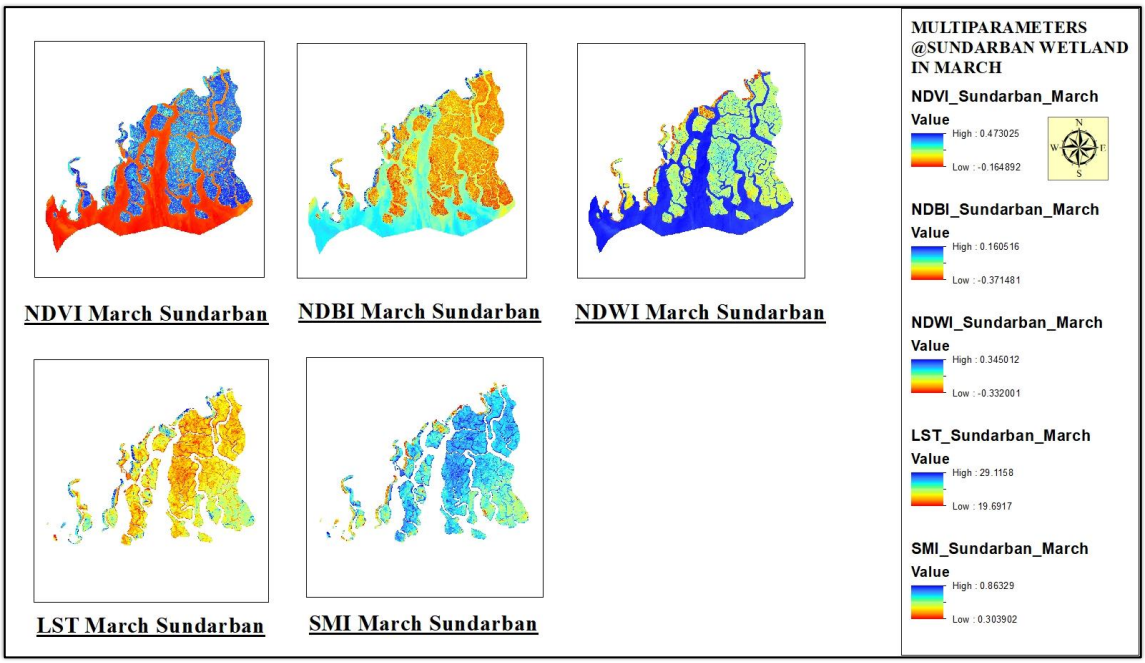

Figure A 2.3: Multiparameter at Sundarban Wetland in March

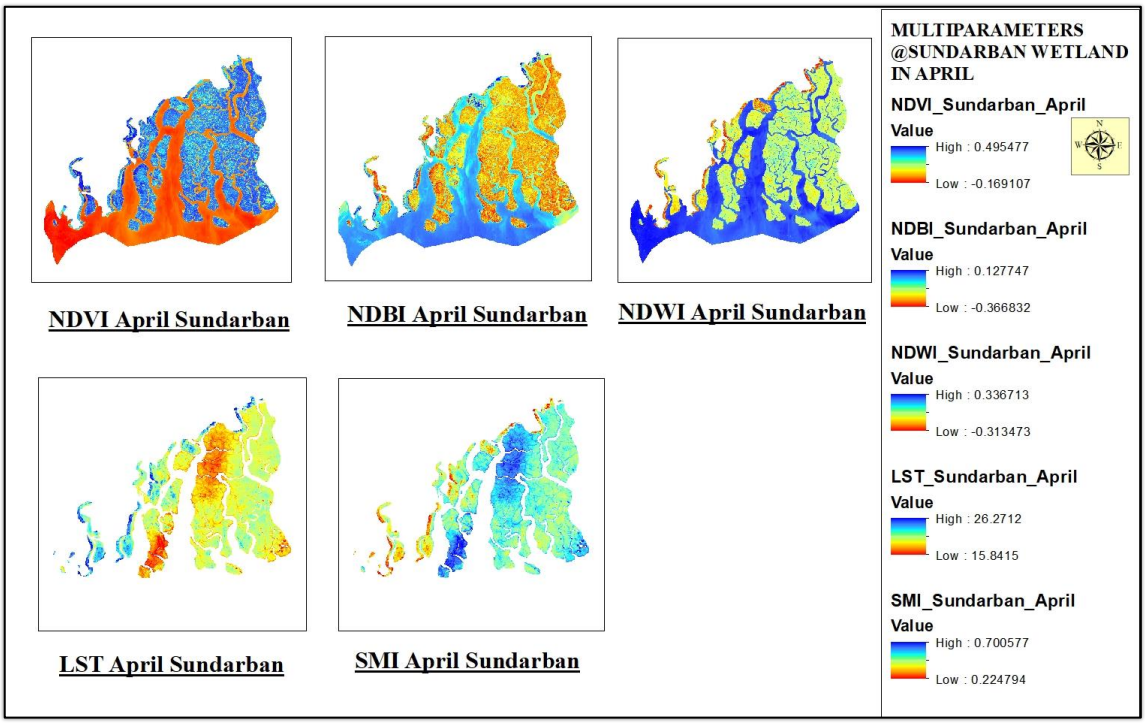

Figure A 2.4: Multiparameter at Sundarban Wetland in April

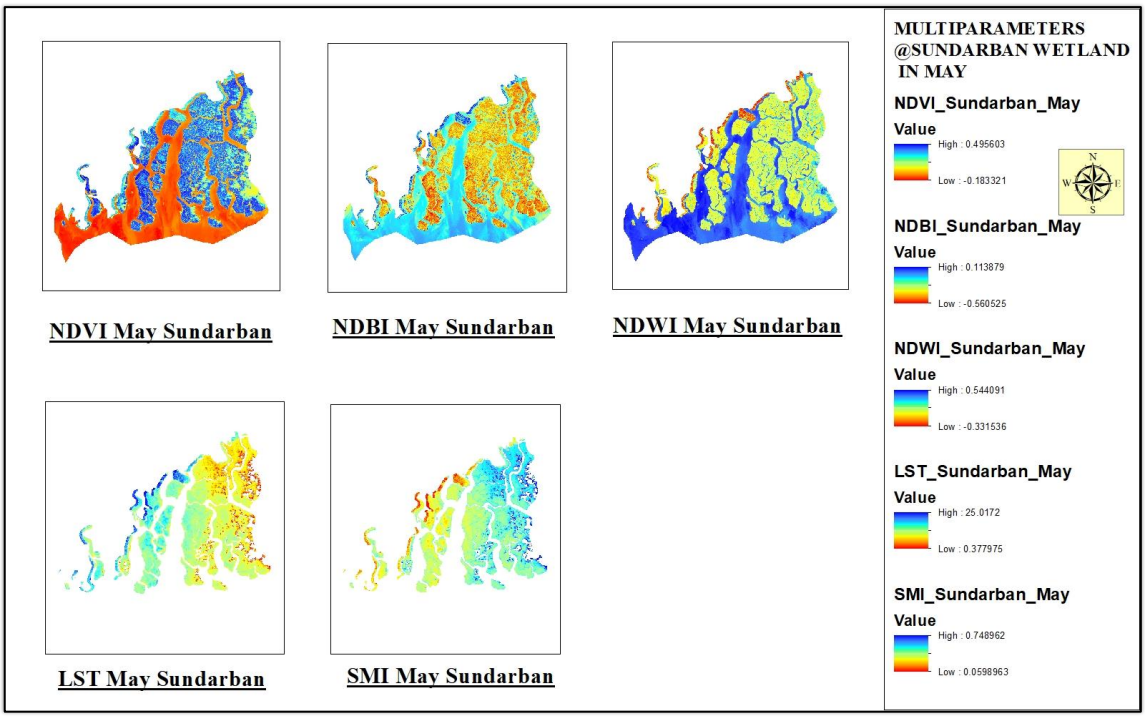

Figure A 2.5: Multiparameter at Sundarban Wetland in May

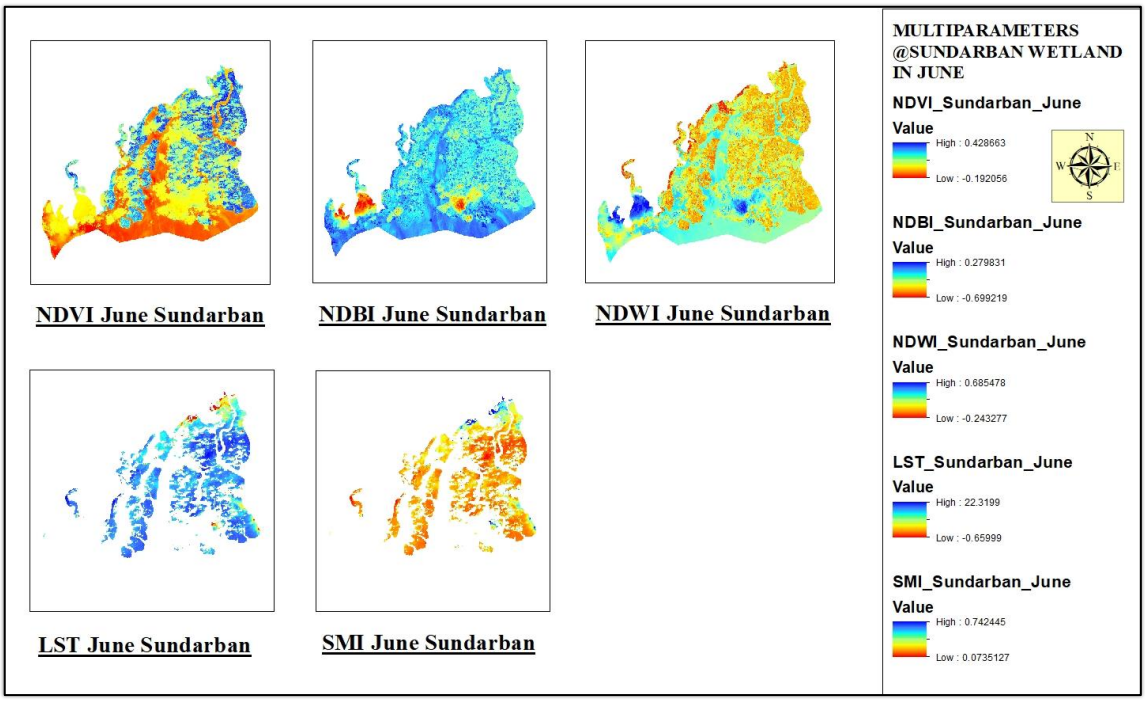

Figure A 2.6: Multiparameter at Sundarban Wetland in June

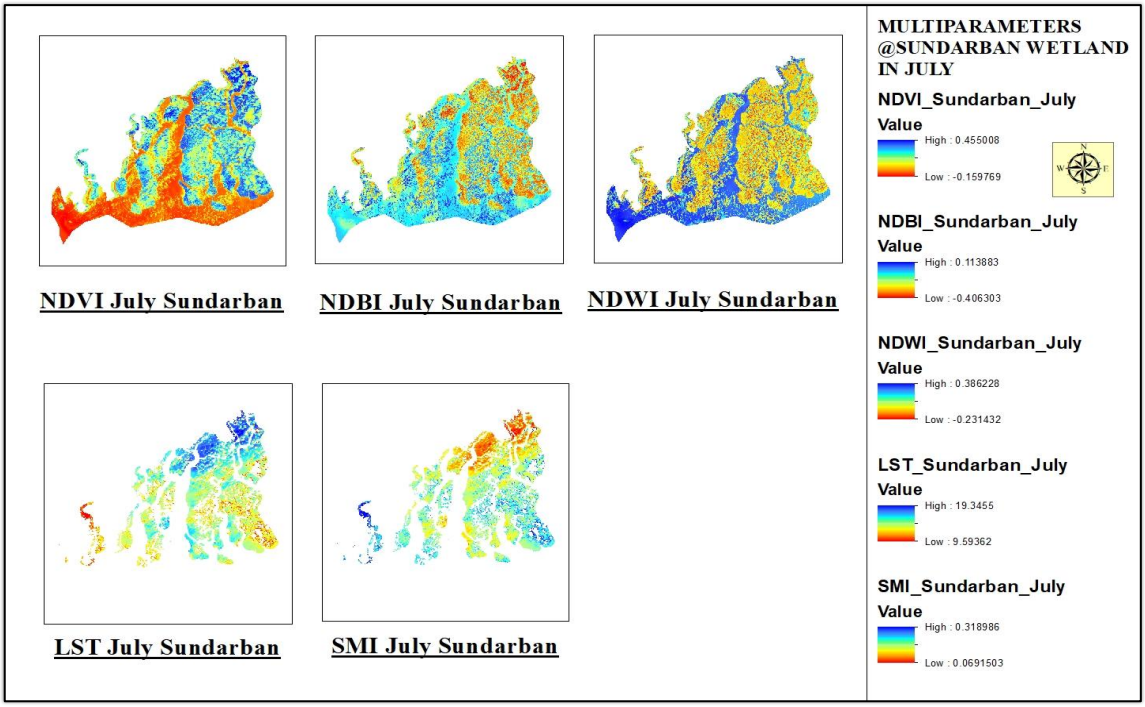

Figure A 2.7: Multiparameter at Sundarban Wetland in July

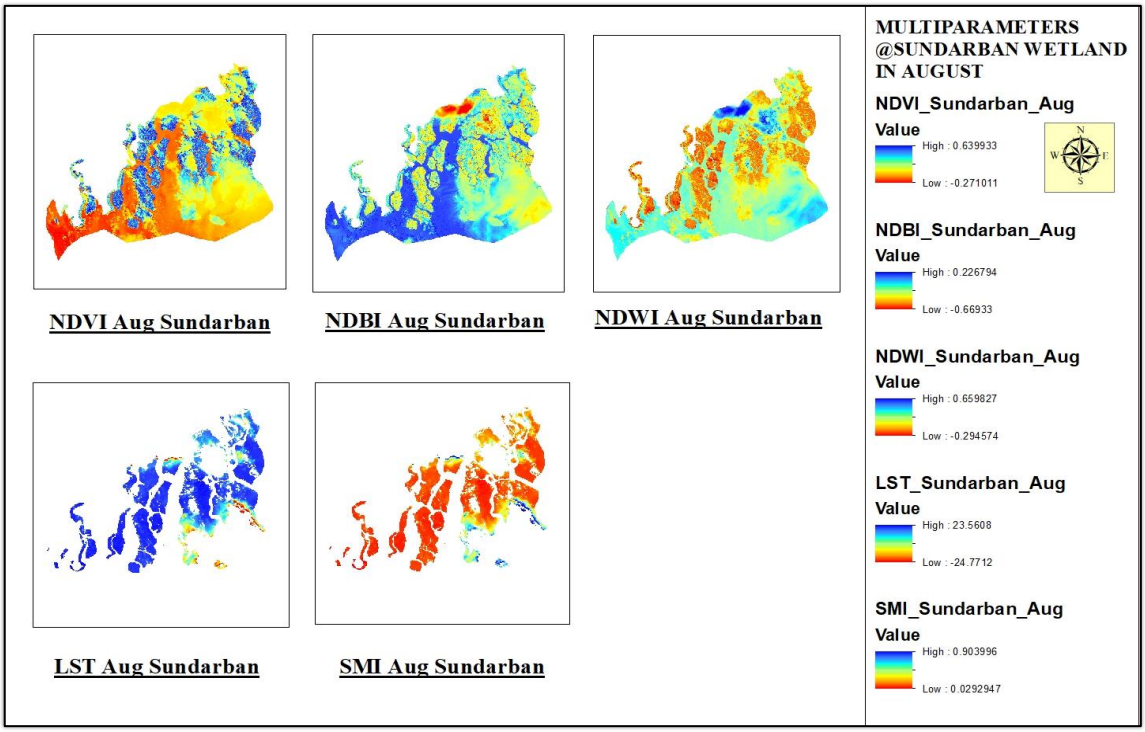

Figure A 2.8: Multiparameter at Sundarban Wetland in August

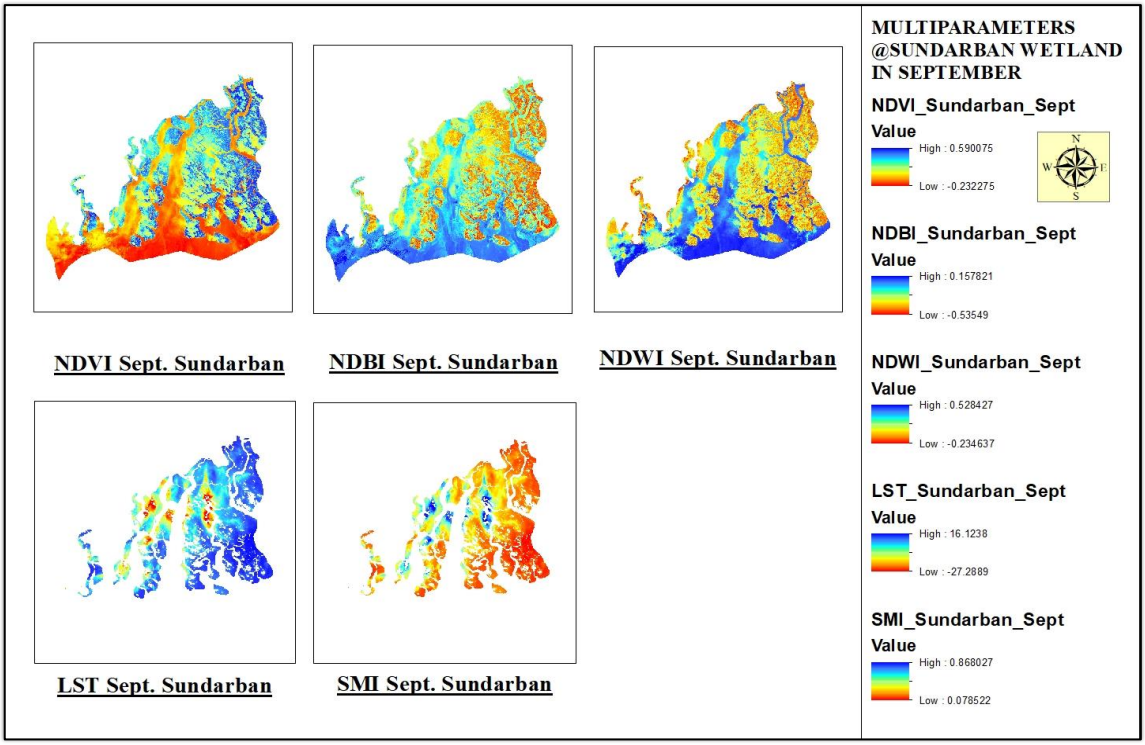

Figure A 2.9: Multiparameter at Sundarban Wetland in September

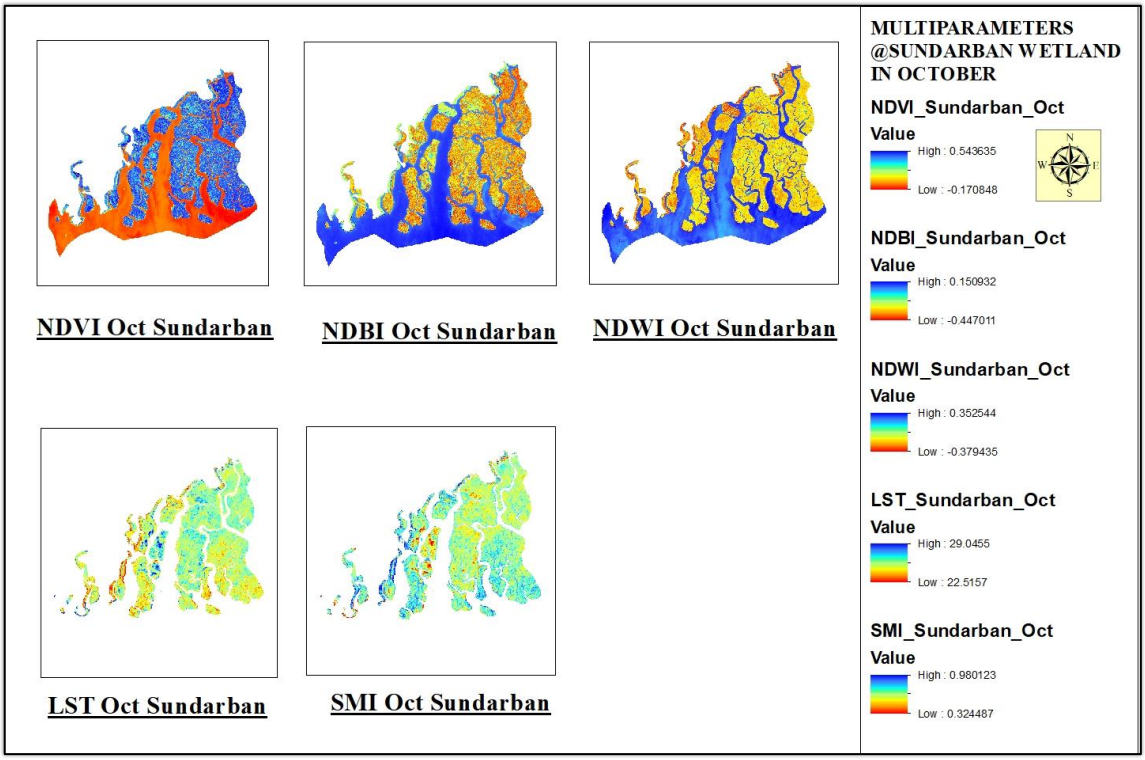

Figure A 2.10: Multiparameter at Sundarban Wetland in October

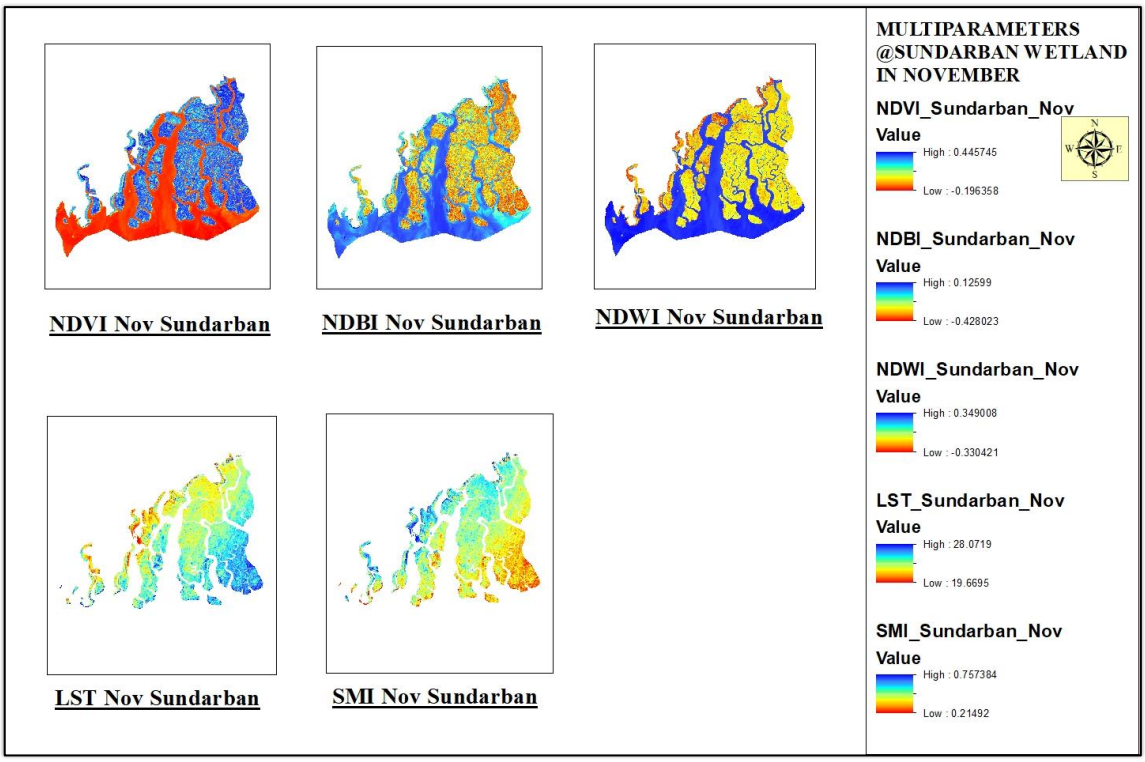

Figure A 2.11: Multiparameter at Sundarban Wetland in November

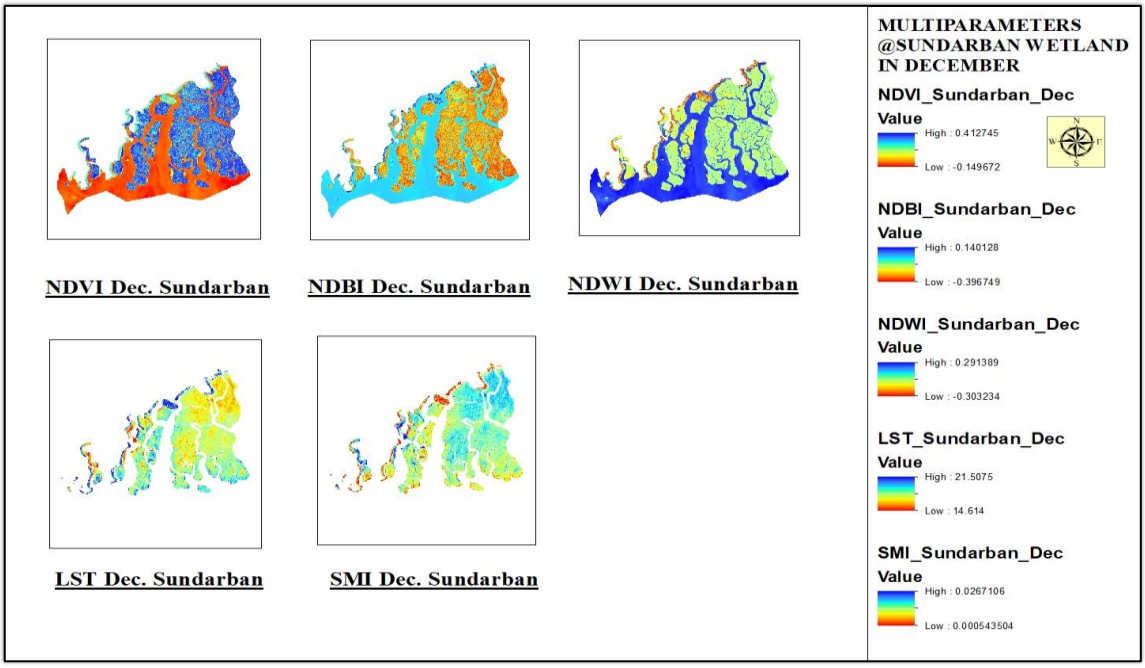

Figure A 2.12: Multiparameter at Sundarban Wetland in December

REFERENCES

[1] **H. Xu**, "A study on information extraction of water body with the modified normalized difference water index (MNDWI)." [Online]. Available: https://www.researchgate.net/publication/284418225

[2] **L. Yang *et al***., "Improving prediction of soil organic carbon content in croplands using phenological parameters extracted from NDVI time series data," *Soil Tillage Res*, vol. 196, Feb. 2020, doi: 10.1016/j.still.2019.104465.

[3] **L. Yang, Y. Cai, L. Zhang, M. Guo, A. Li, and C. Zhou**, "A deep learning method to predict soil organic carbon content at a regional scale using satellite-based phenology variables," *International Journal of Applied Earth Observation and Geoinformation*, vol. 102, Oct. 2021, doi: 10.1016/j.jag.2021.102428.

[4] **P. Kumar *et al***., "Estimation of accumulated soil organic carbon stock in tropical forest using geospatial strategy," *Egyptian Journal of Remote Sensing and Space Science*, vol. 19, no. 1, pp. 109–123, Jun. 2016, doi: 10.1016/j.ejrs.2015.12.003.

[5] **S. Pal, S. Manna, A. Aich, B. Chattopadhyay, and S. K. Mukhopadhyay,** "Assessment of the spatio-temporal distribution of soil properties in East Kolkata wetland ecosystem (A Ramsar site: 1208)."

[6] **K. Ashida *et al***., "Quantitative relationship between organic carbon and geochemical properties in tropical surface and subsurface soils," *Biogeochemistry*, vol. 155, no. 1, pp. 77–95, Aug. 2021, doi: 10.1007/s10533-021-00813-8.

[7] **J. Bae and Y. Ryu**, "Land use and land cover changes explain spatial and temporal variations of the soil organic carbon stocks in a constructed urban park," *Landsc Urban Plan*, vol. 136, pp. 57–67, Apr. 2015, doi: 10.1016/j.landurbplan.2014.11.015.

[8] **S. Pan, X. Zhao, and Y. Yue**, "Spatiotemporal changes of NDVI and correlation with meteorological factors in northern China from 1985-2015," in *E3S Web of Conferences*, EDP Sciences, Nov. 2019. doi: 10.1051/e3sconf/201913101040.

[9] **L. Borromeo, S. Andò, C. France-Lanord, G. Coletti, A. Hahn, and E. Garzanti**, "Provenance of bengal shelf sediments: 1. mineralogy and geochemistry of silt," *Minerals*, vol. 9, no. 10, Oct. 2019, doi: 10.3390/min9100640.

[10] **S. Falahatkar, S. M. Hosseini, S. Ayoubi, and A. Salmanmahiny,** "Predicting soil organic carbon density using auxiliary environmental variables in northern Iran," *Arch Agron Soil Sci*, vol. 62, no. 3, pp. 375–393, Mar. 2016, doi: 10.1080/03650340.2015.1051472.

[11] **J. Foster -Chair, M. Ronan, D. Colin, and O.' Donnell**, "Issues Paper The Role of Wetlands in the Carbon Cycle Wetlands and Waterbirds Taskforce," 2012.

[12] **J. E. Ayala Izurieta *et al.*,** "Multi-predictor mapping of soil organic carbon in the alpine tundra: a case study for the central Ecuadorian páramo," *Carbon Balance Manag*, vol. 16, no. 1, Dec. 2021, doi: 10.1186/s13021-021-00195-2.

[13] **T. Hengl *et al.*,** "SoilGrids250m: Global Gridded Soil Information Based on Machine Learning."

[14] **Y. Zhang *et al***., "Prediction of soil organic carbon based on Landsat 8 monthly NDVI data for the Jianghan Plain in Hubei Province, China," *Remote Sens (Basel)*, vol. 11, no. 14, 2019, doi: 10.3390/rs11141683.

[15] **M. Q. U. Sajib and T. Wang**, "Estimation of land surface temperature in an agricultural region of Bangladesh from landsat 8: Intercomparison of four algorithms," *Sensors (Switzerland)*, vol. 20, no. 6, Mar. 2020, doi: 10.3390/s20061778.

[16] **X. Yu, X. Guo, and Z. Wu**, "Land surface temperature retrieval from landsat 8 TIRS-comparison between radiative transfer equation-based method, split window algorithm and single channel method," *Remote Sens (Basel)*, vol. 6, no. 10, pp. 9829–9852, 2014, doi: 10.3390/rs6109829.

[17] **J. A. Sobrino *et al.***, "Land surface emissivity retrieval from different VNIR and TIR sensors," in *IEEE Transactions on Geoscience and Remote Sensing*, Feb. 2008, pp. 316–327. doi: 10.1109/TGRS.2007.904834.